Technische Universität München
Fakultät für Elektrotechnik und Informationstechnik
Lehrstuhl für Medientechnik

Haptic Communication for Time-delayed Teleoperation

Xiao Xu, M.Sc.

Vollständiger Abdruck der von der Fakultät für Elektrotechnik und Informationstechnik der Technischen Universität München zur Erlangung des akademischen Grades eines

Doktor-Ingenieurs (Dr.-Ing.)

genehmigten Dissertation.

Vorsitzender:		Prof. Gordon Cheng, Ph.D.
Prüfer der Dissertation:	1.	Prof. Dr.-Ing. Eckehard Steinbach
	2.	Prof. Jee-Hwan Ryu, Ph.D.

Die Dissertation wurde am 21.09.2016 bei der Technischen Universität München eingereicht und durch die Fakultät für Elektrotechnik und Informationstechnik am 28.03.2017 angenommen.

To all those who made this happen.

Abstract

Teleoperation systems with haptic feedback allow a human user to immerse into a distant or inaccessible environment to perform complex tasks while simultaneously perceiving the interaction. The communication of haptic information imposes strong demands on the communication network, as it closes a global control loop between the operator and the teleoperator. High packet rate and system stability in the presence of communication delay are the two main challenges for haptic communication in time-delayed teleoperation systems. Teleoperation across communication networks, hence, requires a tight integration of communication and control with the involved robotic systems at the operator and the remote side. So far, the communication and control aspects have been studied mainly independently and by neglecting essential properties of a real communication network.

This thesis focuses on the joint consideration of haptic data communication and stability-ensuring control for time-delayed teleoperation over packet-switched networks. This is to realize a stable system design and an efficient data communication. Two joint solutions are presented: 1) the perceptual deadband-based (PD) haptic data reduction method is combined with the time domain passivity approach. In this context, a novel energy prediction scheme is developed to improve the system transparency of the resulting controller. 2) A modified PD haptic data reduction method is combined with an extended model-mediated teleoperation approach, which is able to deal with environments containing complex geometry and physical properties. The performance of both joint solutions is comprehensively evaluated both objectively and through subjective user studies. These evaluations show that the proposed joint solutions are able to guarantee stable teleoperation while achieving a good trade-off between the teleoperation quality and the packet rate.

Furthermore, this thesis first steps towards an adaptive teleoperation system that can cope with varying network conditions, while still guaranteeing the best possible performance. The proposed approach relies on the systematic comparison of the system performance for different joint communication/control solutions. The experimental results verify that an adaptive use of different communication and control schemes is able to mitigate the drawbacks of each individual method and thus improve the overall system performance in the presence of varying communication delays.

Kurzfassung

Teleoperationsysteme mit haptischer Rückkopplung ermöglichen das Eintauchen eines menschlichen Benutzers in eine entfernte oder schwer zugängliche Umgebung, um sowohl komplexe Aufgaben durchführen zu können, als auch die Interaktion spürbar zu machen. Durch den geschlossenen globalen Regelkreis zwischen Operator und Teleoperator ist die Kommunikation von haptischen Informationen über ein Kommunikationsnetz ausbruchsvoll und mit hohem Regelungsaufwand verbunden. Die Erfordernis von hohen Paketraten sowie die kritische Systemstabilität in Gegenwart von Kommunikationsverzögerungen sind die beiden wichtigsten Herausforderungen für die haptische Kommunikation in zeitverzögerten Teleoperationssystemen. Daher erfordert die Teleoperation über Kommunikationsnetz eine enge Kopplung von Kommunikation und Regelung der Robotiksysteme auf der Operator- und der Teleoperatorseite. Bisher wurden die beiden Aspekte der Kommunikation und Regelung weitgehend unabhängig voneinander untersucht, wodurch ein realistisches Szenario eines Kommunikationsnetz nicht gegeben war.

Diese Arbeit konzentriert sich bewusst auf die gemeinsame Betrachtung von haptischer Datenkommunikation und Regelung für zeitverzögerte Teleoperationen über ein auf paketvermittelndes Kommunikationsnetz. Dies erfordert einen stabilitätsgarantierenden Systementwurf sowie eine effiziente Strategie für die Datenkommunikation. Hierfür werden zwei gemeinsame Lösungsansätze vorgestellt: 1) Zum einen wird Wahrnehmungsmodell-basierte Methode zur haptischen Datenreduktion mit einem Passivitätsansatz im Zeitbereich kombiniert. Hierfür wurde ein neuartiger Ansatz zur Energieprädiktion entwickelt, um die Systemtransparenz des resultierenden Controllers zu verbessern. 2) Zum anderen wird eine modifizierte Methode zur haptischen Datenreduktion in Verbindung mit einem erweiterten modellbasierten Teleoperationsansatz untersucht, welches die Berücksichtigung von Umgebungen mit komplexer Geometrie und anspruchsvollen physikalischen Eigenschaften ermöglicht. Die Leistungsfähigkeit von beiden kombinierten Lösungen wird umfassend objektiv sowie subjektiv durch Nutzerstudien evaluiert. Die Ergebnisse bestätigen, dass die vorgeschlagene kombinierte Lösung stabile Teleoperationen ermöglicht und gleichzeitig einen hervorragenden Kompromiss zwischen der Qualität der Teleoperation und der Höhe der Paketrate auch in schwierigen realen Szenarien gewährleistet.

Zusätzlich befasst sich diese Arbeit mit der gemeinsamen Optimierung der Kommunikation und der Regelung für Teleoperationen mit zeitvarianter Verzögung. Das übergreifende Ziel ist es, ein adaptives Teleoperationssystem zu realisieren, das mit dynamisch veränderbaren Netzwerkbedingungen umgehen kann, ohne dabei auf die bestmögliche Leistungsfähigkeit zu verzichten. Die Resultate verifizieren, dass die adaptive Verwendung von verschiedenen Kommunikations- und Regelungsschemata in der Lage ist, die Nachteile der einzelnen Methoden zu reduzieren und somit die übergreifende Systemperformance trotz der Präsenz von verschiedenen Kommunikationsverzögerungen zu verbessern.

Acknowledgements

The work presented in this dissertation was carried out as a member of the research and teaching staff at the Chair of Media Technology (LMT) at the Technical University of Munich. My research was supported by the European Research Council under the European Union's Seventh Framework Programme (FP7/2007-2013)/ERC Grant agreement no. 258941. Many people have contributed to the success of this work in various personal and professional ways. I am sincerely thankful to all of them; I apologize for not being able to explicitly mention each and every one of them here.

I am eternally grateful to my supervisor Prof. Eckehard Steinbach for giving me the opportunity to investigate the very exciting research field of haptics, and for the trust and the scientific expertise with which he has supported me all throughout my PhD. Despite his busy schedule, he has always been accessible for discussing new ideas and giving me fresh perspectives. His helpful suggestions, advice and guidance significantly contributed to my research work. Furthermore, I would like to thank Prof. Jee-Hwan Ryu for accepting to be the second reviewer of this dissertation and Prof. Gordon Cheng for heading the committee.

My sincere appreciation also goes to all my current and former colleagues of the LMT group. They contributed considerably to this dissertation and many of the achievements presented would not have been possible without their support. I would like to extend my sincere thanks to Dr. Julius Kammerl and Dr. Rahul Chaudhari for initiating me into the world of research. Furthermore, I am very grateful to my colleague Burak Cizmeci for the excellent teamwork in building a reliable teleoperation system in a challenging real-life scenario and his theoretical insights in video coding. Very many thanks go to Clemens Schuwerk for the creative discussion and the joint work on developing the passivity-based control schemes in my research over the past many years. I would like to thank Dr. Nicolas Alt for his extremely reliable support in developing the control platform of the KUKA robotic arm. My sincere appreciation also goes to Dr. Jordi Artigas from the DLR Institute of Robotics and Mechatronics for his insights into robotic teleoperation systems from the control engineering perspective and the intensive support on my implementation of the time domain passivity approach during the winter of 2013. I would like to thank Dr. Robert Huitl, Fernanda Brandi da Silva, Dominik van Opdenbosch, and Anas Al-Nuaimi for giving me their technical

support on various interesting topics. Special thanks go to all my other colleagues and friends, especially Dr. Hu Chen, Dr. Fan Zhang, Dr. Jianshu Chao and Simon Krapf for their interesting discussions on a variety of topics ranging from research, technology, travel, art, philosophy, and international developments. This brings me a lot of passion on the way to my Ph.D. I have learned a lot from all of you.

I would also like to thank all my students who contributed considerably to this dissertation. I sincerely appreciate the efforts of all the highly-motivated students with whom I have worked over the years, especially Zhaoqi Chu, Sili Chen and Ingo Ries. They contributed immensely to the success of my work. Special thanks also go to Ms. Ingrid Jamrath, Ms. Brigitte Vrochte and Dr. Martin Maier for their professional and reliable administrative support. They always kindly and competently helped me in every administrative matter I had.

Finally, I would like to express my deep gratitude to my beautiful girl friend Jie Shen and my parents Hualing Xiao and Yingming Xu for lighting up my world, and for their endless support and forever love.

Munich, June 2016 Xiao Xu

Contents

Contents i

List of Abbreviations v

1 Introduction 1

1.1 Challenges . . . 2

1.2 Major contributions and thesis organization . . . 4

2 Background and Related Work 9

2.1 Bilateral Haptic Teleoperation Systems . . . 9

2.1.1 Master and Slave Subsystems . . . 10

2.1.2 Haptic Communication over Packet-switched Networks . . . 11

2.2 Haptic Data Reduction for the Position-Force Teleoperation Control Architecture 12

2.2.1 Real-time Haptic Data Reduction Approaches . . . 12

2.2.2 Passivity-based Control Schemes . . . 17

2.2.3 Joint Data Reduction and Control Solutions . . . 22

2.3 Model-mediated teleoperation . . . 23

2.3.1 Historical Development of MMT . . . 25

2.3.2 Challenges of MMT . . . 31

2.4 Evaluation Methods . . . 37

2.4.1 Objective Quality . . . 37

2.4.2 Subjective Quality . . . 38

2.5 Chapter Summary . . . 39

3 Time-delayed Teleoperation: Combing Perceptual Data Reduction with the Time Domain Passivity Approach 41

3.1 PD+TDPA . . . 42

3.1.1 System Structure . . . 42

3.1.2 Feasibility evaluation . . . 45

3.1.3 Conservative Control Behavior during Communication Interruptions . . . 47

3.2 Energy Prediction for Less Conservative Control . . . 50
3.2.1 Energy Prediction for Constant Delays . . . 50
3.2.2 Energy Prediction for Time-varying Delays . . . 54
3.2.3 Energy Overestimation for Position Drift Compensation . . . 56
3.3 Evaluation of Teleoperation Quality . . . 57
3.3.1 Objective quality evaluation . . . 57
3.3.2 Subjective quality evaluation . . . 62
3.4 Discussion . . . 69
3.5 Chapter Summary . . . 70

4 Point Cloud-based Model-mediated Teleoperation 73
4.1 System Design . . . 74
4.1.1 Pre-processing . . . 74
4.1.2 Environment modeling . . . 77
4.1.3 Model update . . . 79
4.1.4 Point cloud-based force rendering . . . 79
4.1.5 Point cloud compression . . . 81
4.2 Radial function-based deformation method for real-time modeling of deformable objects using point clouds . . . 81
4.2.1 A model of deformable objects . . . 82
4.2.2 Radial function-based deformation . . . 83
4.2.3 Feasibility Evaluation . . . 87
4.3 Slave update controller: dynamic and perception-based model update . . . 89
4.3.1 Updating the object geometry . . . 89
4.3.2 Updating the physical properties of the objects . . . 91
4.4 Master update controller: passivity-based model update . . . 92
4.4.1 Overview of master system with environment model . . . 93
4.4.2 Passivity condition . . . 94
4.4.3 Evaluation . . . 97
4.5 Evaluation of the pcbMMT system . . . 100
4.5.1 Setup . . . 100
4.5.2 Results . . . 101
4.5.3 Subjective test . . . 104
4.6 Discussion . . . 105
4.6.1 Modeling of complex environments . . . 106
4.6.2 Modeling of human behavior . . . 107
4.6.3 Selective transmission of model parameters . . . 108
4.6.4 System transparency . . . 108

4.7 Chapter Summary 109

5 Toward Joint Optimization of Communication and Control for Networked Teleoperation 111

5.1 Experimental Case Study 112
5.1.1 Experimental setup 113
5.1.2 Experimental procedure 114
5.1.3 Results 115
5.1.4 Conclusions 120
5.2 Discussion and Open Research Questions 121
5.3 Chapter Summary 122

6 Conclusion and Future Work 125

6.1 Haptic Data Reduction using the Time Domain Passivity Approach 125
6.2 Point Cloud-based Model-mediated Teleoperation 126
6.3 Toward Joint Optimization of Communication and Control for Networked Teleoperation 128

A A Summary of Relevant Studies on Model-mediated Teleoperation 131

Bibliography 133

List of Figures 147

List of Tables 151

List of Abbreviations

Abbreviation	Description	Definition
TOP	Teleoperator	page 1
OP	Operator	page 1
3D	3-dimensional	page 6
DoF	Degree of Freedom	page 12
JND	Just Noticeable Difference	page 14
DBP	Deadband Parameter	page 14
PD	Perceptual Deadband	page 14
ZOH	Zero Order Hold	page 16
WV	Wave Variable	page 18
PO	Passivity Observer	page 20
PC	Passivity Controller	page 20
TDPA	Time Domain Passivity Approach	page 20
MMT	Model-mediated Teleoperation	page 23
EP	Energy Prediction	page 52
PDC	Position Drift Compensation	page 56
RPT	Region of Perceived Transparency	page 62
ISS	Input-to-State Stability	page 70
pcbMMT	Point Cloud-based Model-mediated Teleoperation	page 73
RFBD	Radial Function-based Deformation	page 74
pcbHR	Point Cloud-based Haptic Rendering	page 79
HIP	Haptic Interacting Point	page 79
PMU	Passivity-based Model Update	page 93
QoS	Quality of Service	page 111

Chapter 1

Introduction

Remote interaction solutions such as voice or video conferencing have reached a high level of sophistication and widespread use. While the feeling of being present in a remote environment is clearly available with these systems, a complete immersion cannot be realized without the possibility of physical interaction with the remote environment. To this end, bilateral haptic teleoperation systems have been developed. These systems supply the user with multimodal sensor information concerning the remote environment while commanding a robotic system in the remote space. Haptics, as an extension of visual and auditory modalities, refer to both kinesthetic and tactile information and include position, velocity, force, torque, vibration, etc. In this thesis, we use the word *haptic* to refer to kinesthetic components such as force and motion.

Using a teleoperation system with haptic feedback, the users can thus truly immerse themselves into a distant environment, i.e., modify it, and execute tasks without physically being present but with the feeling of being there. A typical teleoperation system with haptic feedback (referred to as a teleoperation system) comprises three main parts: the human operator (OP)/master system, the teleoperator (TOP)/slave system, and the communication link/network in between [43]. During teleoperation, the slave and master devices exchange multimodal sensor information over the communication link. As illustrated in Fig. 1.1, the slave robot equipped with multimodal sensors follows the received position or velocity commands sent by the master. The haptic, visual, and audio signals captured by the sensors on the slave side are sent back to the master and displayed to the OP. The communication network realizes the exchange of the command and sensor signals between the master and the slave.

Use of haptic feedback, in addition to visual and audio information, increases the sense of being present in the remote environment. Consequently, teleoperation systems are already established in many fields of application allowing an OP to perform dangerous tasks at a safe distance and to execute complex tasks in reduced time with lower costs and improved precision/performance [26]. This applies to hazardous environments such as the handling of nu-

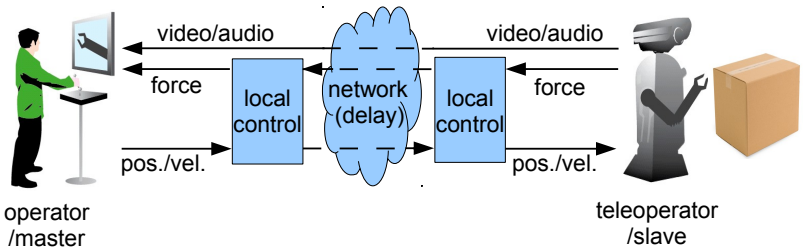

Figure 1.1: Overview of a bilateral teleoperation system with haptic feedback (adapted from [43]).

clear/toxic/explosive materials [86] or the exploration of space and underwater [70, 113, 128]. Further interest can be found in the medical field, where telesurgery systems follow surgeons for applying remote treatment on patients [54]. In 2001, the first completely remote surgery on a human patient was performed over a distance of 7000 km between Strasbourg (France) and New York (USA) with a latency of 135 ms [100]. Moreover, using tele-teaching/tele-training systems, a full skill transfer can be achieved without the experts being present [24, 39, 40, 57, 121].

Communication of haptic information between the master and slave plays a key role in teleoperation systems. For geographically distributed teleoperation systems, communication over the Internet (a typical packet-switched network) is the most attractive medium as it provides low cost, easy access, worldwide coverage and high flexibility. However, the high packet rate required for exchanging haptic information leads to high communication load and results in potential network congestion. Furthermore, time delay, delay variation, and packet loss, which are introduced by the Internet, distort the communication of haptic information. This jeopardizes the stability of teleoperation systems and degrades user performance. The main challenges faced by the communication of haptic information in time-delayed teleoperation systems are summarized in the following.

1.1 Challenges

For teleoperation in remote environments, the communication of haptic information imposes strong demands on a communication network. This presents the following challenges for the design of a reliable teleoperation system.

Haptic data reduction

During teleoperation, haptic signals are typically sampled at a rate of 1 kHz or even higher [19, 31, 87]. The samples are packetized and transmitted immediately once available. In this way, an additional processing delay, which is crucial for system stability and transparency [31,

90, 136], is avoided. Teleoperation systems, hence, transmit 1000 or more haptic data packets per second bidirectionally over the network. The resulting high packet load on the network leads to substantial data overhead due to the transmission of packet header information. At a packet rate of 1 kHz, this can become a critical factor and the overhead can even dominate the actual payload data [65, 108]. In addition, haptic signals usually need to provide to the user visual and audio feedback from the slave subsystem. A high packet rate of haptic communication consequently makes the management and synchronization of these data streams very challenging [29]. Hence, it is desirable to develop approaches that reduce the amount of haptic packets to be exchanged between the master and slave.

Stability-ensuring control schemes

The communication between geographically distributed master and slave systems is typically afflicted by time delay, delay variation, and packet loss. This is particularly the case if packet-switched networking, e.g., on the Internet, or even wireless communication hops are involved. Studies have shown that even small delays or packet loss rate jeopardize system stability and transparency [16, 90, 105]. Transparency, in this context, is defined as the ability to present the undistorted impedance of the remote environment to the human operator [90]. To realize a stable and transparent (high-quality) teleoperation, stability-ensuring control schemes are required in the presence of communication delay.

Joint solutions

So far, the haptic data reduction or stability-ensuring control schemes have been studied mainly independently and by abstracting or neglecting important properties (e.g. channel resources, communication delays, and delay jitters) of the communication network. More specifically, for the state-of-the-art haptic data reduction approaches [61, 65], communication delay, which is the main source for the stability issues in teleoperation systems, has been neglected completely. For the conventional stability-ensuring control schemes [16, 18, 105, 119], the challenge resulting from the required high packet rates has been ignored.

For real networked teleoperation in remote environments, communication delays as an important network characteristic cannot be neglected. The haptic data reduction approaches and the stability-ensuring control schemes need to be jointly considered to realize a stable system design and an efficient data communication. The control and haptic data reduction approaches introduce different types of artifacts/distortions into the system, their performance varies between tasks, and they also differ in their robustness towards different network parameters. The artifacts introduced by the control schemes can aggravate the distortion introduced by the data reduction approach, and vice versa. One of the major questions relates to the extent to which the packet rate can be reduced such that the system still preserves stability and high teleoperation quality in the presence of communication delay.

Earlier studies combined the state-of-the-art haptic data reduction methods [65] with the wave-variable transformation scheme [105] to address the aforementioned challenge. The authors of [68] applied the haptic data reduction approach directly on the wave variables and found the subjectively best deadband parameter for an interaction with a rigid wall in the presence of a 100 ms round-trip communication delay. In contrast, the authors of [145] proposed a method that enables the use of the haptic data reduction approach in the time domain (i.e., on the force and velocity signals). Both methods, however, are applicable only for constant delays without packet loss.

1.2 Major contributions and thesis organization

This thesis focuses on the kinesthetic components of haptic data. The aim is to develop efficient haptic (kinesthetic information) communication approaches for time-delayed teleoperation over packet-switched networks. Kinesthetic haptic data reduction approaches and control schemes are jointly considered to achieve a stable teleoperation and a good trade-off between teleoperation quality and the consumed network resources. To this end, this thesis proposes two solutions:

1. a combination of the state-of-the-art haptic data reduction approaches with the conventional stability-ensuring (passivity-based) control schemes. Both schemes are modified to adapt to each other.

2. an extension of the model-mediated teleoperation (MMT) for dealing with complex environments (e.g. deformable objects or objects with complex surface geometry) with the help of 3D sensors (named the point cloud-based model-mediated teleoperation). The main challenges for designing a reliable MMT system, such as precise environment modeling, efficient data transmission, and stable haptic rendering during model mismatches, are addressed for the investigated scenarios.

A comparison between these two solutions is also presented in this thesis. It aims to jointly optimize control and communication for various network characteristics. The main contributions of this work together with an outline are presented in the following.

Haptic data reduction using the time domain passivity approach (Chapter 3)

Haptic data reduction for time-delayed teleoperation can be achieved by combining existing haptic data reduction methods with the conventional stability-ensuring control schemes (e.g. passivity-based control methods). Early attempts such as [68, 145] combined the wave-variable (WV) transformation scheme [105] with the perceptual deadband-based haptic data reduction approach (PD approach) [65]. These methods, denoted as PD+WV, however, are applicable

only for constant delays. For teleoperation over real communication networks, delay variation is a non-negligible characteristic.

Chapter 3 presents a joint solution which combines the PD scheme with the time domain passivity approach (TDPA) [120]. The goal is to reduce the packet rate over the communication network while preserving system stability in the presence of time-varying and unknown delays. This solution is first studied based on a simple combination, denoted as PD+TDPA. Theoretical and numerical analysis as well as subjective tests show that the PD+TDPA method improves subjective quality and user preference compared to the PD+WV method, while achieving a comparable data reduction in the presence of time-varying communication delays.

Chapter 3 provides furthermore an extension of the PD+TDPA method. The PD approach leads to irregular updates between the master and slave, resulting in degraded system transparency and reduced teleoperation quality (e.g., due to strong force jumps) when the PD approach is combined with the TDPA. Chapter 3 proposes a novel energy prediction (EP) scheme that adaptively predicts system energy during communication interruptions and allows for larger energy output. This achieves less conservative control and improves teleoperation quality. Evaluation of objective and subjective quality shows that the PD+TDPA+EP method achieves the best system transparency, when compared with the PD+TDPA method and other related approaches from literature. According to a subjective user study, the PD+TDPA+EP method, compared with the PD+TDPA and other related approaches from literature, allows for a higher packet rate reduction without noticeably affecting interaction quality.

Point cloud-based model-mediated teleoperation (Chapter 4)

Conventional teleoperation control schemes, such as the passivity-based control schemes, require the exchange of motion (position/velocity) and force signals between the master and slave. Model-mediated teleoperation (MMT) is an alternative control scheme that does not require the transmission of force signals. MMT systems generate non-delayed force feedback based on a local model on the master side. The model parameters describing the slave environment are continuously estimated in real time and transmitted back to the master. For static or slow-varying environments, the transmission/update of the model parameters is not necessary to be 1 kHz; hence the packet rate in the backward channel is reduced.

MMT was first proposed by Hannaford in [58], and later extended by Niemeyer et al. in [103, 148]. Compared to the passivity-based control schemes, MMT technique is relatively young and not comprehensively investigated. Challenges such as dealing with complex environments and achieving efficient data communication are still not intensively studied.

Chapter 4 extends the state-of-the-art MMT technique for dealing with complex environ-

ments. Particularly, the following contributions are presented to address the main challenges facing the design of a reliable MMT system.

- **Environment modeling for complex geometry and deformable objects**
  The most important challenge of MMT is the environment modeling. A precise and quickly converging model estimation algorithm is the key for designing an efficient MMT system. Sec. 4.1 presents an overview of the proposed point cloud-based model-mediated teleoperation (pcbMMT) approach, which allows for handling of complex object geometry. Sec. 4.2 proposes an online environment modeling methods for deformable objects. External 3-dimensional (3D) sensors are employed to improve modeling accuracy.

- **Efficient data transmission**
  In the backward channel of MMT systems, the transmitted data are the model parameters. To avoid excessive and unnecessary model updates, transmission of the estimated model parameters can be reduced in the following ways: 1) reduction of the estimation rate. This is to increase the time period of the estimation process on the slave side. 2) selected transmission. This is to selectively send the relevant model parameters. In Sec. 4.3, these two methods are discussed and evaluated in a MMT system.

- **Stable local haptic rendering**
  This is to ensure stability of the local haptic loop on the master side during the period when the local model is in mismatch with the remote environment. If model mismatch is detected, a model update on the master side is required. Ideally, the parameters of the local model need to be updated to the correct ones as quickly as possible. However, improper update schemes, e.g., a sudden change in stiffness or model position, result in a suddenly changed force that is displayed to the human user. This is called the model-jump effect. Sec. 4.4 presents a passivity-based model update schemes, which can avoid model-jump effects while guaranteeing system stability and allowing sufficiently quick model update.

Toward Joint Optimization of Control and Communication for Networked Teleoperation (Chapter 5)

Chapter 5 presents an experimental case study toward joint optimization of control and communication for networked teleoperation systems. It aims to verify that an adaptive teleoperation system can cope with varying network conditions, while still guaranteeing the best possible performance. This requires an adaptive switch between different control and haptic communication schemes for various quality of service (QoS) offered by the network. Section 5.1 evaluates the two joint solution methods that are introduced in Chapter 3 and 4, and presents the first result of the joint optimization work. The experimental results show that

an adaptive teleoperation system is able to mitigate the drawbacks of each individual control scheme and subjectively improve system performance for different communication delays. Section 5.2 discusses the factors that affect system performance (both objective and subjective) and outlines further research directions toward a comprehensive joint optimization work.

The thesis is concluded in Chapter 6 with a summary and an outlook of future research directions.

Parts of the work presented in this thesis have been published in various international peer-reviewed scientific journals [1–3] and conferences [4–10].

Chapter 2

Background and Related Work

Bilateral haptic teleoperation systems, also known as telehaptic systems [126] (referred to as teleoperation systems in the following of this thesis), usually consist of one human operator using a haptic interface (master device) on one end, one teleoperator (slave actuator) on the other end, and a communication channel between them (Fig. 1.1). For short distance applications the communication channel can be a single wired or wireless point-to-point communication. Long distance applications benefit from packet-switched network infrastructures, such as the Internet. The goal of teleoperation systems, as implied by their name, is to provide the human users with the feeling of presence and the capability to operate in the remote environment.

This chapter introduces the general architecture and important design objectives of teleoperation systems. Haptic data communication and stability-ensuring control schemes are reviewed with the focus on reducing the haptic packet rate and stabilizing teleoperation systems over packet-switched networks. Furthermore, relevant measures for evaluating teleoperation quality are discussed.

2.1 Bilateral Haptic Teleoperation Systems

A typical teleoperation system includes a human user, a master and a slave device, a communication network between the master and slave, local control loops, and an environment that the slave interacts with (see Fig. 2.1). The human operator interacts with the master device (a haptic interface) which senses and transmits the motion data (position or velocity discrete-time data) to the slave subsystem. The slave is equipped with sensors and actuators; it is controlled by the received motion commands, senses the interaction with the remote environment, and returns the visual, auditory, and haptic feedback to the master. These multimodal feedbacks are displayed to the human user, allowing the human user to immerse themselves into the distant environment. The two local control blocks on both the master and slave side are used for ensuring system stability in the presence of communication delay

and packet loss, and guaranteeing a high sampling rate of the motion/force signals that are required for a stable and transparent global/local close-loop control.

A teleoperation structure, which sends motion (position/velocity) signals and receives force signals, is referred to as position-force teleoperation architecture [16, 105, 120] as illustrated in Fig. 2.1. Another widely-used teleoperation architecture is the position-position structure; where the master sends its position/motion signals to the slave, and also receives the slaves position/motion signals. The force feedback is then rendered based on the master and received slave motion signals [18, 119]. This thesis focuses on the position-force teleoperation architecture.

In the case of a user interacting with a remote surface using appropriate hardware that can render texture information, the slave subsystem is also responsible for transmitting texture data as well.

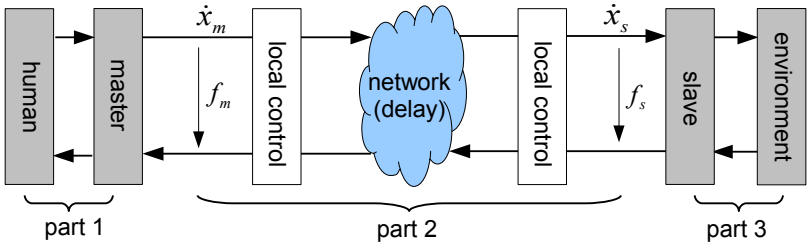

Figure 2.1: Components of a position-force teleoperation architecture.

2.1.1 Master and Slave Subsystems

Haptic devices which are used as master subsystems, also called haptic manipulators, are comprised of actuators and sensors which form the kinesthetic and tactile device subsystems.

Master subsystems are able to reproduce and process kinesthetic or tactile, or both types of haptic data. Table 2.1 shows a selection of the most popular haptic devices providing kinesthetic feedback, which are applied for research or commercial use. Many haptic interfaces, such as the CyberGrasp [13] (an exoskeleton device), can also be entirely wearable or have wearable components in order to provide tactile feedback more effectively. It is possible to use more than one actuator for each finger. A recent product applies the tactile display techniques to the screen of mobile phones, called TPad [151], providing tactile feedback to the fingers.

The slave subsystem can be either a physical device which interacts with a physical remote environment or a virtual device of any form (e.g. a virtual hand) that operates in a virtual environment. A key difference between them is that the effect of the slave impedance and the control of the slave actuator can be neglected in virtual environments, which simplifies the whole teleoperation systems. Virtual environments, even though it is not feasible to perfectly replicate a physical environment, have the advantage of allowing for safer simulation in differ-

	Degrees of Freedom	Maximum Force (N)	Maximum Stiffness (N/mm)
Geomagic Touch (formerly Sensable Phantom Omni)	up to 6	3.3	X-axis:1.26 Y-axis:2.31 Z-axis:1.02
Force Dimension Omega 3 / Omega 6 / Omega 7	3 / 6 / 7	12 / 12 / 12 and ±8 (grasping)	14.5
Novint Falcon	3	8.9	14.5
MPB Freedom 6S / 7S	6 / 7	2.5	2

Table 2.1: Overview of popular commercial kinesthetic haptic devices.

ent situations, faster tele-training for various environments, and easier setup for interaction among multiple users in remote locations [121].

2.1.2 Haptic Communication over Packet-switched Networks

The bidirectionally exchanged motion/haptic signals in a teleoperation system close a global control loop between the master and the slave. Accordingly, even a small communication delay in the haptic communication channel jeopardizes system stability and degrades teleoperation quality [90]. In order to keep the communication delay of the real-time transmission of haptic signals as small as possible, haptic sensor readings are packetized and transmitted once available. Typically, haptic signals are sampled at a rate of 1 kHz or even higher [19, 31, 87]. This sampling rate has been widely used in many teleoperation applications. Rigorously, 1 kHz sampling rate is not a strict requirement for teleoperation systems. However, according to the stability analysis in [11, 32, 38, 99], the sampling rate is lower bounded by the maximum displayable stiffness and the system damping for ensuring system stability. Teleoperation systems can be stable for sampling rates lower than 1 kHz (e.g. 100 Hz). In this case, however, the maximum displayable stiffness is quite smaller than that for higher sampling rate (e.g. 1 kHz). Meanwhile, the system requires large damping for stabilizing a hard contact when the sampling rate is small. Therefore, 1 kHz is a good choice for many teleoperation applications, and it leads to 1000 or more haptic data packets per second to be transmitted between the master and the slave. For Internet-based communication, such high packet rates are hard to maintain [48, 61, 65].

In addition, for teleoperation in remote environments over Internet or mobile networks, communication delay and delay variation are inevitable. Communication delay normally ranges from a few milliseconds up to several hundred milliseconds, depending on distance and the communication infrastructure. The delay can even increase to several seconds in

space applications. Even for sufficiently high packet rate in the haptic channel, communication delay destabilizes teleoperation systems [16, 90].

Approaches that reduce the amount of haptic packets over the network and control schemes that guarantee system stability in the presence of communication delay, are hence the key objectives of communicating haptic data in time-delayed teleoperation systems.

2.2 Haptic Data Reduction for the Position-Force Teleoperation Control Architecture

For conventional position-force teleoperation control architectures, to tackle the challenges of haptic communication over packet-switched networks, simply improving the communication channel infrastructure to provide higher quality of service is not enough. Improvements have been proposed in the literature by means of signal processing and control methods which guarantee efficient use of channel resources and system stability. Such techniques to address the aforementioned challenges, either individually or jointly, are discussed further in the following subsections.

2.2.1 Real-time Haptic Data Reduction Approaches

Haptic data reduction can be achieved by reducing either the packet size or packet rate or both. For communication of haptic data at a packet rate of 1 kHz or higher, reduction of packet rate is the more important task. To improve haptic immersion and manipulative flexibility for extensive haptic interaction, position tracking and force feedback display (e.g. more joints), the integration of more degrees of freedom (DoF) in haptic multimedia systems is clearly a recent trend. For instance, Immersions CyberGrasp/CyberGlove HSI device [13] integrates 22 DoF to enable the haptic modality for a human hand. As each DoF needs to be continuously sampled and controlled, the amount of sensor/actuator data quickly increases. In this case, both haptic packet rate and packet size need to be reduced.

Haptic data reduction techniques, according to the human haptic perception system, can be classified either as kinesthetic data reduction or tactile data reduction. These techniques can be considered as lossy data reduction/compression schemes as full recovery of the original raw data is not possible. Since this thesis focuses on kinesthetic haptic data, in the following subsections, the state-of-the-art kinesthetic haptic data reduction schemes are introduced.

2.2.1.1 Human Haptic Perception System

Human haptic perception describes the human sense of feeling and the sense of touch. The human body, when in motion or in contact with other objects, detects and transmits the

sensed information through the human haptic system to the brain. The human haptic system, referring to both kinesthetic and tactile perception, is briefly discussed in the following.

- *The kinesthetic sense:* The kinesthetic perception refers to the sense of the position of limb joints, limb movements, and the perception of forces and torques acting on the body. In addition, stimuli such as velocity, acceleration, force changes, etc. can be also perceived through the kinesthetic perception system. The kinesthetic sensory information is captured by mechanoreceptors in muscles and tendons. The kinesthetic sense enables the human to identify physical properties such as mass/inertia, stiffness, and viscosity of currently touched objects. A comprehensive overview of the human kinesthetic perception system is presented in [84].

- *The tactile sense:* The tactile perception refers to the sense of touch on the skin. Tactile sensory information is captured by different types of mechanoreceptors in the skin. This enables the human to perceive tactile information such as temperature, roughness, geometry/shape of touched objects. Additionally, vibrations (repetitive pressure stimuli) can be also detection through the tactile perception system within the frequency range of 3-500 Hz [51]. A detailed discussion on human tactile perception can be found in [123].

Both kinesthetic and tactile subsystems, responsible for the modalities of proprioception and touch. Through haptic perception system, the human is thus able to sense the physical properties and surface information of interacted objects.

2.2.1.2 Lossy Compression of Kinesthetic Signal

Early attempts exploit the statistical properties of the kinesthetic signals to compress the packet size. To this end, predictive models are employed to reduce the data redundancy. Quantization techniques (e.g., Adaptive DPCM) for kinesthetic data reduction were presented in [125]. In [156], kinesthetic data was represented with 32-bit IEEE floating-point values. After the master and slave device have exchanged enough raw data, a simple position prediction method was used. Compression was achieved by performing an exclusive-or operation between the predicted and the previously predicted value and the result being reduced to the eight most important bits.

Apart from prediction, lossy kinesthetic data compression and decompression has also been achieved by using discrete cosine transform (DCT) [137], similarly to the JPEG codec, in a teleoperation system with force feedback with a compression ratio near 20%. Moreover, a Wavelet Packet Transform (WPT)-based compression method has been tested on 1-DoF haptic data [88].

2.2.1.3 Perceptual Deadband-based Approaches for Kinesthetic Packet Rate Reduction

The first proposal that targets packet rate reduction for networked control systems can be found in [108]. If the difference between the most recently sent update and the current input value exceeds a fixed threshold, signal updates are triggered. The receiver reacts to a missing sample by holding the value of the most recently received sample. The approach in [108], however, is conservative for the studied teleoperation systems, as it ignores that the human operator comes with strong limitations in terms of perceivable signal changes.

State-of-the-art methods have shown that it is possible to exploit the limitations of human haptic perception towards achieving lossy data reduction. It is known from psychophysics that the human haptic perception system is limited, and it is often described using Weber's law [49, 147]. This law states that the perceivable difference between two stimuli, the just noticeable difference (JND), is proportional to the initial stimulus itself:

$$\Delta I = k \cdot I \tag{2.1}$$

where k is a constant and I and ΔI denote the initial stimulus and the JND, respectively. The constant k, also called the Weber fraction, depends on the investigated stimulus, e.g. force, stiffness or velocity. A brief summary of the Weber fraction k of human perceptual discrimination for haptic signals is shown in Table 2.2.

Physical property	k	Experimental conditions
Force	ca. 10%	arm/forearm
Movement	$8\% \pm 4\%$	arm/forearm
Stiffness	$23\% \pm 3\%$	arm/forearm
Viscosity	$34\% \pm 5\%$	arm/forearm
Inertia	$21\% \pm 3.5\%$	pinch-fingers, at 12 kg

Table 2.2: Weber fraction of human perceptual discrimination for haptic signals [66].

The perceptual deadband-based (PD) approach is a lossy haptic packet rate reduction scheme that employs a mathematical model of human haptic perception to keep the signal distortion below human perception thresholds [61, 65, 69, 134, 135]. The PD approach exploits this limitation to reduce the number of force and velocity signal packets in teleoperation systems. For a given force signal I, the deadband parameter (DBP) p defines a deadband zone (DBZ) $2pI$ (see Fig. 2.2). Samples that lie in the DBZ are dropped. When the difference between the most recently sent sample and the current signal violates the DBZ, the current signal is transmitted. At the receiver side, an upsampling method is used to interpolate the irregularly received signal samples to a high sampling rate, which is required for the local control loop. Figure 2.2 illustrates the 1-DoF PD approach. The input signal in Fig. 2.2(a)

is irregularly downsampled and only the values represented with black-filled circles are transmitted. In Fig. 2.2(b), the output signal is interpolated back to the original sampling rate (e.g. 1 kHz) using the zero-order hold strategy. With a proper choice of p (e.g. $p < k$), the input data can be strongly reduced without significantly distorting the interaction quality.

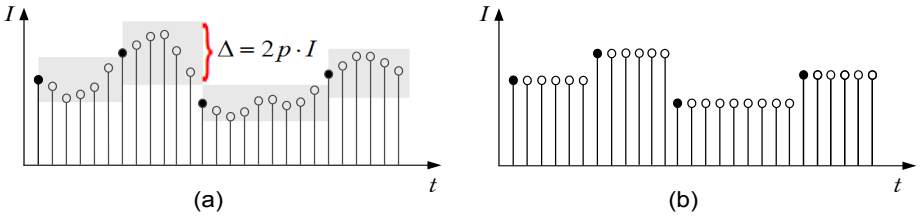

Figure 2.2: Illustration of the 1-DoF perceptual deadband approach. (a) The input signal, i.e., the sensor readings at the sender. (b) The reconstructed signal at the receiver.

For multi-dimensional haptic signals, the DBZ defined by the DBP becomes a sphere or a cone [64, 134]. Considering the direction masking effect of human haptic perception [134], more than one DBP are necessary to define the DBZ in high dimensional space.

2.2.1.4 Perceptual Deadband Approaches with Predictive Coding

Haptic signal predictors can be used to estimate future haptic samples from previous data. By this, a further reduction of the haptic packet rate is achievable [62, 135]. As illustrated in Fig. 2.3, the same predictors run in parallel at both the sender and receiver sides. On the sender side, the predictor generates the predicted haptic signal at every sample instant. If the prediction error is smaller than the corresponding JND, no update is triggered. Otherwise, the input sample is transmitted to the other side and the transmitted sample is used for updating the predictor. On the receiver side, if a packet is received, it is directly applied as the output and the received haptic signal is used for updating the predictor. Otherwise, the predictor generates the predicted haptic signal as the current output.

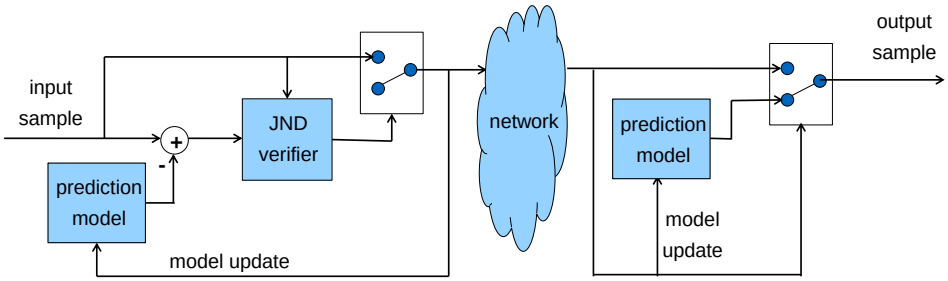

Figure 2.3: Structure of the perceptual haptic data reduction scheme with predictive coding (adapted from [135]).

Different kinds of predictors, for example a linear first order or higher order predictors, can be used to estimate the future haptic samples. The original PD approached introduced in Section 2.2.1.3 can be considered to use a zero-order hold (ZOH) predictor.

A first-order linear predictor as presented in [61, 62] can be expressed as

$$I_i = I_{i-1} + \frac{I_{new-1} - I_{new-2}}{t_{new-1} - t_{new-2}}(t_i - t_{i-1}) \tag{2.2}$$

where $\{I_i, I_{i-1}, I_{i-2}, \dots\}$ are the predicted signals given by the predictor and $\{t_i, t_{i-1}, t_{i-2}, \dots\}$ are the corresponding time instances. $\{I_{new}, I_{new-1}, I_{new-2}, \dots\}$ and $\{t_{new}, t_{new-1}, t_{new-2}, \dots\}$ are the last transmitted/received signals and the corresponding time instances, respectively. According to (2.2), the predicted signal value lies on a straight line determined by the last two received signal values. Once the difference between the predicted value and the actual value is larger than the JND, a new value I_{new} is transmitted and the parameters of the predictor are updated accordingly. Figure 2.4 illustrates the input, predicted, and output signals using the linear predictor.

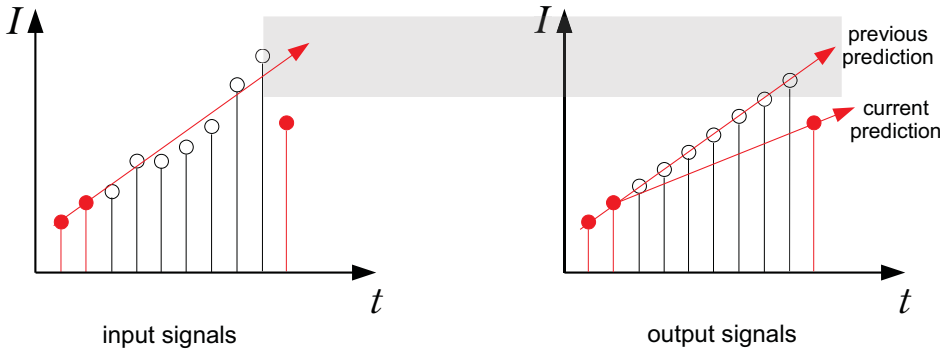

Figure 2.4: Principle of linear prediction. The red values are transmitted and used to predict the current haptic value. If the predicted value differs by more than the JND from the actual value, a new value is transmitted and the predictor is updated.

Compared to the ZOH method, this linear predictor can lead to a lower packet rate with comparable subjective quality. The velocity signal approximation used in the prediction model, however, is very sensitive to noise. For real teleoperation systems, position updates are more critical than the force as the slave is controlled by the motion signals. Noised motion signals can quickly lead to noticeable position drift as well as artifacts, limiting the usefulness of predictive coding on real teleoperation systems. Therefore, haptic samples need to be filtered such as using a scalar Kalman filter on the input signals [63]. An augmented version of the linear prediction method, which is more robust against noise, was introduced in [23] by employing the linear regression analysis. The transmitted data are the slopes and offsets of the predicted lines.

Typical higher order prediction approaches, such as the third-order autoregressive model and the quadratic curve-based prediction, can be found in [52, 53, 122]. After an initialization and training process, the coefficients are computed so that the predicted values are produced. Instead of sending haptic signals directly, the coefficients of the prediction model calculated in real time are transmitted.

2.2.1.5 Passivity of the PD Approaches

The PD approaches irregularly downsample the signals at the senders and interpolate the received signal samples to a high sampling rate that is required for the local control loop. Note that if the signals are reconstructed by a simple ZOH strategy, the PD approach is not passive in general [67]. The authors of [65, 145] proposed a passive PD approach by modifying the reconstructed signal to guarantee system passivity when using the ZOH reconstruction strategy.

Figure 2.5 illustrates the PD approach with the passive ZOH reconstruction strategy. Assuming that from the time t^* to t there is no packet arrived due to the deadband data reduction, the reconstructed force and velocity signals on the master and slave sides are

$$\begin{aligned} f_m(t) &= f_m^{recv}(t^*) + sign(v_m)\Delta_v \\ v_s(t) &= v_s^{recv}(t^*) - sign(f_s)\Delta_f \end{aligned} \tag{2.3}$$

where Δ_v and Δ_f represent the deadband zone with regard to the current velocity and force signals. This method reconstructs the velocity and force values either at the lower or the upper bound of the deadband zone such that passivity is preserved. It can also be used for ensuring the passivity of the PD approaches with predictive coding.

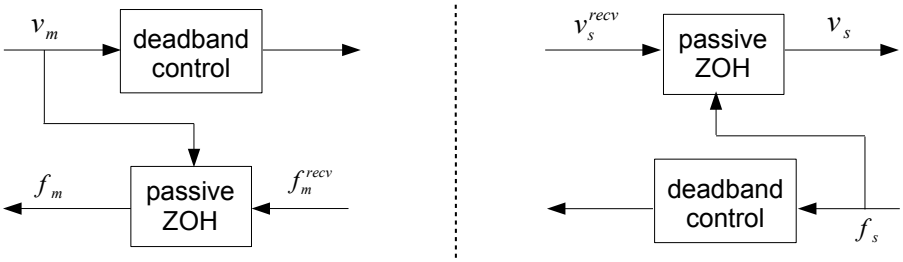

Figure 2.5: PD approach with passive ZOH reconstruction strategy (adapted from [65]).

2.2.2 Passivity-based Control Schemes

Passivity is a powerful and widely used tool for the analysis of system stability for teleoperation systems [16, 105, 120]. It provides a sufficient condition for the input/output stability. A teleoperation system can be represented by a cascade of two one-port subsystems (human

operator and environment, part 1 and part 3 in Fig. 2.1) and one two-port subsystem (data communication over the network, part 2 in Fig. 2.1). A one-port system has only one pair of terminal with an input and an output, while a two-port system has two pairs of terminals with an input port and an output port to connect to external systems (see Fig. 2.6).

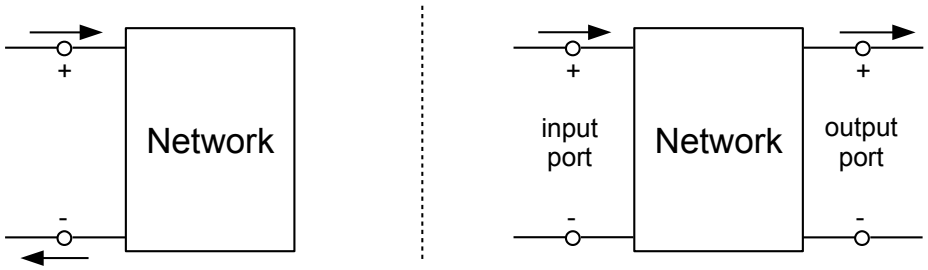

Figure 2.6: Illustration of a one-port system (left) and a two-port system (right).

System passivity characterizes the energy exchange in and between these subsystems. The human and the environment are considered to always behave in a passive manner. Thus, passivity-based control schemes need to guarantee the passivity of the two-port subsystem for haptic data communication.

2.2.2.1 Passivity of the Two-port System

Intuitively, a system is passive if it absorbs more energy than it produces. The communication network can be considered as an equivalent two-port system. The master and slave velocity vector $\mathbf{u} = (\dot{x}_m, -\dot{x}_s)$ are the inputs, and the master and slave force vector $\mathbf{y} = (\dot{f}_m, \dot{f}_s)$ are the outputs. Passivity condition requires a non-negative net energy balance at any time instant (assuming zero initial energy). For continuous-time systems at time instant t, the passivity condition is

$$E(t) = \int_0^t \mathbf{u}^T(\tau) \cdot \mathbf{y}(\tau) d\tau \geq 0 \tag{2.4}$$

For discrete-time systems at the n^{th} sampling instant $t = nT$, the passivity condition is

$$E(n) = \sum_{k=0}^{n} \mathbf{u}^T(k) \cdot \mathbf{y}(k) \geq 0 \tag{2.5}$$

Note that a positive energy balance indicates that the two-port system, which either stores or dissipates energy, is passive. A negative energy balance, in turn, indicates an active system which can general energy.

2.2.2.2 Wave-variable Transformation

The wave-variable (WV) transformation [105], also referred to as the scattering transformation [16], guarantees passivity of the global haptic control loop of a teleoperation system

under the assumption of arbitrarily large, but constant time delay (can be unknown) in the communication channel. The wave variable control architecture is illustrated in Fig. 2.7. The wave variables u_l, u_r, v_l and v_r are linear combinations of the force and velocity signals:

$$\begin{aligned} u_l &= \tfrac{1}{\sqrt{2b}}(f_m + b\dot{x}_m), \quad u_r = \tfrac{1}{\sqrt{2b}}(f_s + b\dot{x}_s), \\ v_l &= \tfrac{1}{\sqrt{2b}}(f_m - b\dot{x}_m), \quad v_r = \tfrac{1}{\sqrt{2b}}(f_s - b\dot{x}_s), \end{aligned} \tag{2.6}$$

where b is a scalar constant denoting the wave impedance. It describes the damping character of the transmitted wave variables. A larger value of b enables a higher interaction stiffness during contact. However, it adds an additional inertia in free space motion. A smaller value of b, in turn, enables a free space motion with lower inertia, while the contact stiffness becomes also lower [66].

Instead of the power variables (velocity and forces), the wave variables u_l (forward path) and u_r (backward path) are transmitted over the two-port network. They arrive at the corresponding receiver (v_r and v_l) with time delays T_1 and T_2.

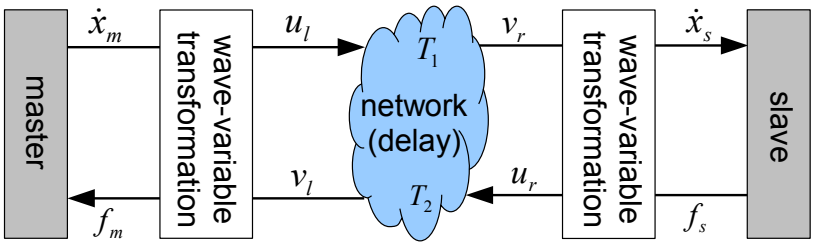

Figure 2.7: Overview of the wave-variable transformation for time-delayed teleoperation.

Assuming zero initial energy storage $E(0) = 0$, the net energy balance in the wave domain can be computed as [105]

$$E_{wv}(t) = \int_0^t (\dot{x}_m f_m - \dot{x}_s f_s)d\tau = \frac{1}{2}\int_0^t (u_l^2 - u_r^2) + (v_r^2 - v_l^2)d\tau = \frac{1}{2}\int_{t-T_1}^t u_l^2 d\tau + \frac{1}{2}\int_{t-T_2}^t v_r^2 d\tau \geq 0 \tag{2.7}$$

Hence, the communication of the haptic information including the wave variables transformation over the network is passive.

The WV method has been extended also for time-varying delay [98], in which case, however, the knowledge of the change rate of the delay is required.

The WV transformation control scheme is a conservative control design and leads to distortions in the displayed environment properties. Hard objects are displayed softer as they actually are and an increased inertia is displayed during free-space motion [66]. Comprehensive surveys of the WV transformation control schemes can be found in [73].

2.2.2.3 Time-domain Passivity Approach

The time-domain passivity approach (TDPA) is another passivity-based control architecture. Stability of TDPA-based teleoperation systems is guaranteed in the presence of arbitrary communication delays with the help of passivity observers (PO) and passivity controllers (PC). The concept of TDPA was first presented in [59] for haptic interaction with virtual environments. It was later extended for teleoperation systems using the position-position architecture [18, 119] and the position-force architecture [120]. The TDPA is able to deal with time-varying delays and packet loss without explicit knowledge about the network characteristics.

The structure of the original TDPA [120] can be observed in Fig. 2.8. The POs compute the current system energy. The PCs adaptively adjust the damping α and β to dissipate energy and thus guarantee the net energy balance to be non-negative.

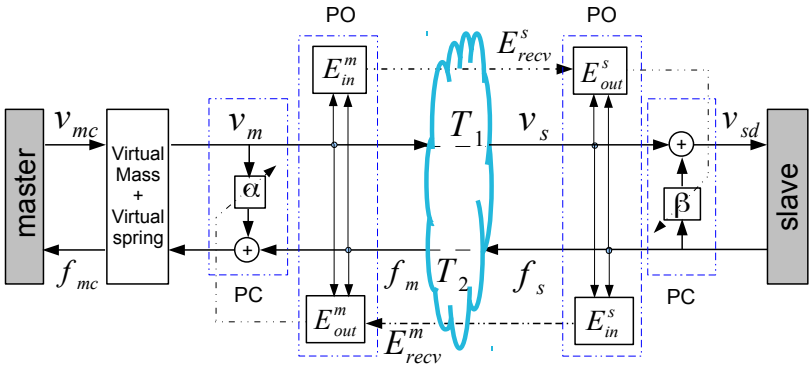

Figure 2.8: A time-delayed teleoperation system with the TDPA and the virtual mass-spring filter (adopted from [120]).

The TDPA separates the net energy balance into the input energy E_{in} and the output energy E_{out}. The passivity condition requires $E_{in}(k) \geq E_{out}(k)$ at any sampling instant k (system initial energy is assumed to be zero). With the assumption that the sampling rate on the velocity and force signal is substantially faster than the dynamics of the system, input and output energy flows on both the master and slave sides are further divided into the master-side energy $E^m_{in}(k)$ and $E^m_{out}(k)$, and the slave-side energy $E^s_{in}(k)$ and $E^s_{out}(k)$. The computation of all the energy flows presented in [120] proceeds as follows:

$$E^m_{in}(k) = \begin{cases} E^m_{in}(k-1) + \Delta E^m(k), & \text{if } \Delta E^m(k) > 0 \\ E^m_{in}(k-1), & \text{else} \end{cases} \tag{2.8}$$

$$E^m_{out}(k) = \begin{cases} E^m_{out}(k-1) - \Delta E^m(k), & \text{if } \Delta E^m(k) < 0 \\ E^m_{out}(k-1), & \text{else} \end{cases} \tag{2.9}$$

$$E^s_{in}(k) = \begin{cases} E^s_{in}(k-1) + \Delta E^s(k), & \text{if } \Delta E^s(k) > 0 \\ E^s_{in}(k-1), & \text{else} \end{cases} \tag{2.10}$$

$$E^s_{out}(k) = \begin{cases} E^s_{out}(k-1) - \Delta E^s(k), & \text{if } \Delta E^s(k) < 0 \\ E^s_{out}(k-1), & \text{else} \end{cases} \tag{2.11}$$

where $\Delta E^m(k) = v_m(k) f_m(k) \Delta T$ and $\Delta E^m(k) = v_s(k) f_s(k) \Delta T$ are the energy changes on the master and slave sides during the k^{th} sampling period. ΔT is the sampling time. f_m and v_m denote the force and velocity signal on the master side, and f_s and v_s are the force and velocity signal on the slave side.

All four energy values computed with (2.8)-(2.11) are positive and monotonically increasing. The passivity condition

$$E_{in} = E^m_{in}(k) + E^s_{in}(k) \geq E^m_{out}(k) + E^s_{out}(k) = E_{out} \tag{2.12}$$

can be guaranteed by satisfying a sufficient and more conservative condition [120]:

$$E^m_{in}(k) \geq E^s_{out}(k), \text{ and } \quad E^s_{in}(k) \geq E^m_{out}(k) \tag{2.13}$$

Note that $E^m_{in}(k)$ and $E^m_{out}(k)$ are computed on the master side, and $E^s_{in}(k)$ and E^s_{out} are computed on the slave side. In order to examine the system passivity according to (2.13), $E^m_{in}(k)$ must be sent to the slave side, and $E^s_{in}(k)$ must be sent to the master side. Due to the communication delay, the received E^m_{in} on the slave side and the received E^s_{in} on the master side at the sampling instant k are $E^m_{in}(k - T_1(k))$ and $E^s_{in}(k - T_2(k))$, where $T_1(k)$ and $T_2(k)$ denote the forward and backward communication delays at sampling instant k. Thanks to the monotonic increase of the input/output energy, it is sufficient to satisfy (2.14) in order to satisfy (2.13):

$$\begin{aligned} E^m_{in}(k) &\geq E^m_{in}(k - T_1(k)) = E^s_{recv}(k) \geq E^s_{out}(k) \\ E^s_{in}(k) &\geq E^s_{in}(k - T_2(k)) = E^m_{recv}(k) \geq E^m_{out}(k) \end{aligned} \tag{2.14}$$

where $E^m_{recv}(k)$ and $E^s_{recv}(k)$ are the currently received input energies on the master and slave sides, respectively. According to (2.13) and (2.14), the system is passive if $E^{m/s}_{recv}(k) \geq E^{m/s}_{out}(k)$.

If the passivity condition is satisfied, the received velocity or force signal is directly applied. If not, the PC is activated and the adaptive dampers α and β are computed to dissipate output energy:

$$\alpha(k) = \begin{cases} 0, & \text{if } E^m_{recv}(k) \geq E^m_{out}(k) \\ \frac{E^m_{out}(k) - E^m_{recv}(k)}{\Delta T v^2_m(k)}, & \text{eles, if} |v_m(k)| > 0 \end{cases} \tag{2.15}$$

$$\beta(k) = \begin{cases} 0, & \text{if } E^s_{recv}(k) \geq E^s_{out}(k) \\ \frac{E^s_{out}(k) - E^s_{recv}(k)}{\Delta T f^2_s(k)}, & \text{eles, if} |f_s(k)| > 0 \end{cases} \tag{2.16}$$

Note that the dissipated energy should be deducted from the corresponding $E_{out}^{m/s}$, if the PC is activated.

Similar to the WV approach, the TDPA also distorts the displayed environment impedance. Compared to the WV approach, the TDPA does not introduce additional inertia into the system for free space motion. On the other hand, it can lead to sudden force changes when the PCs are activated to dissipate the system output energy. This effect becomes stronger with increasing communication delays [120].

2.2.3 Joint Data Reduction and Control Solutions

The haptic data reduction approaches and control schemes mentioned in Sec. 2.2.1 and Sec. 2.2.2 have been initially developed independently to address the two challenges of haptic communication for teleoperation systems (reduction of haptic packet rate and ensuring system stability). Considering realistic network conditions, the haptic data reduction approaches have to be combined with stability-ensuring control schemes.

The first joint solution combined the WV control scheme with the PD approach [68]. This method applied the PD approach directly on the wave variables after the WV transformation. The transmission of the wave variables depended on their absolute and relative changes. For an interaction with a rigid wall in the presence of a 100 ms round-trip communication delay, the authors experimentally found that the absolute PD approach led to an average data reduction of 97%, while the relative PD approach led to an average data reduction of 93%. Since researches on human perception for the wave variables were not available from the literature, further analysis on the experimental results was left for future work.

The combination of the WV scheme and the PD approach was later extended in [145]. The PD approach was applied directly in the time domain (i.e., on the force and velocity signals, namely power variables). If the communication delay is known and constant, the transmission of the wave variables becomes equivalent to the transmission of the power variables with the help of communication buffers. In addition, the haptic data reduction and reconstruction scheme was extended in a passivity-guaranteed procedure. Compared to the method presented in [68], the extended method proposed in [145] achieved improved system transparency and more efficient haptic data reduction.

The above mentioned joint solutions are applicable only for constant delays. This is their main drawback, since delay variation is a non-negligible characteristic for realistic networks such as the Internet. Combining the PD approach with the extended WV architecture [98] which is able to deal with time-varying delays can be a potential solution. However, the change rate of the delay must be known, as it is one of the parameters for computing the passivity condition. This requires online parameter estimation on the communication network. Considering potential packet loss in the network and the irregular packet transmission

obtained when using the PD approach for data reduction, a precise online estimation becomes challenging. For these reasons, a simpler and more flexible system structure for haptic data reduction in delayed teleoperation systems is required.

To overcome the limitations mentioned above, the combination of the PD approach and the TDPA is presented and analyzed in Chapter 3 of this thesis. This method achieves comparable data reduction compared to the methods presented in [68, 145], while robustly dealing with time-varying delays without explicitly knowing the network characteristics. It also achieves less conservative control and improves teleoperation quality. Table 2.3 compares the method proposed in Chapter 3 with the methods from literature.

	Network characteristic	Passivity	Data reduction
[68] (PD+WV)	unknown constant delay	Yes	wave variables
[145] (PD+WV)	known and constant delay	Yes	power variables
Chapter 3 (PD+TDPA)	time-varying delay, packet loss	Yes (less conservative)	power variables

Table 2.3: A comparison of the existing haptic data reduction approaches for time-delayed teleoperation with the presented approaches in this thesis.

2.3 Model-mediated teleoperation

The conventional teleoperation architectures, which exchange velocity and force signals over the network, have very strong restrictions on the communication delay of the sampled data, resulting in high packet rates and necessitating the use of stability-ensuring control schemes (e.g. the passivity-based control schemes). One of the main issues of the passivity-based control schemes developed for conventional teleoperation architectures is that system passivity and transparency are conflicting objectives [90]. This means that the system gains stability at the cost of degraded transparency [16, 34, 66, 78, 105]. For example, hard objects are displayed softer as they actually are, and this effect becomes stronger with increased communication delay [66]. This leads to a degradation of the teleoperation quality. Thus, to develop new teleoperation architectures which simultaneously guarantee system stability and achieve high system transparency is imperative.

Model-mediated teleoperation (MMT) has been proposed to address both stability and transparency issues in the presence of communication delays [58, 103, 148] and packet loss [44]. In the MMT approach, a local object model is employed on the master side to approximate the slave environment. The model parameters describing the object in the slave environment are continuously estimated in real time and transmitted back to the master whenever the slave obtains a new model. On the master side, the local model is reconstructed or updated on

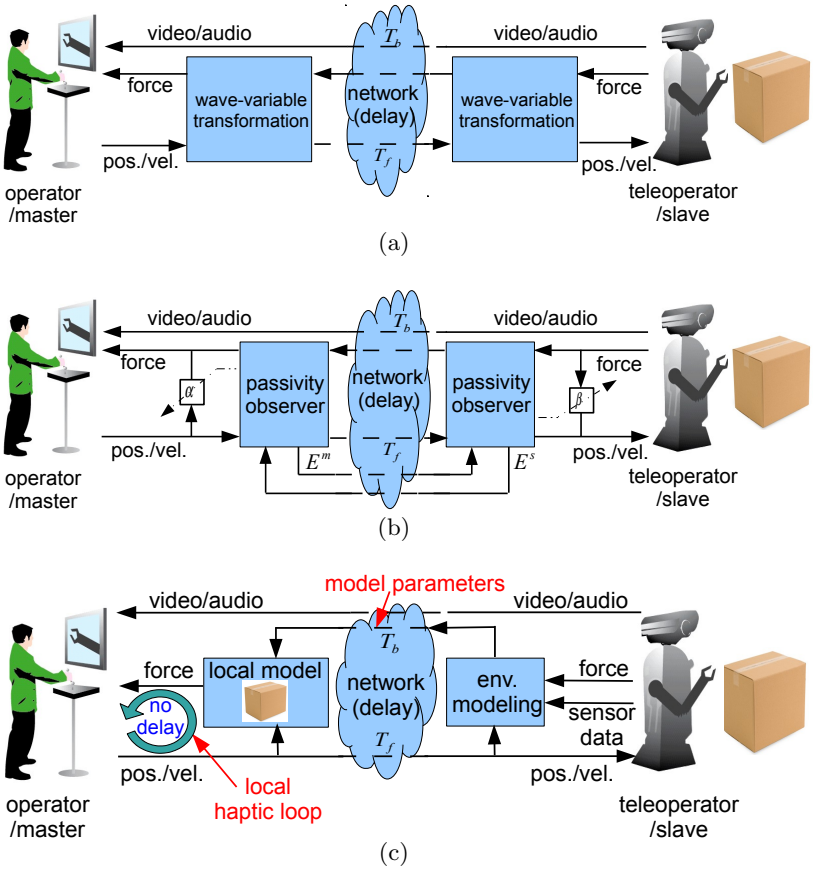

Figure 2.9: (a) Passivity-based teleoperation using the wave-variable transformation. (b) Passivity-based teleoperation using the time-domain passivity approach. For (a) and (b), the velocity and force signals are modified to guarantee system passivity. (c) A state-of-the-art model-mediated teleoperation architecture. The use of the local model enables non-delayed haptic rendering thus guaranteeing system stability.

the basis of the received model parameters, and the haptic feedback is computed on the basis of the local model without noticeable delay (see Fig. 2.9(c)). If the estimated model is an accurate approximation of the remote environment, both stable and transparent teleoperation can be achieved [103, 111, 112].

Figure 2.9(c) shows a comparison between the conventional passivity-based teleoperation architectures (the WV method and the TDPA, Fig. 2.9(a) and 2.9(b)) and the MMT architecture (Fig. 2.9(c)). In the passivity-based architectures, the control blocks (wave-variable transformation or passivity observer) ensure system passivity by dissipating system output energy by modifying the corresponding velocity and force signals. Additionally, in the TDPA architecture, the computed system energy needs to be exchanged between the master and slave. Compared to the passivity-based architectures, the MMT approach requires neither a modification of the velocity and force signals nor the exchange of information about the system energy. MMT systems do not send the delayed force signals back to the master. In-

stead, they generate non-delayed force feedback based on a local model on the master side which is an approximation of the remote environment. Continuously updating the already accurately estimated model parameters is not necessary. For static or slowly varying environments, there is also no need to update the model parameters at a high rate. Hence, MMT systems in general do not require high packet rate in the backward channel.

The authors of [17] compared 10 different control schemes including the passivity-based control and predictive control (an early version of MMT) in terms of their stability region, position and force tracking performance, displayed impedance, position drift, etc. For the passivity-based architectures, balancing system conservatism (amount of dissipated energy) and system passivity is one of the main challenges for achieving high system transparency [90, 154]. For the MMT architecture, the challenges are quite different from the passivity-based architectures. In general, an MMT system requires a fast and accurate environment modeling method. In addition, data communication, local model updating, and stable slave controlling are also important challenges for MMT. The number of studies on MMT and MMT-relevant challenges has rapidly increased in recent years due to the benefits of MMT in terms of system stability and transparency. In the following subsections, we briefly review the development of MMT and discuss the challenges MMT-based teleoperation faces.

2.3.1 Historical Development of MMT

MMT has been studied by a great number of researchers since the late 1980s. Different names have been suggested for the general concept of MMT. Among them, the most frequently used ones are adaptive impedance-reflecting teleoperation [58, 97, 140–142], model-based teleoperation [85, 155], model predictive/prediction-based teleoperation [30, 74, 104, 127, 131, 132], virtual-reality-based teleoperation[106], and MMT [103, 130, 143, 148].

2.3.1.1 Origins

The key idea of MMT is to use a predicted environment model on the master side to locally provide a stable and non-delayed force feedback. The idea of environment prediction can be traced back to 1957, the year that the Smith Predictor was developed to eliminate the potential instability caused by delayed feedback signals [133]. This method, named after its inventor Otto J. M. Smith, however, was not proposed for teleoperation systems but for stabilizing a general feedback control system in the presence of time delay.

The use of prediction of the remote environment for teleoperation systems originated in the late 1980s. At that time, the so-called predictive display approach was developed to visually compensate for the communication delay [20, 21]. In [21], a computer graphics model of the slave arm was overlayed on real video images. This allowed the OP to locally view the motion of the slave robot before it actually moved and, hence, to avoid possible collisions.

An extension of this idea in [25] additionally provides the user with a photorealistic view on the remote slave using three-dimensional (3D) environment reconstruction in combination with texture-mapping. A predictive display with force feedback for teleoperation systems was presented in [85] by Kotoku. The force signals were generated based on a predefined spring-damper model.

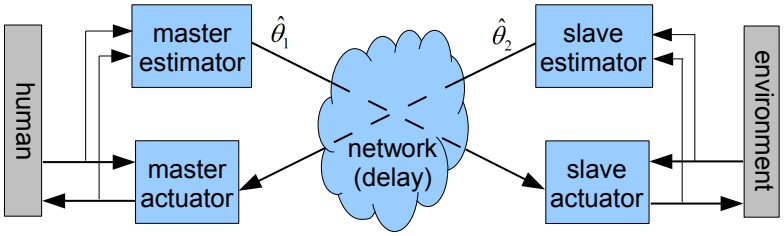

Figure 2.10: First prototype of the MMT control architecture. The exchanged parameters $\hat{\theta}_{1,2}$ contain the effort (force/torque) and impedance on both the master and slave sides (adapted from [58]).

In 1989, Hannaford [58] proposed an online environment estimation scheme for teleoperation systems, called bilateral impedance control. This concept of using an online estimated environment model to provide non-delayed force feedback signals is very similar to the state-of-the-art MMT approach. Hence, we consider the structure proposed in [58] to be the first prototype of MMT. The online estimation algorithm focused on estimating the impedance of the OP and the environment (H-matrix). As illustrated in Fig. 2.10, the estimator calculates the applied force/torque and the equivalent impedance at the OP port and the environment port and transmits the estimates $\hat{\theta}_{1,2}$ to the other side for position/force tracking. It was proved that if the estimates of the environment model approach their actual quantities, and if the actuator is able to represent a large impedance, then the teleoperation system can be fully transparent in the presence of communication delay.

2.3.1.2 Smith Predictor-based predictive control

From the early 2000s, predictive control was studied for stabilizing teleoperation systems with time delays [14, 15, 47, 74, 127, 131, 132], wherein the most typical system structure was based on the Smith Predictor.

The Smith Predictor [133] was originally designed to stabilize a linear time-invariant (LTI) system in the presence of time delays. As illustrated in Fig. 2.11(a), the transfer function of the example system is

$$\frac{Y}{X} = \frac{G_1 G_2 e^{-sT}}{1 + G_1 G_2 e^{-2sT}} \tag{2.17}$$

The delay term e^{-2sT} in the denominator indicates potential instability. The use of the Smith Predictor in Fig. 2.11(b) leads to a modified transfer function:

$$\frac{Y}{X} = \frac{\hat{G}G_2e^{-sT}}{1+\hat{G}G_2e^{-2sT}} \tag{2.18}$$

where $\hat{G} = \frac{G_1}{1+G_1\hat{G}_2(1-e^{2sT})}$. If $\hat{G}_2$ is an accurate prediction of G_2 ($\hat{G}_2 = G_2$), the transfer function of Fig. 2.11(b) becomes

$$\frac{Y}{X} = \frac{G_1G_2e^{-sT}}{1+G_1G_2} \tag{2.19}$$

which ensures a stable system if G_1 and G_2 are stable. Obviously, the Smith Predictor can eliminate the potential instability caused by the delayed feedback signal.

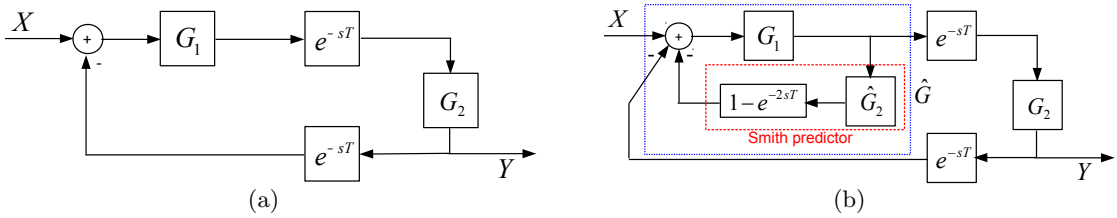

Figure 2.11: (a) An example system block diagram with delays. (b) The use of the Smith predictor to compensate for the delays (adapted from [133]).

Based on the Smith Predictor, Huang and Lewis proposed a recurrent neural network (RNN)-based predictive control scheme for a position-position teleoperation architecture [74]. The authors employed a predefined linear time-invariant (LTI) model to approximate the non-linear behavior of the slave-environment system. A linear system/model in this context means that a linear relationship exists between the inputs and outputs. A widely-used linear model is the Kelvin-Voigt model [42, 56].

The assumption of an invariant linear part in the slave-environment non-linear behavior limits the system capacity for dealing with time-varying slave-environment behavior, since the linear predictor on the master side is predefined and not updated in real time. However, for teleoperation with rich knowledge about the remote environments (e.g., pre-scanning and available history data for the current environment), a precisely predefined environment model can also provide stable haptic interaction without the need for parameter estimation. The idea of using predefined models has been adopted for many applications, such as predictive aid in teleoperation systems [27, 85], in-orbit space robot teleoperation [155], and MMT systems with a pre-scan process [157]. The use of predefined models in MMT systems shows some level of improved stability in the presence of communication delay, and also robustness against small modeling errors [155].

A consequence of using a predefined model is obviously the potential modeling error. This error originates from the difficulty of modeling complex environments and the limited resolution of the sensor measurements. In practice, there are situations in which we have limited knowledge about the remote environment, especially when the slave enters a new environment or interacts with dynamic (movable or deformable) objects. Therefore, online environment modeling and model updating are inevitable. This requires the slave system to be able to extract the environment geometry and impedance in real time. The geometry represents the position and shape of the object model, while the impedance describes the physical properties of the environment model, including mass/inertia, stiffness/compliance, damping, friction, etc.

The authors of [14, 15] discussed Smith predictor-based predictive control structures which allowed for an online environment modeling method. Fite et al. proposed a model-based prediction approach in [47] to enable a teleoperation system to deal with a time-varying environment. The environment is assumed to be a linear spring model, and the model parameter (stiffness) is continuously estimated and updated online on both the master and slave sides. In [131, 132], a neural network (NN)-based prediction scheme for dealing with both non-linear and time-varying environments has been developed. As illustrated in Fig. 2.12(a), the NN estimator is trained online to model the environment input-output dynamics. The trained weights of the NN estimator $\mathbf{W}_{ji}$ are transmitted back to the master to update the local NN model. If the estimation is accurate, the estimated force $\hat{f}_e$ on the master side with the delay term $e^{-s(T_f+T_b)}$ is able to cancel the received (and delayed) slave contact force f_e. Note that although the transmitted weights are delayed, they converge to stable values and have minimal changes after the initial learning period is passed.

This scheme retains the original structure of the Smith Predictor. The communication delay, however, must be known to eliminate the effect of the delayed force signal on the master side. In addition, imprecise modeling of the environment leads to incomplete cancellation of the contact force from the slave side, and results in potential contact oscillation and control difficulties. Alfi et al. proposed a modified structure in [15] to improve system robustness against uncertainties of time delay and model parameters. In the presence of measurement errors in time delay and model parameters, simulation results showed good performance of their method in motion and force tracking. To completely avoid these issues, the authors of [131, 132] presented a zero-feedback NN-based predictive control scheme, where the slave force is no longer sent back to the master (Fig. 2.12(b)). The force signal on the master side is only computed based on the local NN-model. Thus, knowing the communication delay is not required. Improvements on system performance while using the zero-feedback structure are shown in [131, 132]. However, the system stability of this control architecture highly depends on the accuracy of the environment model and the employed schemes for model update on

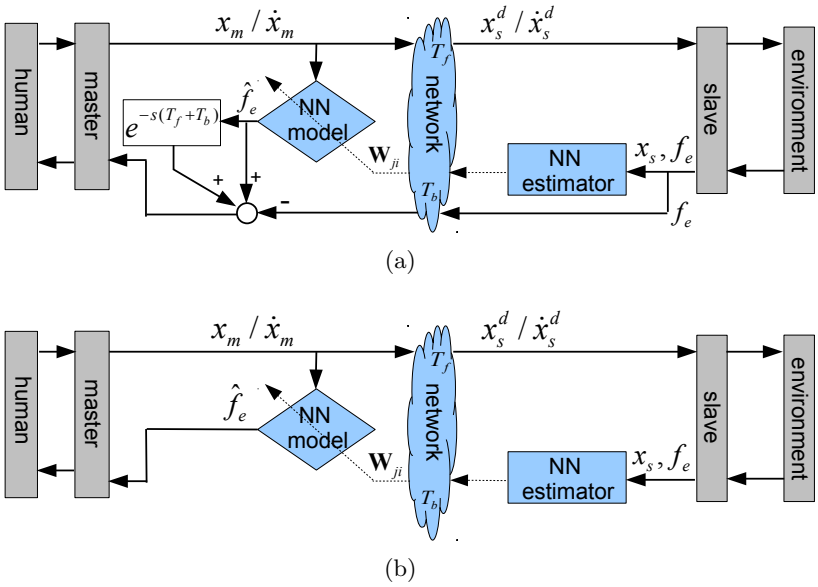

Figure 2.12: (a) Predictive control architecture using a Smith Predictor for a position-force teleoperation system with the force feedback term. (b) Predictive control architecture using a Smith Predictor for a position-force teleoperation system without force feedback term.

the master side.

The capability of dealing with nonlinear and varying environments in the presence of unknown communication delay enables the zero-feedback predictive control scheme to serve as a benchmark for studies of the MMT approach. In fact, the general structure in Fig. 2.12(b) is conceptually identical to the state-of-the-art MMT architecture illustrated in Fig. 2.9(c). We use the architecture illustrated in Fig. 2.9(c) to represent an MMT system in this thesis, if no further specification is made.

2.3.1.3 MMT in complex environments

The Smith Predictor-based studies on MMT introduced in Sec. 2.3.1.2 mainly focus on 1D environments without modeling the environment geometry. From the year 2000 onward, studies on MMT have turned to the matter of efficiently modeling complex environments, including their impedance and geometry in 3D space, and how to stably update the local model on the master side and stably control the slave system when the local model and the environment do not match. In fact, model mismatch can lead to a mismatch in position tracking on the slave side, resulting in dangerous slave behavior such as undesirably deep penetration into an object or improperly large forces acting on the environment.

Mitra and Niemeyer were the first to use the name MMT in [103] to indicate an alternative type of information exchange between the master and slave. Different from the conventional teleoperation architecture wherein the force signals are transmitted in the backward channel,

MMT systems send the estimated model parameters back to the master. The authors also presented a qualitative analysis of the trade-off between the level of communication delay and the level of abstraction in control schemes. They suggested that the abstraction for control schemes should adapt to the communication delay in order to maintain successful teleoperation. As illustrated in Fig. 2.13, the MMT approach, according to this analysis, is able to deal with relatively larger communication delays. The relatively lower update rate of MMT implies that the MMT approach is unsuitable for quickly changing environments, since frequent updating of the model parameters could lead to stability issues. In [103], a constrained model update scheme on the master side and a position-force-switching control scheme on the slave side are proposed to avoid instability when the slave is first establishing an environment model or a model update is needed. A general discussion of the system stability of MMT can be found in [149].

For MMT with an unknown environment geometry, Tzafestas et al. in [141], Verscheure et al. in [144], and Xu et al. in [7] proposed online estimation algorithms for 1D, 2D, and 3D environment models, respectively. These algorithms use the position and force signals measured on the slave side to estimate the environment geometry and impedance. The geometry and impedance parameters, however, can be estimated only after the slave's first contact with the environment.

Using additional sensors, e.g., a laser range finder for a 1D environment [104], a stereo camera for a 2D environment [148], or a time-of-flight camera for a 3D environment [1, 6], the environment geometry can be estimated even prior to contact. Prior knowledge of the environment geometry minimizes the modeling error at the time of the slave's first contact with the environment, and improves system stability when the slave establishes a hard contact with rigid objects.

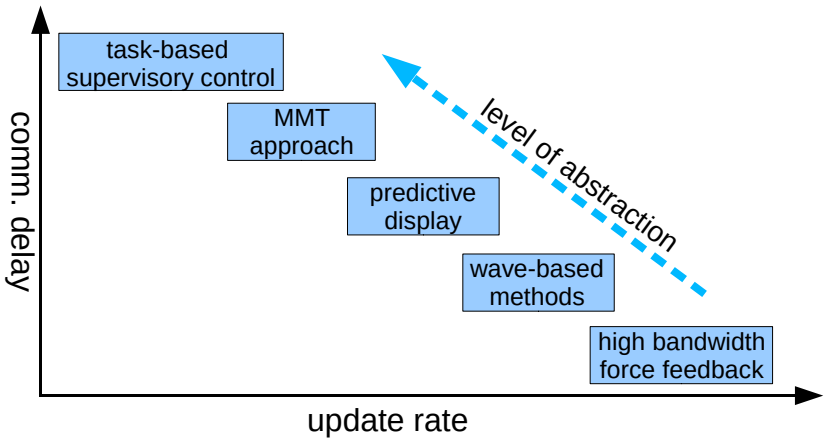

Figure 2.13: The level of abstraction and data complexity with update rates and robustness to delays (adapted from [103]).

2.3.2 Challenges of MMT

After more than 25 years of development from the first MMT prototype to present, some challenges of MMT have already been intensively studied, while others are still lacking solutions. The main challenges facing MMT techniques are summarized in the following.

2.3.2.1 Environment Modeling

Environment modeling is the foremost challenge in MMT, since a perfect match between the local model and the environment enables stable teleoperation in the presence of arbitrary communication delays. If the models of the master and the slave environment are mismatched (which happens normally due to environment changes, improper model approximation, or inefficient parameter estimation methods), a model update on the master side is required. According to whether the local model matches the remote environment, the following two states for MMT are defined:

- **Steady state:** The estimated model parameters have converged to the actual quantities, and the local model on the master side matches the environment. Model updates in this state are not required. For an efficient MMT system, the teleoperation system should be in steady state as often and as long as possible.
- **Transition state**: Due to environment changes or inaccurate environment estimation, a model mismatch between the local model and the actual environment can occur. In this case, the local model needs to be updated as quickly as possible. Transition states occur irregularly during teleoperation.

Modeling methods

The task of environment modeling is to identify the input-output response of the slave-environment system. Depending on whether environment models are known or not, the identification can be divided into parametric and non-parametric methods, respectively.

In parametric methods, an environment model is assumed based on certain pre-knowledge or previously available information. The identification involves the estimation of the model parameters including the geometry and the physical properties in real time. This is referred to as *online parameter estimation* or *online contact dynamics identification*. Studies focused on modeling objects with known geometry [37, 55, 97] and with unknown geometry but simple (e.g. planar surface) environment [92, 144, 7]. Studies also focus on modeling soft/deformable objects without surface friction [12] (no tangential motion on the object surface) .

For non-parametric methods, no assumption is made for the environment models, and the aim of the identification is to directly estimate a linear or non-linear input-output mapping for the slave-environment system. To this end, online neural network approaches [74, 131, 132]

have been proposed for modeling simple environments. The main challenges of using the NN-based estimation method are the reciprocal relationships among the computational complexity, estimation accuracy, and convergence rate. Online NN-based estimation works only for a limited number of hidden layers and neurons. This limitation degrades the estimation accuracy for complex environments.

The point cloud-based MMT (pcbMMT) system presented in Sec. 4.1 of this thesis extends the MMT approach to deal with arbitrarily complex and unknown 3D environment geometries. In addition, the radial function-based deformation (RFBD) method presented in Sec. 4.2 of this thesis enables an online modeling of 3D deformation objects with frictional contact on the object surface. Please refer to Table 2.4 for a comparison of the related literature and this work.

	[148]	[7]	[12]	Sec. 4.1 and 4.2
Geometry	2D plane	3D plane/sphere	-	3D point cloud
Dynamics	rigid	rigid	3D deformable (no friction)	3D deformable (frictional contact)

Table 2.4: A comparison of the state-of-the-art environment modeling methods for MMT with the extensions presented in this thesis.

2.3.2.2 Efficient Data Communication

Attention must be also paid to data transmission over the communication network. First, network resources and transmission conditions limit the update rate of the model parameters. Second, the potential loss of the packets that contain environment parameter updates can introduce additional model mismatch. Both these increase the time period of the transition state and can lead to aggravated stability issues. Thus, it is necessary to design an efficient and reliable communication protocol for transmitting model parameters to achieve a stable MMT system.

Although the packet rate in the backward channel is not necessarily to be 1 kHz, excessive updating of model parameters also leads to high packet rate and increases communication load. Thus, packet rate reduction for MMT is also required. For the standard MMT structure as illustrated in Fig. 2.9(c), data transmission in the forward channel is the same as that for the conventional teleoperation structure. Thus, the packet rate in the forward channel can be reduced using the state-of-the-art PD approach. In the feedback channel, the transmission of the estimated model parameters can be reduced in the following two ways:

1. **Reduction of the estimation rate:** Model parameters are estimated only when necessary. For a slowly varying environment, there is no need to estimate the model

parameters at a high rate. For example, if we estimate the environment parameters every 100 ms, the packet rate is maximally 10 packets/s. However, a too low estimation rate slows down the estimation convergence and is not able to follow the change of the environment, even though the change is not frequent.

2. **Selected transmission:** This is to apply the PD approach to the estimated model parameters: not every estimate is transmitted, but only those for which the difference between the current estimate and the most recently sent estimate leads to a perceptual change at the OP larger than the JND given by Tab. 2.2. This scheme, in addition to the estimation rate reduction, can further reduce the packet rate in the network.

For the reduction of the estimation rate, a very simple way is to use a time-triggered approach. The model estimator is activated every T seconds, where T is a pre-defined estimation period. The maximum update rate (packet rate) is then $\frac{1}{T}$ packets/s. This method, however, has some drawbacks in following environment changes (e.g., stiffness change). In addition, a too large estimation period slows down the estimation convergence when the slave encounters a new environment. For the case when the slave is in contact with a static environment but stops moving, signals such as the position, velocity, and force are constant. These constant signals cannot provide persistent excitation for the parameter estimation, resulting in invalid estimates.

To overcome the drawbacks of the time-triggered estimation, Verscheure et al. proposed an event-triggered estimation approach in [144]. The activation of the model estimator is not based on time but is in accordance with the slave behavior and the measured data. For example, the estimation is activated only if the robot is moved, either in normal or tangential direction, beyond a threshold while remaining in contact. Robustness of the estimation can be increased by using the event-triggered estimation approach, since the persistent excitation condition can be fulfilled. In addition, the estimation algorithm will not be triggered with singular measurements such as zero velocity, thus avoiding meaningless estimation results.

The above two methods focus on the reduction of the estimation rate. On the other hand, the work presented in Sec. 4.3 of this thesis focuses on the second data reduction method: selected transmission. It adaptively selects and transmits the estimated model parameters which are sufficiently important for human perception. Thus, unnecessary transmission is avoided, and the packet rate reduction can be better achieved in the backward communication channel in the presence of noise and measurement errors. Table 2.5 summarizes the difference between the methods proposed in Chapter 4 and in [144].

	Reduction of the estimation rate	selected transmission
Event-triggered method [144]	yes	no
Sec. 4.3	yes	yes (perception-based)

Table 2.5: A comparison of the data reduction schemes for MMT.

2.3.2.3 Stability in the Transition State

Beside online model estimation and efficient data transmission, handling the stability issues in the transition state is another important challenge for MMT. An analysis of the MMT control block helps us to understand the concrete issues related to this challenge. First, the MMT structure that is illustrated in Fig. 2.9(c) is modified to the control block diagram in Fig. 2.14. The estimated environment parameters are denoted as $\hat{\theta}$.

Unlike the conventional teleoperation architecture, the MMT approach opens the control loop between the master and slave and leads to two decoupled control loops, one on the master and one on the slave side as illustrated in Fig. 2.14. The stability of the MMT system can be determined using the stability of the human-master local model closed loop (loop 1) and the slave-environment closed loop (loop 2), which has been discussed in [12, 111, 112]. During the transition state, the geometry and impedance of the local model could dramatically change, resulting in unstable haptic rendering in loop 1. Meanwhile, due to the model mismatch in the transition state, the master could use an improperly large force signal to command the slave or could command the slave to access an unreachable position, e.g., deep penetration of a rigid object. This could lead to the damage of both the slave robot and the objects in the remote environment. Thus, a stable haptic rendering (model updating) approach and a stable slave control scheme in the transition state are required. These are also important challenges for MMT.

Stable model update for the master loop

As discussed above, the local model on the master side needs to be updated if the slave detects a new model, or if there is a significant model mismatch between the local model

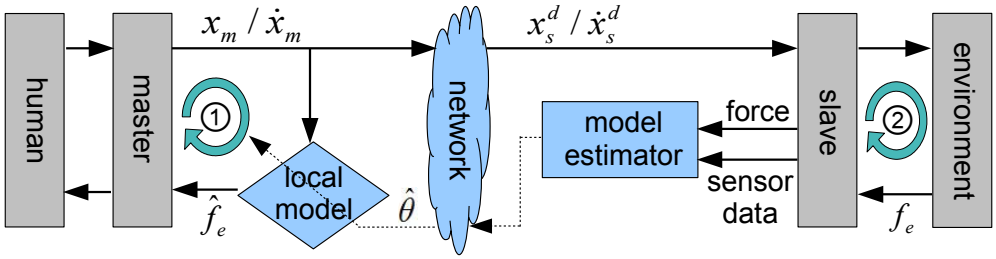

Figure 2.14: Overview of an MMT control architecture without force transmission in the backward channel.

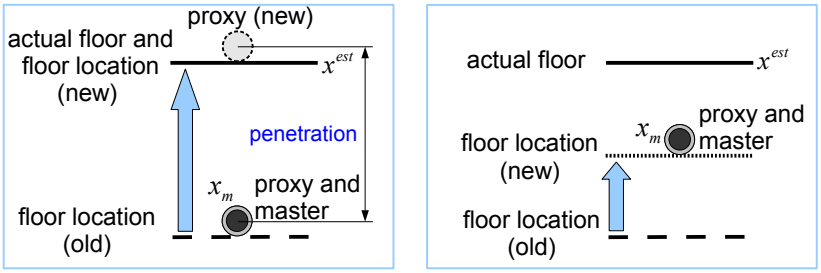

Figure 2.15: Two methods for updating object position. Left: direct updating leads to suddenly increased penetration and thus injects energy into the system. Right: gradual updating without injecting energy into the system. Adapted from [103].

and the environment. In this case, the slave triggers an update. The parameters of the local model are updated according to the received data. Improper update schemes, e.g., a sudden change in stiffness or model position, result in a suddenly changed force that is displayed to the human user. This is called the model-jump effect [149]. If the users cannot adjust their arm impedance quickly enough to follow (stabilize) this force change, an unexpected motion occurs, causing dangerous slave behavior. Therefore, smooth and stable model updating is required. Using the concept of passivity, stability during model updating can be ensured. The key point is to avoid energy injection into the system, or to ensure that the injected energy can be dissipated by system damping or friction.

Mitra and Niemeyer have proposed a constraint-based scheme for updating model position in 1D environment to avoid energy injection [103] (referred to as zero energy injection method). For this approach, any position updating that introduces energy injection will be delayed, unless the user's motion allows for a position update that will not introduce energy injection.

As illustrated in Fig. 2.15, the master is in contact with the current local model (a 1D floor), while a new floor position x^{est} is detected and transmitted to the master. If the position of the floor on the master side is immediately updated to the actual position x_{est}, the penetration is increased and energy is injected into the system. This leads to a suddenly increased contact force being displayed to the user.

The solution proposed in [103] is to constrain the master floor position x_m^f to be below the master position x_m:

$$x_m^f = \min\{x^{est}, x_m\} \tag{2.20}$$

This means that if the master proxy moves upward, the master floor moves accordingly, but always below the proxy position. If the master moves downward, the master floor keeps still to provide a rigid contact (Fig. 2.15). Until the master floor reaches its actual position (the estimated position), the system switches to the steady state.

Without actively injecting energy during model update on the master side, system passivity can be guaranteed. This approach, however, is designed only for position updating rather

than for impedance updating. Meanwhile, the updating period can be very long, since the updating process depends on the master's motion. Only when the master reaches the actual floor position can the entire update period be completed. Mitra et al. found that compared with some non-passive update approaches, e.g., gradually moving the master floor from the old location to the actual position at a fixed velocity, the user does not haptically prefer this passive updating scheme [102]. Therefore, further studies on the passivity-based model updating scheme are required.

In Sec. 4.4 of this thesis, a non-zero energy injection model updating scheme is presented. This approach allows for the updating of both impedance and geometry parameters in 3D environments, and can update the local model in a quicker and user-preferred way. Table 2.6 shows the main points of difference between these two approaches.

	[102, 149]	[103]	Sec. 4.4
Feature	gradual update (non-passive)	zero energy injecting (passive)	non-zero energy injecting (passive, less conservative)

Table 2.6: A comparison of the state-of-the-art model update methods for MMT with the approach presented in this thesis.

Stable motion control for the slave loop

Model mismatch can lead to a mismatch in position tracking on the slave side, resulting in dangerous slave behavior such as undesirably deep penetration into an object or improperly large force acting on the environment. The state-of-the-art transition-state slave control approaches for dealing with such issues are the switching position control/force control method [103, 148] and the relative tracking method [150]. Both methods guarantee stable and safe interaction between the slave and environment in the transition state.

2.3.2.4 Summary

According to the discussion above, the main challenges of MMT are summarized as follows.

1. A stable and quickly convergent parameter estimation method for a model that approximates the environment on the slave side, discussed in Sec. 2.3.2.1.

2. An efficient and reliable data transmission for model parameters over the network, discussed in Sec. 2.3.2.2.

3. A stable haptic rendering algorithm with changing model parameters on the master side and a stable slave control scheme during the period of model mismatch, discussed in Sec. 2.3.2.3.

All these challenges directly deal with the issues in transition states. However, this does not mean that the MMT system is absolutely stable in steady state without any constraints. In fact, the haptic rendering (loop 1 in Fig. 2.14) suffers from various stability issues in the steady state. For instance, stability of haptic rendering in the steady state is influenced by environment stiffness, damping, and sampling period [11, 32, 38, 99]. In addition, the slave-environment interaction (loop 2 in Fig. 2.14) in the steady state can also be unstable, especially when the slave establishes a hard contact [72, 96]. However, these stability problems in the steady state are not particular issues for MMT but general issues for teleoperation systems. As there have already been intensive studies on these issues for general teleoperation systems, most MMT-relevant researches only focus on the aforementioned three challenges particular to MMT systems. A summary of relevant studies on MMT is shown in the Appendix A.

Chapter 4 of this thesis presents a series of approaches to address the aforementioned challenges. These approaches extend MMT systems to deal with complex environment geometry and to interact with deformable objects including frictional contact. The work presented in Chapter 4 also provides an efficient data transmission method and a better solution to guarantee system stability during model update in the transition states.

2.4 Evaluation Methods

Methods for evaluating teleoperation quality are instrumental for the design of teleoperation systems. In the following, methods for evaluating the objective and subjective quality are briefly discussed.

2.4.1 Objective Quality

Objective quality typically focuses on the transparency of teleoperation systems. System transparency describes the accuracy with which a teleoperation system can display a remote environment to the human user. In the traditional sense, a teleoperation system is called transparent if the master and the slave position/force signals are perfectly matched [154], or if the environment impedance on the slave side and the displayed impedance on the master side are identical [90]. For the former definition, the slave behaves identical as the master. For the latter one, dynamics of the remote environment are exactly represented on the master side during teleoperation.

Ideal transparency is normally not achievable due to several factors, such as the influence of system dynamics, a limited amount of degrees of freedom, communication delay, insufficient sensor resolution, etc. Lawrence [90] has proposed a definition of impedance error Z_{error} to describe the difference between the displayed impedance Z_h and the environment impedance

Z_e over a certain frequency range:

$$Z_{error} = \frac{1}{\omega_{max} - \omega_{min}} \int_{\omega_{min}}^{\omega_{max}} |Z_{diff}(j\omega)| d\omega \tag{2.21}$$

with

$$Z_{diff}(j\omega) = |\log Z_h(j\omega)| - |\log Z_e(j\omega)| \tag{2.22}$$

The lower the value of Z_{error}, the higher is the degree of transparency.

2.4.2 Subjective Quality

By considering human factors, subjective quality reflects a subjective impression on the perceived teleoperation quality. A teleoperation system is called subjectively transparent if the user cannot distinguish the perceptions between a tele-interaction and a direct interaction with the same environment.

Due to several reasons, such as system noise, communication delay, and the use of haptic data reduction approaches, the displayed/perceived impedance cannot exactly match the environment impedance. Considering the limitations of human haptic perception, one of the major questions relates to the extent to which the displayed impedance can differ from the actual impedance such that the human user still perceives them to be the same. The concept of **perceived transparency** is introduced in [66] to take human perceptual limitations into account. A teleoperation system is perceived transparent if the displayed impedance lies within the range of the JND of the corresponding human perception:

$$Z_h(j\omega) \in [Z_e(j\omega) - \Delta Z_e(j\omega), Z_e(j\omega) + \Delta Z_e(j\omega)] \tag{2.23}$$

The JNDs for haptic stimuli are quite different for various physical properties. For example, the JND for forces is about 7% to 10% [81, 109], whereas the JND for stiffness is about 15% for soft contact and 23% for hard contact [82, 139]. Classical psychophysical techniques, such as the method of constant stimuli, the method of limits, the method of adjustment, the method of staircase, etc., are very useful to detect the JNDs of different haptic stimulus for various tasks. These methods can determine relative and absolute thresholds according to statistical assumptions on human behavior and based on sufficiently large amount of sample data from subjective experiments. A review of application of psychophysical techniques to haptic research was presented in [83].

Studies also investigate the overall subjective quality as a function of different parameters, such as communication delay, packet rate over the network, etc. In this case, post-test questionnaires containing different questions on the experienced quality of the displayed multimodal information can be adopted ([124, 152]). Subjective rating is usually used to evaluate the experienced quality. Table 2.7 illustrates the rating scheme for method of magnitude estimation that is used in several experiments in this thesis. It is able to evaluate the perceived

quality in the presence of distortion introduced by different parameter settings of teleoperation systems, comparing with the undisturbed signals.

In addition to the determination of perceptual threshold and the overall quality, statistical analysis methods (e.g. the T-test, the ANOVA, the Friedman test, etc.) are often applied to investigate statistical significance of the results among different experimental conditions, different parameter settings, or different subjects. A comprehensive overview of subjective presence measurements was presented in [76].

Table 2.7: Rating scheme for subjective evaluation.

Rating level	Description
5	no difference to the undisturbed signal (perfect)
4	slightly perceptible disturbing (high quality)
3	disturbed (low quality)
2	strongly disturbed (very low quality)
1	completely distorted (unacceptable)

2.5 Chapter Summary

Reduction of haptic packet rate and guaranty of system stability are the two main challenges for networked teleoperation systems in the presence of communication delay. This chapter has covered the background of current researches on individual and joint solutions to the two challenges, and outlined how the work presented in this thesis makes original contributions to address the two challenges.

For a conventional teleoperation structure which exchanges position/velocity and force signals over the communication channel, a combination of the PD approach and the WV control schemes has successfully addressed these challenges under the assumption of constant delay and no packet loss. This thesis presents a novel combination of the PD approach and the TDPA, which allows for a comparable data reduction rate while robustly dealing with time-varying delay and packet loss. Use of the conventional teleoperation structures, however, cannot simultaneously guarantee system stability and transparency.

For the MMT architecture which uses a local model on the master side to approximate the remote environment on the slave side, it guarantees both system stability and transparency while not requiring a packet rate as high as 1 kHz. The state-of-the-art MMT techniques can only deal with relatively simple environment geometry and dynamics, such as rigid planar objects or deformable objects without friction. Stability of MMT systems during the transition state is still not intensively investigated. This thesis extends the current MMT techniques to deal with arbitrary environment geometry and complex dynamics such as deformable ob-

jects with frictional interaction. In addition, a perception-based model updating scheme is integrated into MMT systems to additionally reduce the packet rate in the backward channel. Furthermore, a passivity-based model update scheme is presented to guarantee system stability during model update in the transition states.

Chapter 3

Time-delayed Teleoperation: Combing Perceptual Data Reduction with the Time Domain Passivity Approach

Haptic communication approaches for teleoperation systems which are deployed over real-world packet-switched networks require the joint consideration of control and communication aspects to achieve a stable, transparent and efficient system design. The joint solutions require the combination of control approaches with haptic data reduction schemes. In [68, 145], the WV control scheme was combined with the PD approach. These methods, denoted as the PD+WV scheme, efficiently reduce the haptic packet rate in the communication channel for constant communication delays. For time-varying delays, however, no approach exists in literature. The innovation in this chapter is the development of a joint communication/control solution, which combines the PD approach with the TDPA to reduce the packet rate over the network while preserving system stability in the presence of time-varying and unknown delays.

The combination, denoted as PD+TDPA, is introduced in Section 3.1, including the stability analysis, necessary modifications of the system architecture to maintain the stability conditions, and feasibility evaluation. Furthermore, Section 3.1.3 describes the situation that the resulting control behavior is overly conservative when the PD approach is combined with the TDPA. The PD approach leads to irregular updates between the master and slave, which can be considered as a special case of packet loss. As described in [120], packet loss interrupts the communication of system energy between the master and slave and causes conservative control. Thus, during time periods when no packets are transmitted, the system is more conservatively controlled due to the use of the PD approach. Although stability is ensured, the conservative control behavior results in degraded system transparency and poor teleoperation quality such as frequent and strong force jumps.

To address this issue, Section 3.2 proposes an energy prediction (EP) scheme that deals with the conservative behavior of the resulting controller. The EP scheme adaptively predicts

the system energy during communication interruptions and allows for larger energy output. This achieves less conservative control and improves teleoperation quality.

Evaluations of the teleoperation quality, both objectively and subjectively, are presented in Sec. 3.3. For the objective quality evaluation, we compare the displayed impedance for the schemes proposed in this chapter and related approaches from literature. For subjective quality evaluation, we experimentally find the subjectively optimal system parameters which allow for the strongest data reduction among the tested methods without introducing perceptible distortion. This way, the best possible trade-off between the teleoperation quality and the consumed network resources is achieved.

3.1 PD+TDPA

This section presents two structures of the PD+TDPA method. The original PD approach with the zero-order-hold (ZOH) reconstruction scheme as discussed in Section 2.2.1.3 and presented in [61, 65] is employed for data reduction and reconstruction. The employed PD approach is a non-passive scheme. However, the TDPA [120], as discussed in Section 2.2.2.3 and illustrated in Fig. 2.8, is able to guarantee the passivity of the two-port network between the two PCs. With a proper adaptation between the PD approach and the TDPA, system stability is ensured.

3.1.1 System Structure

3.1.1.1 Type A

For structure A, the control blocks for data reduction are placed after the POs. As illustrated in Fig. 3.1, the blocks *Deadband Data Reduction*, on both the master and slave sides, control the transmission rate of the velocity, force, and energy signals based on the predefined deadband parameter. Due to the use of the PD approach, not every velocity or force sample is transmitted. If no update is received, the block *Deadband Reconstruction* outputs the same signal as the most recently received one (original ZOH reconstruction scheme). Compared to the original TDPA architecture [120], the computation of the energy in the POs for the proposed approach is modified. The energy changes on both the master and slave sides at each time instant k can be described as follows:

$$\Delta E^m(k) = v_m(k) f_m(k) \Delta T = \begin{cases} v_m(k) f_m^{recv}(k) \Delta T, & \text{if signal received} \\ v_m(k) f_m^{recv}(k^*) \Delta T, & \text{else} \end{cases} \tag{3.1}$$

$$\Delta E^s(k) = v_s(k) f_s(k) \Delta T = \begin{cases} v_s^{recv}(k) f_s(k) \Delta T, & \text{if signal received} \\ v_s^{recv}(k^*) f_s(k) \Delta T, & \text{else} \end{cases} \tag{3.2}$$

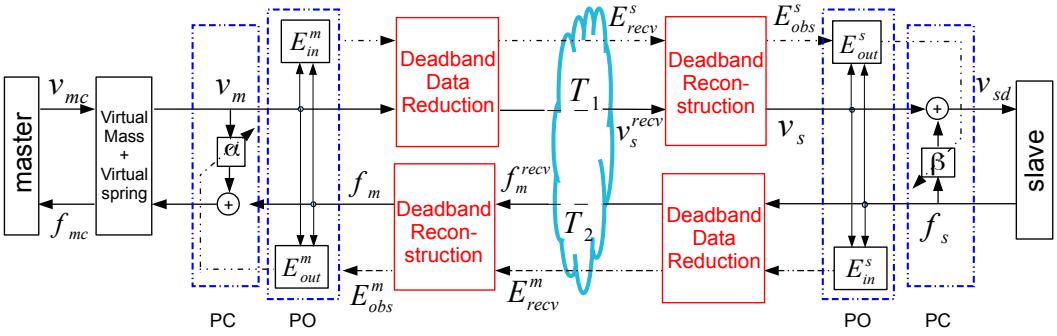

Figure 3.1: Combination of the PD approach with the TDPA, type A.

where $k^* < k$ is the time instant of the most recently received signal update, $v_s^{recv}(k^*)$ and $f_m^{recv}(k^*)$ are the most recently received velocity and force signals, respectively, and $v_s^{recv}(k)$ and $f_m^{recv}(k)$ denote the currently received velocity and force signals, respectively. Based on the signs of the energy change, the input or output energy on both the master and slave sides can be computed according to (2.8)-(2.11).

The exchange of energy information follows the transmission of the haptic data. This means that the energy information on the master or slave side is transmitted only when there is a corresponding velocity or force value transmission. Since the energy information is not transmitted at every time instant, the most recently received energy value is used for passivity observation, if there is no update

$$E_{obs}^s(k) = \begin{cases} E_{recv}^s(k) = E_{in}^m(k - T_1(k)), & \text{received} \\ E_{recv}^s(k^*) = E_{in}^m(k^* - T_1(k^*)), & \text{not received} \end{cases} \tag{3.3}$$

$$E_{obs}^m(k) = \begin{cases} E_{recv}^m(k) = E_{in}^s(k - T_2(k)), & \text{received} \\ E_{recv}^m(k^*) = E_{in}^s(k^* - T_2(k^*)), & \text{not received} \end{cases} \tag{3.4}$$

Assuming the received haptic packets are in order, due to the monotonic increase of the computed input/output energy (discussed in 2.2.2.3), it is always true that

$$\begin{aligned} E_{recv}^s(k^*) < E_{recv}^s(k) = E_{in}^m(k - T_1(k)) \\ E_{recv}^m(k^*) < E_{recv}^m(k) = E_{in}^s(k - T_2(k)) \end{aligned} \tag{3.5}$$

Hence, the entire system remains passive, if the output energy on both the master and slave sides ($E_{out}^{m/s}$) are controlled to be no larger than the corresponding energy observation $E_{obs}^{m/s}$:

$$\begin{aligned} E_{out}^s(k) \le E_{obs}^s(k) \le E_{recv}^s(k) = E_{in}^m(k - T_1(k)) \\ E_{out}^m(k) \le E_{obs}^m(k) \le E_{recv}^m(k) = E_{in}^s(k - T_2(k)) \end{aligned} \tag{3.6}$$

3.1.1.2 Type B

An alternative structure for the PD+TDPA approach is to monitor the energy after the block of perceptual deadband data reduction. As illustrated in Fig. 3.2, the transmission of the velocity or force signals is controlled before the POs. Since the deadband data reduction blocks are out of the control range of the two PCs and, the employed PD approach is non-passive as discussed in Sec. 2.2.1.5, a passive PD approach that is similar to the methods presented in [65, 68, 145] is applied to guarantee the passivity of the two-port subsystems of the structure type B (part 1 and 3). For this passive PD approach

$$v_m(k) = \begin{cases} v_{md}(k), & \text{if transmit} \\ v_{md}(k^*) - sign(f_{md})\Delta_{v_{md}}, & \text{else} \end{cases} \tag{3.7}$$

$$f_s(k) = \begin{cases} f_{sd}(k), & \text{if transmit} \\ f_{sd}(k^*) + sign(v_{sd})\Delta_{f_{sd}}, & \text{else} \end{cases} \tag{3.8}$$

where Δ denotes the corresponding deadband zone with regard to the most recently transmitted signal and is always positive. Apart from this, the computation of the energy observation in the POs is the same as in structure A. In addition, the exchange of energy information also follows the transmission of the haptic data.

For the two-port subsystems part 1 and 3 in the structure B,

$$\begin{aligned} P_1 &= v_{md}f_{md} - v_m f_{md} = (v_{md} - v_m)f_{md} = sign(f_{md})\Delta_{v_{md}} \cdot f_{md} > 0 \\ P_3 &= v_{sd}f_s - v_{sd}f_{sd} = (f_s - f_{sd})v_{sd} = sign(v_{sd})\Delta_{f_{sd}} \cdot v_{sd} > 0 \end{aligned} \tag{3.9}$$

Consequently, the individual two-port subsystems are passive. Meanwhile, the two PCs guarantee the passivity of the two-port subsystem part 2. Hence, the cascade connection of the three subsystems, each of them dissipating energy, leads to a stable overall system. This structure, however, cannot fully take advantage of the TDPA. The PCs dissipate output energy

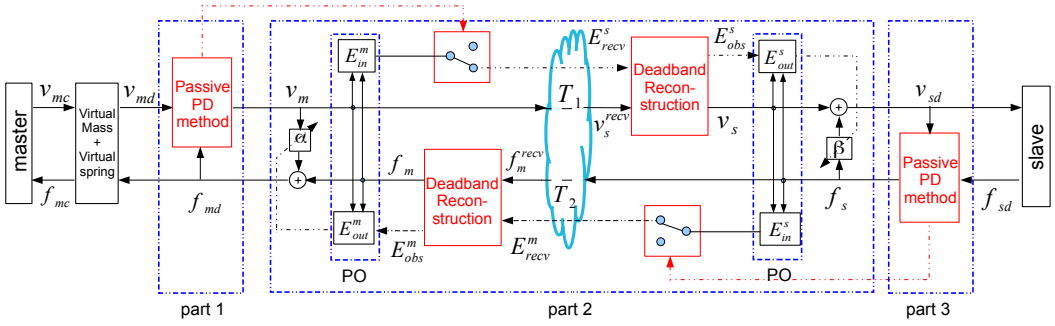

Figure 3.2: Combination of the PD approach with the TDPA, type B.

to ensure system passivity. The use of the passive deadband control before the PCs leads to additional energy dissipation. Thus, the entire system dissipates the output energy twice on each side, once by the PC of the TDPA and again by the passive PD approach. This results in a more conservative control behavior.

Therefore, we adopt the structure A as described in Sec. 3.1.1.1 in the following.

3.1.2 Feasibility evaluation

This section evaluates the feasibility of the type A structure in terms of packet rate reduction and user experience (subjective rating) for constant and time-varying communication delays. The experiment was conducted in a virtual environment (VE) with a real haptic device (Phantom Omni). The VE was developed based on the Chai3D library (www.chai3d.org). A 1-DoF rigid wall with a stiffness of 700 N/m is placed in the middle of the VE as the object on the slave side. A virtual slave was simulated in the VE, with a mass of 0.05 kg and a damping of 0.5 Ns/m. The slave was controlled by a proportional-derivative controller with a proportional gain of 300 N/m and a derivative gain of 1 Ns/m. The sampling rate was 1 kHz.

3.1.2.1 Setup and procedure

The round-trip delay (RTT) of a typical Internet communication is in the range from zero to hundreds of milliseconds depending on distance, network resources, traffic load, etc. Three different RTTs were tested in this experiment: 1) 10 ms constant delay, 2) 100 ms constant delay, and 3) varying delay with a mean delay of 100 ms and a Gaussian distributed delay variation (jitter) with a standard deviation of 30 ms. The selection of these delay values was motivated by RTT measurements from Germany to the east coast of the US where a mean delay of 95 ms was observed. For each tested delay scenario, a series of DBP values were tested: 0%, 2%, 5%, 8%, 10%, and 15%. A DBP of 0% corresponds to the performance of the original TDPA architecture without haptic data reduction.

During the experiment, the DBPs were randomly arranged. The subjects were asked to interact with the virtual wall by pressing on the surface and slowly vary the applied force with a frequency of about 0.5 Hz. This constraint in motion corresponded to the assumption of low frequency inputs for the passivity condition as used in the experiment in [120]. Moreover, position drifts introduced by the TDPA ([120]) were corrected after each trial when the virtual slave was in free space.

Note that the PD approach reduces the packet rate, leading to communication interruptions during the exchange of haptic signals over the network. This can introduce unpredictable artifacts in the haptic signals. Besides demonstrating the achievable data reduction preference, the other main purpose of this experiment was to investigate the effect of the DBP on the user experience compared to the case when no data reduction scheme was used. Thus,

the subjects were asked to give a rating for each DBP by comparing the perceived similarity of the haptic interaction between the case of using the given DBP value and the case of using a reference. The reference, the same delay as the current experiment trial with 0% DBP (designated level 5 according to Table 2.7), was considered as the "best" performance of the original (uncompressed) TDPA architecture for a tested delay. The rating scheme was based on Table 2.7 as discussed in Section 2.4.2. The reference setup could be recalled at any time during the experiment.

Fifteen subjects participated in the experiment, ranging in age from 25-45. A headset with active noise cancellation was worn to isolate the subjects from ambient noise.

3.1.2.2 Results

The packet rate vs. the DBP for the three tested communication delays is shown in Fig. 3.3(a). As expected, higher DBPs lead to lower packet rates. Obviously, the DBP has a dominant effect on the packet rate. On the other hand, the tested communication delays influence the damping of the passivity controller, which leads to modified velocity and force values. The modified velocity and force signals in turn affect the packet rate. Thus, the communication delays have an indirect influence on the packet rate. However, the resulting packet rate curves are very close to each other, which indicates that the effect of communication delay on the packet rate is small for the tested delays.

The subjective rating vs. the DBP is shown in Fig. 3.3(b). Higher DBPs lead to lower subjective ratings, since the subjects perceive stronger artifacts with increasing DBPs compared to the reference (no data reduction).

One can ask the question why the subjective rating for 10 ms delay is quite similar to the 100 ms delay case. Note that the ratings with the same DBP for different delays are not directly comparable, since the experiment used different references for different delays. All the references in each delay case are designated as rating level 5. For each delay, the subjects need to only rate the similarity of the haptic interaction between the reference (DBP=0) and the case with DBP>0. Thus, the subjective rating shows a relative quality with respect to different references for the given delays.

The combined curves from Fig. 3.3(a) and Fig. 3.3(b) are shown in Fig. 3.4, which illustrates the relationship between the subjective rating and the packet rate. Note again that the three curves in Fig. 3.4 are not directly comparable due to the use of different references for different delays. If a DBP of 5% is applied, the packet rate can be reduced by up to 80%, while the subjective rating remains sufficiently high (at about level 4). Hence, the PD+TDPA method approach is able to achieve high packet rate reduction without significantly disturbing the user experience compared to the original TDPA for the tested delay scenarios.

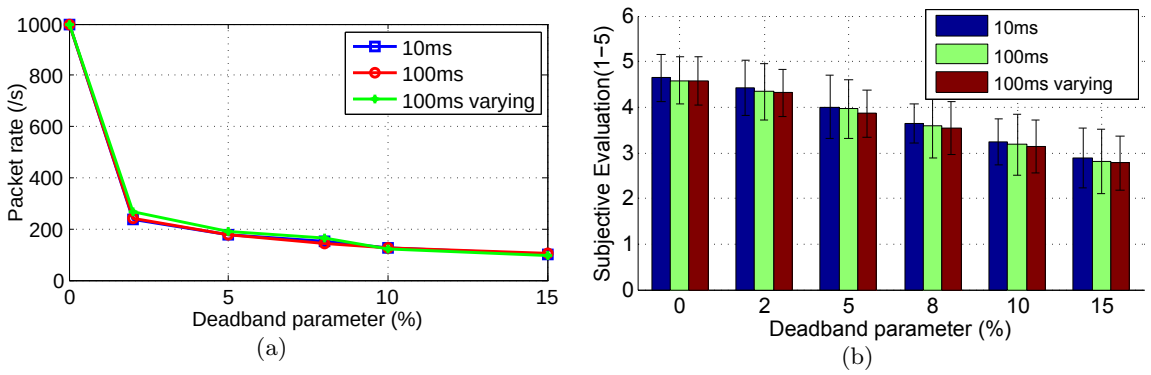

Figure 3.3: Experimental results. (a) Packet rate vs. deadband parameters for different delays. (b) Mean and standard deviation of the subjective ratings vs. DBP.

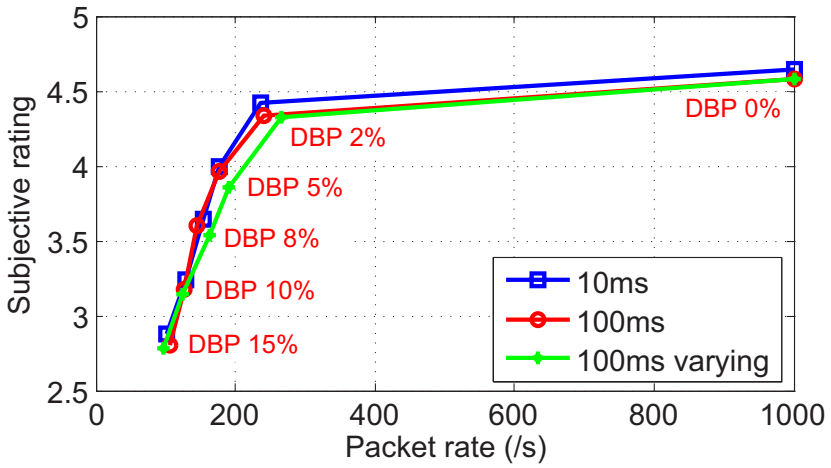

Figure 3.4: Subjective rating vs. packet rate.

3.1.3 Conservative Control Behavior during Communication Interruptions

Compared to the original TDPA [120], the use of the PD+TDPA method leads to a more conservative control. This is due to the communication interruptions caused by the PD approach. This section discusses and analyzes the reasons and the resulting effects. In the following discussion, we assume that the received packets are in order.

As discussed in [120], a TDPA-based teleoperation system is controlled conservatively during communication interruptions, for which the energy information is lost. The irregular downsampling of the haptic data caused by the PD approach can be considered as a special case of packet loss. Thus, the PD approach leads to communication interruptions and results in conservative control. According to (3.3) and (3.4), the master and slave systems use the most recently received energy for the POs, if they do not receive any update. The corresponding

Figure 3.5: Teleoperation setup with adjustable time delay.

output energy is controlled to be below the most recently received energy value:

$$\begin{aligned} E^s_{out}(k) &\leq E^s_{obs}(k^*) = E^m_{in}(k^* - T_1(k^*)) \\ E^m_{out}(k) &\leq E^m_{obs}(k^*) = E^s_{in}(k^* - T_2(k^*)) \end{aligned} \tag{3.10}$$

According to (3.5), this is more conservative compared to the original TDPA without data reduction, which monitors the output energy below $E^{s/m}_{in}(k - T_{2/1}(k))$. Since the system is already passive if $E^m_{out}(k) \leq E^s_{in}(k - T_2(k))$ and $E^s_{out}(k) \leq E^m_{in}(k - T_1(k))$, using (3.10) as the passivity condition leads to more conservative control, when the communication of the energy information is interrupted.

We illustrate this issue with the help of a real teleoperation system (see Fig. 3.5*). Two Phantom Omni devices were used as the master and slave. The slave was controlled by a proportional-derivative controller with a proportional gain of 200 N/m and a derivative gain of 2 Ns/m. The sampling rate was 1 kHz. According to [80], these control parameters ensure that the slave is controlled in its stability region.

The slave was controlled to establish contact with a metal plate. The round-trip communication delay was $T_d = T_1 + T_2 = 200$ ms and the DBP was 0.3. The measured energy, position, and force signals are shown in Fig. 3.6.

In Fig. 3.6(a) and 3.6(b), the green bars represent the time instants when packets are received. The black dashed lines are the delayed input energy value of the remote side if every packet is transmitted and received, namely $E^{m/s}_{in}(k - T_{1/2})$. The actually received energy information $E^{m/s}_{recv}$ for passivity observation is denoted by the dash-dotted blue lines, which are constant when no packet is received. The output energy, represented by the solid red line, is monitored so that it stays below the received energy value. This can lead to conservative behavior during the communication interruptions as shown in Fig. 3.6(a) and 3.6(b). Actually, the system is still passive if the output energy is above the dash-dotted blue line and below the dashed black line. This means that the system could be allowed for higher output energy.

*Please refer to http://www.lmt.ei.tum.de/forschung/projekte/prohaptics.html#demos/videos for more video demos.

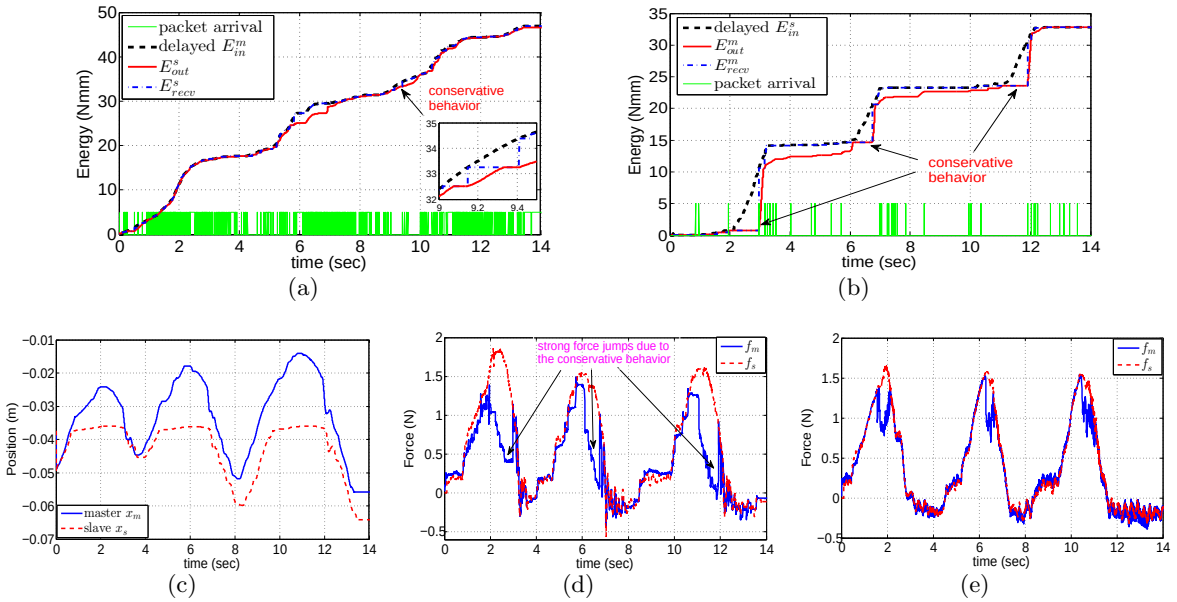

Figure 3.6: Illustration of the conservative control behavior of the PD+TDPA method. Delay 200 ms, DBP 0.3, average packet rate: 179 packets/s. (a) Computed and received energy signals at the slave side. (b) Computed and received energy signals at the master side. (c) Position signals. (d) Force signals with the PD approach. (e) Force signal without the PD approach.

The TDPA guarantees system passivity by damping the desired slave velocity and the displayed master force. The main consequence of the aforementioned conservative control issue is that the PCs are activated more frequently, and the desired slave velocity and displayed master force are damped unnecessarily. This results in increased position drift on the slave side if the slave output energy is monitored conservatively, and more force jumps on the master side if the master output energy is monitored conservatively. According to Fig. 3.6(a), the velocity values are frequently received on the slave side, leading to short communication interruptions. Therefore, the conservative behavior due to the communication interruptions on the slave side is quite small. Thus, the position drift observed in Fig. 3.6(c) is mainly caused by the TDPA and less by the PD approach. However, large durations of communication interruptions are observed in Fig. 3.6(b), which results in strong conservative behavior on the master side. Thus, there are strong force jumps in the displayed master force signals in Fig. 3.6(d). Figure 3.6(e) illustrates the force signals recorded for the original TDPA without the PD approach. Obviously, the force jumps without the PD approach are significantly less than those with the PD approach.

Note that the step effect in the force signals in Fig. 3.6(d) is due to the use of the PD approach. For small DBPs, this effect is not necessarily perceivable by human users. However, if the DBP is sufficiently large, the step effects (low-amplitude high-frequency vibrations) become perceivable.

3.2 Energy Prediction for Less Conservative Control

To compensate for the aforementioned conservative control behaviors, the input energy values of the remote side need to be estimated/predicted during communication interruptions. A proper energy prediction algorithm can, to a certain extent, compensate for the conservative control behavior, while maintaining system passivity. In this section, we assume that the communication interruptions of the haptic signals (information loss) are caused only by the PD approach. This means that no packet is lost during transmission over the network.

The conservative control behavior is caused by the communication interruptions of the energy information. If we can locally predict the actual input energy of the remote side during the communication interruptions, the lost energy can be compensated for and the system can be controlled less conservatively. In other words, we need to compute the predicted energy for the POs ($\hat{E}^{m/s}_{obs}(k)$) during the communication interruptions such that $\hat{E}^{m/s}_{obs}(k)$ is as close as possible to (but no larger than) the delayed input energy of the remote side. In the best case, the predicted energy for POs is identical to the delayed input energy of the remote side, namely $\hat{E}^{m/s}_{obs}(k) = E^{s/m}_{in}(k - T_{2/1}(k))$

Hence, we modify (3.3) and (3.4) to be

$$\hat{E}^{s}_{obs}(k) = \begin{cases} E^{s}_{recv}(k) = E^{m}_{in}(k - T_1(k)), & \text{received} \\ E^{s}_{recv}(k^*) + E^{s}_{comp}(k^*, k), & \text{else} \end{cases} \tag{3.11}$$

$$\hat{E}^{m}_{obs}(k) = \begin{cases} E^{m}_{recv}(k) = E^{s}_{in}(k - T_2(k)), & \text{received} \\ E^{m}_{recv}(k^*) + E^{m}_{comp}(k^*, k), & \text{else} \end{cases} \tag{3.12}$$

where $E^{m}_{comp}(k^*, k)$ and $E^{s}_{comp}(k^*, k)$ are the locally compensated energies on the master and slave sides, respectively, which predict the input energy of the remote side from the time instant of the most recently received packet k^* to the current time instant k.

3.2.1 Energy Prediction for Constant Delays

Assume that the communication delays T_i $(i = 1, 2)$ are known and constant. If a packet is received at time instant k^*, the delayed input energy of the master and slave ports at the current time k can be computed as

$$E^{m}_{in}(k - T_1) = E^{s}_{recv}(k^*) + \sum_{j=k^*+1}^{k} \max\{v_m(j - T_1) \cdot f_m(j - T_1) \cdot \Delta T,\ 0\} \tag{3.13}$$

$$E^{s}_{in}(k - T_2) = E^{m}_{recv}(k^*) + \sum_{j=k^*+1}^{k} \max\{v_s(j - T_2) \cdot f_s(j - T_2) \cdot \Delta T,\ 0\} \tag{3.14}$$

where $E_{recv}^{m/s}(k^*) = E_{in}^{s/m}(k^* - T_{2/1}(k^*))$.

Note that the sums in (3.13) and (3.14) accumulate only the **positive terms** (i.e., when $v_m \cdot f_m \geq 0$ or $v_s \cdot f_s \geq 0$) into the input energy $E_{in}^{m/s}$. This follows the definition of the energy computation in (2.8)-(2.11).

If every packet is transmitted, namely

$$v_s(k) = v_m(k - T_1) \text{ and } f_m(k) = f_s(k - T_2), \ \forall k \tag{3.15}$$

the master and slave are able to locally compute the delayed input energy of the remote side by combining (3.13), (3.14), and (3.15),:

$$E_{in}^{m}(k - T_1) = E_{recv}^{s}(k^*) + \sum_{j=k^*+1}^{k} \max\{v_s(j) \cdot f_s(j - T_1 - T_2) \cdot \Delta T, \ 0\} \tag{3.16}$$

$$E_{in}^{s}(k - T_2) = E_{recv}^{m}(k^*) + \sum_{j=k^*+1}^{k} \max\{v_m(j - T_1 - T_2) \cdot f_m(j) \cdot \Delta T, \ 0\} \tag{3.17}$$

However, due to the use of the PD approach, not every packet is transmitted. Thus, (3.15) is no longer available. The local prediction of the delayed input energy of the remote side needs to be derived in another way. According to the PD approach, the non-transmitted velocity or force signal during the communication interruptions must be within the deadband zone defined by the most recently transmitted signal update. This means that the receiver knows the **range** of the signal values on the sender side, even if it receives nothing. For example, if the slave receives no packet update at time instant k, the non-transmitted velocity signal on the master side can be estimated using the DBP and the most recently received velocity on the slave side:

$$|v_m(k - T_1)| \geq |v_m(k^* - T_1)| \cdot (1 - p) = |v_s(k^*)| \cdot (1 - p) \tag{3.18}$$

Meanwhile, the slave can also estimate the force signals on the master side according to the transmission buffer $\tilde{f}_s(k)$:

$$f_m(k) = \tilde{f}_s(k - T_2) = \begin{cases} f_s(k - T_2), & \text{if transmitted} \\ f_s(k'), & \text{else} \end{cases} \tag{3.19}$$

where $k' < k - T_2$ is the time instant of the most recently transmitted force signal with respect to time instant $k - T_2$. According to (3.13), (3.18), and (3.19):

$$E_{in}^{m}(k - T_1) \geq E_{recv}^{s}(k^*) + \underbrace{\Delta T(1 - p) \sum_{j=k^*+1}^{k} \max\{v_s(k^*)\tilde{f}_s(j - T_1 - T_2), \ 0\}}_{E_{comp}^{s}(k^*, k)} = \hat{E}_{obs}^{s} \tag{3.20}$$

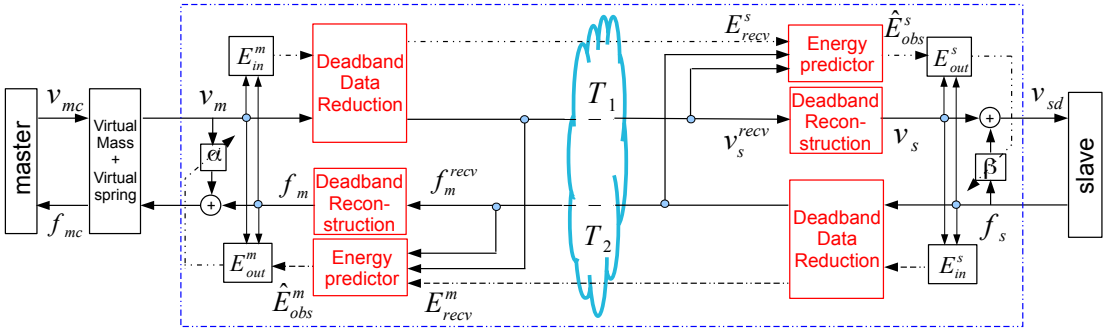

Figure 3.7: Control architecture of the TDPA-based haptic data reduction approach with the use of the energy prediction scheme.

Similarly, the non-transmitted force signal on the slave side can be locally estimated on the master side:

$$|f_s(k-T_2)| \geq |f_s(k^*-T_2)| \cdot (1-p) = |f_m(k^*)| \cdot (1-p) \tag{3.21}$$

With the help of the transmission buffer $\tilde{v}_m(k)$

$$v_s(k) = \tilde{v}_m(k-T_1) = \begin{cases} v_m(k-T_1), & \text{if transmitted} \\ v_m(k'), & \text{else} \end{cases} \tag{3.22}$$

(3.14) can be rewritten as

$$E^s_{in}(k-T_2) \geq E^m_{recv}(k^*) + \underbrace{\Delta T(1-p) \sum_{j=k^*+1}^{k} \max\{f_m(k^*)\tilde{v}_m(j-T_1-T_2),\ 0\}}_{E^m_{comp}(k^*,k)} = \hat{E}^m_{obs} \tag{3.23}$$

Equations (3.20) and (3.23) indicate that the master and the slave can locally predict the lower bound of the delayed input energy of the remote side during the communication interruptions; thereby partly compensating for the conservative control issue. Similar to (3.13) and (3.14), the sums accumulate only the positive terms. Since $\hat{E}^m_{obs} \leq E^s_{in}(k-T_2)$ and $\hat{E}^s_{obs} \leq E^m_{in}(k-T_1)$ are always true according to (3.20) and (3.23), monitoring the output energy on both the master and slave sides to be no larger than the predicted energy will not violate the system passivity condition.

The overall structure of the PD+TDPA method with the energy prediction (EP) scheme, denoted as PD+TDPA+EP, is illustrated in Fig. 3.7. If a packet is received, the energy predictor outputs the received value. If nothing is received, it computes the predicted energy according to (3.20) and (3.23) and uses it for the POs.

The performance of the proposed EP scheme is evaluated using the same teleoperation setup and the same communication parameters as shown in Sec. 3.1.3. The measured energy,

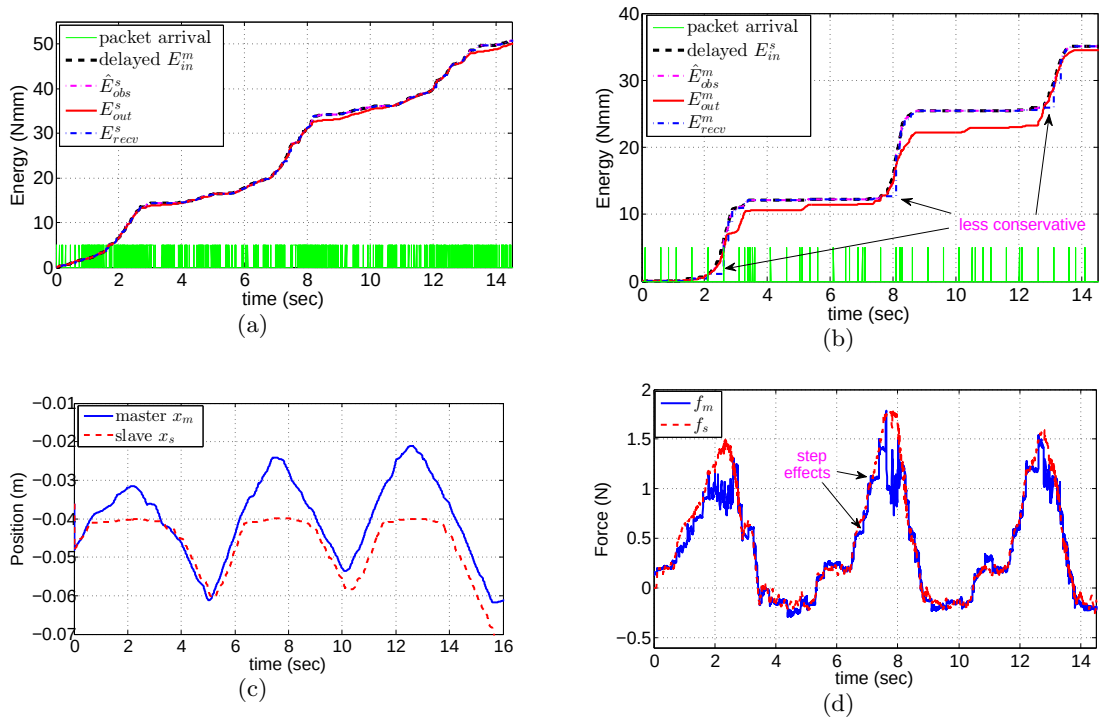

Figure 3.8: Measurements for the PD+TDPA+EP method. Delay 200 ms, DBP 0.3, average packet rate: 151 packets/s. (a) Computed and received energy signals at the slave side. (b) Computed and received energy signals at the master side. (c) Position signals. (d) Force signals.

position, and force signals are shown in Fig. 3.8. Compared to Fig. 3.6(a) and 3.6(b), less conservative behavior can be observed especially in Fig. 3.8(b). Due to the prediction scheme, the output energy of the slave and master (solid red lines) are controlled to be beyond the most recently received energy (dash-dotted blue lines) during communication interruptions, but they are monitored to maintain them below the predicted energy (dash-dotted purple lines). According to (3.20) and (3.23), the predicted energy is no larger than the delayed input energy of the remote side (dashed black lines); hence, the system is passive.

The position drift shown in Fig. 3.8(c) is comparable to the drift shown in Fig. 3.6(c). As discussed in Sec. 3.1.3, the conservative behavior of the PD+TDPA method on the slave side is relatively small. Thus, the potential for reducing the position drift is limited. On the other side, the conservative behavior on the master side during the communication interruptions is compensated to a large extent as shown in Fig. 3.8(b). Therefore, the force jumps are significantly reduced in Fig. 3.8(d) compared to those in Fig. 3.6(d). The force signals in Fig. 3.8(d) show a very similar behavior as those in Fig. 3.6(e). This indicates that the EP scheme can effectively compensate for the conservative behavior during communication interruptions and thus improves force feedback quality.

Note that (3.20) and (3.23) provide a conservative prediction (lower bound of the delayed

input energy of the remote side). Thus, there might still be gaps between the predicted energy and the delayed input energy of the remote side. In addition, the EP scheme only compensates for the conservative behavior during communication interruptions due to the PD approach. If the packet rate is not strongly reduced, the duration of the communication interruptions is relatively short and the conservative behavior is small. In this case, the improvement of using the EP scheme is limited. This is why the position drift is not significantly compensated for by the EP scheme in our evaluation.

3.2.2 Energy Prediction for Time-varying Delays

Section 3.2.1 presented the EP scheme for known and constant delays and communication without packet loss. The EP scheme can estimate the value range of the signals on the remote side, even if nothing is received. This is the key for locally predicting the input energy of the remote side.

However, if packet loss is taken into account and the receiver receives nothing, it is challenging to distinguish between the communication interruptions caused by the use of the PD approach and those caused by actual packet loss. In this case, the value range of the signal on the remote side cannot be correctly estimated, which leads to the violation of (3.18) and (3.21) and results in energy overestimation, namely $\hat{E}_{obs}^{m/s}(k) > E_{in}^{s/m}(k - T_{2/1})$. Energy overestimation can cause active behavior if $\hat{E}_{obs}^{m/s}(k) \geq E_{out}^{m/s}(k) > E_{in}^{s/m}(k - T_{2/1})$.

For time-varying delays, T_1 and T_2 in (3.20) and (3.23) have to be replaced by $T_1(k)$ and $T_2(k)$. This requires a precise and reliable real-time measurement of the communication delays, which is challenging in practice and requires additional resources from the network. A compromise is to use the expected value of the delay. This, however, can also lead to energy overestimates if the delay is suddenly and strongly increasing.

In order to avoid the accumulation of the energy overestimation in the presence of time-varying delay and packet loss, the activation time of the energy prediction must be limited. Since the delay and packet loss are not deterministic, the EP scheme cannot find the critical point when the energy prediction should be deactivated. Thus, potential energy overestimation is always present. However, we can limit the bound of the active energy by introducing the following procedure

- Set a forced regular packet transmission (e.g. 2 packets/s).
- Set a maximum activation time for the EP (e.g. 500 ms). After this time, the EP scheme is deactivated until the next packet is received.
- Deactivate the EP scheme once a packet is received and an overestimation is detected. Activate the EP scheme only when no overestimation is detected.

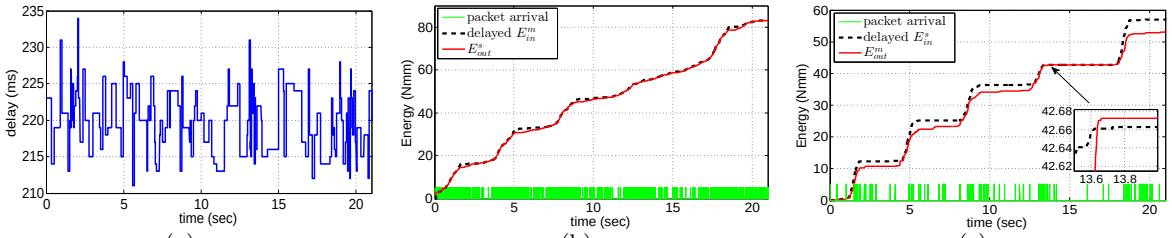

(a) (b) (c)

Figure 3.9: The modified EP scheme for time-varying delay and packet loss. Average packet rate: 137 packets/s (10% packet loss). (a) Round-trip-delay in the communication channel. (b) Output energy at the slave side and delayed input energy at the master side. (c) Output energy at the master side and delayed input energy at the slave side.

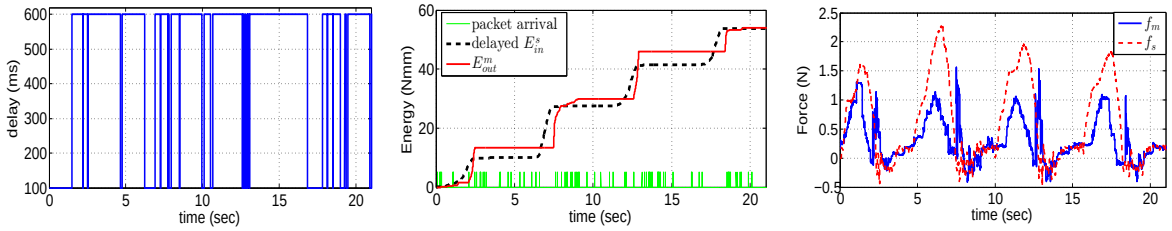

(a) (b) (c)

Figure 3.10: The modified EP scheme for an extreme case. Average packet rate: 118 packets/s (50% packet loss). (a) Round-trip-delay. (b) Output energy at the master side and delayed input energy at the slave side. The system is still piece-wise passive. (c) Force signals.

The first item guarantees that a packet is transmitted every 500 ms. This forced regular transmission does not introduce a significant communication load (only 2 packets/s). Thus, communication interruptions larger than 500 ms are caused by the increased delay or packet loss. For the second item, a maximum activation time of the EP scheme (500 ms) ensures an upper-bounded energy prediction. Although the predicted energy also depends on the operator behavior, the operator cannot output unbounded energy. For low frequency inputs, the overestimated energy can be limited into a small range during the 500 ms prediction period. Note that not every packet loss or delay variation causes energy overestimation. The limited EP activation time can reduce the probability of energy overestimation and consequently limit the active behavior. In addition, the third item avoids the accumulation of the energy overestimation. Please note that the velocity and force are maximally damped to zero by the damper α and β, but not to altered signs.

The same teleoperation setup was used to evaluate the modified EP scheme. The communication delay follows a Gamma-like distribution with $\Gamma_{\alpha,\beta}(20, 1)$ plus a deterministic delay of 200 ms. This model is based on Internet delay measurements [22]. The packet loss rate is 10%. The DBP is 0.3.

Only very slight active behavior is observed in more than 20 teleoperation trials. Fig-

ure 3.9 illustrates the recorded energy signals and round-trip-delay for one exemplary trial. In Fig. 3.9(c), the active behavior is limited and the energy overestimation does not accumulate with time. The active behavior due to the previous energy overestimation is terminated with the increasing system energy during teleoperation. Considering that passivity is a conservative condition of system stability and that the human user also contributes to the stability because of their own damping [50], the teleoperation system is very likely stable for the tested teleoperation behavior and network characteristics.

The active behavior is strong but still limited for extreme cases (Fig. 3.10). The packet loss rate in this example is 50%. In Fig. 3.10(b), strong active behavior can be observed. However, the active energy is bounded and does not accumulate. Thus, piece-wise passive behavior can be achieved during teleoperation. The force signals in Fig. 3.10(c) do not show strong vibration. This implies that the system is still operable for the tested teleoperation behavior even in this extreme case.

3.2.3 Energy Overestimation for Position Drift Compensation

Position drift is one of the main issues of TDPA. This is due to the velocity modification (damping) by the slave PC. The authors of [28] presented a scheme to compensate the position drift. After using the position drift compensation (PDC) scheme, the slave is able to follow the master's position command with only minimum drift. To take full advantage of the EP and the PDC schemes, their integration into the PD+TDPA structure is necessary (i.e., PD+TDPA+EP+PDC), as illustrated in Fig. 3.11.

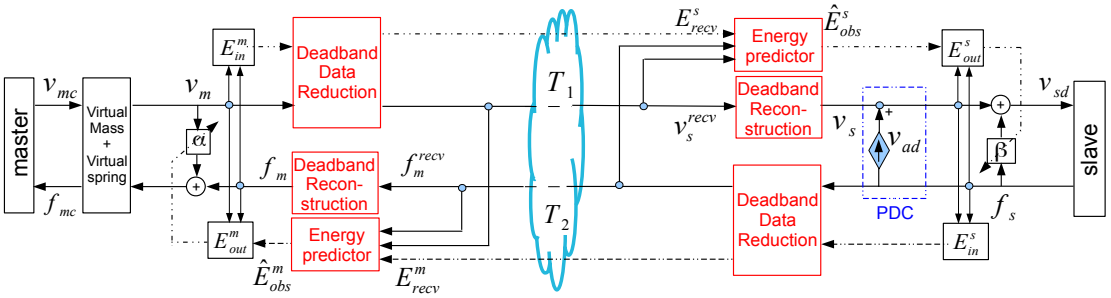

Figure 3.11: Control architecture of the TDPA-based haptic data reduction approach with the use of the energy prediction and position drift compensation schemes (PD+TDPA+EP+PDC). The velocity signal v_{ad} is used to compensate for the position drift.

However, this integration is quite challenging, even for constant delays. The reason is that the PDC scheme compensates for the position drift by altering the received slave velocity before the slave PC. This modification is out of the control of the PD approach and can push the slave velocity out of the deadband zone defined by the most recently transmitted master velocity. In some cases, even the direction of the slave velocity is modified. According to

[28], the modification of the slave velocity depends only on the previous slave force and the damping of the slave PC: $v_{ad}(k) = -\beta(k-1)f_s(k-1)$. The master cannot be informed about the damping β and the slave force f_s at every time instant due to the packet rate reduction of the PD approach. Therefore, the master can no longer locally predict the value range of the slave velocity. Hence, (3.23) is no longer fulfilled. Therefore, the predicted energy on the master side ($\hat{E}^m_{obs}$) can be beyond the delayed input energy of the slave side, violating the passivity condition. Note that (3.20) is still fulfilled, and the slave can correctly predict the input energy on the master side. This is because the master does not apply any compensation in the force signals.

Fig. 3.12 illustrates the active behavior on the master side if the EP and the PDC schemes are used simultaneously. The time delay is 200 ms and the DBP is 0.3. Although the overall passivity cannot be guaranteed, the active behavior is limited and does not accumulate if the procedure introduced in 3.2.2 is used. The whole system is piece-wise passive.

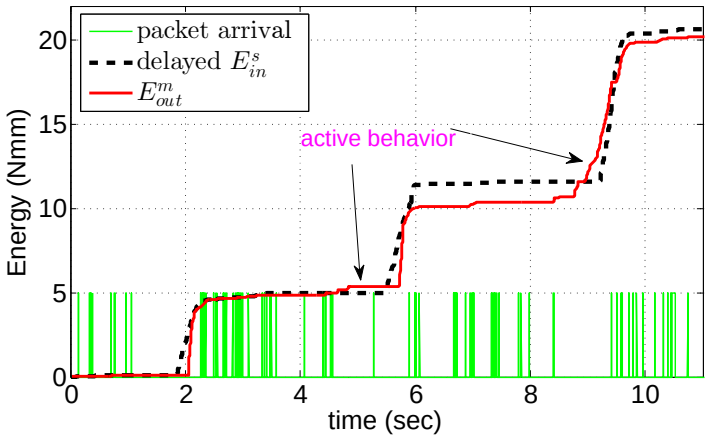

Figure 3.12: Output energy at the master side and delayed input energy at the slave side while simultaneously using the EP scheme and the PDC scheme. Limited active behavior is observed.

3.3 Evaluation of Teleoperation Quality

This section evaluates the teleoperation quality for the proposed combination schemes. The evaluation was made both objectively and subjectively.

3.3.1 Objective quality evaluation

3.3.1.1 System Transparency

System transparency is a common performance metric for objective quality of teleoperation systems. As discussed in 2.4.1, system transparency describes the accuracy with which a tele-

operation system can display a remote environment to a human user. According to [90], if the impedance displayed to the human (denoted as Z_h) matches the real environment impedance (denoted as Z_e) the teleoperation system is transparent. A measurement of transparency is the impedance error, which integrates the absolute difference between the displayed impedance and the environment impedance over a certain frequency range [90]:

$$Z_{error} = \frac{1}{\omega_{max} - \omega_{min}} \int_{\omega_{min}}^{\omega_{max}} |Z_{diff}(j\omega)| d\omega \tag{3.24}$$

where Z_{diff} is the impedance difference between Z_h and Z_e. The lower the value of Z_{error}, the higher is the degree of transparency.

The impedance error can be used as a measure of objective quality. If a valid linear approximation exists, the mechanical impedance is given as the mapping between the velocity $V(s)$ and the force $F(s)$ in the Laplace domain as $Z(s) = F(s)/V(s)$. Although the PD approach changes the dynamics of the system and no linear model for the displayed impedance $Z_h(s)$ can be derived, it can be assumed that a linearization of the displayed impedance $Z_h(s)$ around some working points exists. Hence, the standard frequency response measurement with correlation functions as suggested in [66, 68, 77, 145] is used to measure Z_h for the tested frequency range. In addition, the impedance difference is computed relative to the environment impedance as

$$Z_{diff} = \frac{|Z_h(j\omega) - Z_e(j\omega)|}{|Z_e(j\omega)|} \tag{3.25}$$

3.3.1.2 Simulation results

This section presents the simulation results for evaluating system transparency. The evaluation was made for the proposed haptic data reduction scheme for time-delayed teleoperation, and for the related approaches from literature.

Two virtual devices were simulated as the master and slave, with a mass of 0.05 kg and a damping of 0.5 Ns/m. The master commanded the slave into contact with a rigid wall (linear spring with stiffness of 10000 N/m). The slave was controlled by a proportional-derivative controller with proportional gain of 300 N/m and a derivative gain of 1 Ns/m. The master motion was a sinusoidal velocity input within a frequency window $[f_{min}, f_{max}] = [10^{-2}, 10^{2}]$ Hz and an amplitude of 0.1 m/s. The sampling rate was 1 kHz.

Figure 3.13 shows the Bode plot of the displayed impedance for a round-trip delay of $T_d = 100$ ms, DBP=0.1, and the use of the PD+TDPA+EP scheme. The environment impedance (the solid red line) shows a linear behavior across the tested frequency range. The displayed impedance (dashed blue line) follows the linear behavior at low frequency inputs. For input frequencies larger than 1 Hz, the displayed impedance shows a complex non-linear behavior.

The average impedance error for the tested frequency range according to (3.24) and (3.25) is about 45%. Note that the environment impedance is the coupled impedance of the virtual slave and the spring environment.

The tested delays (T_d) are constant and range from 0 to 1000 ms. The DBP values range from 0 to 0.3. For each tested (T_d, DBP) pair, the corresponding average impedance error and the average packet rates were recorded. Different combination schemes such as the PD+TDPA, the PD+TDPA+EP, the PD+TDPA+PDC, and the PD+WV as presented in [145] were evaluated. Note that the PD+TDPA+EP+PDC method cannot guarantee system passivity even for constant delay as discussed in Section 3.2.3. Therefore, this combination scheme was not evaluated.

The overall simulation results are shown in Fig. 3.14.

The average impedance error of the PD+TDPA method is illustrated in Fig. 3.14(a). Increased delay leads to an increased impedance error (degraded transparency). This implies that the PCs need to dissipate more energy to ensure system passivity for large communication delays, and the environment is displayed softer than it should be. In addition, the change of the DBP value has also influence on the average impedance error, though the effect is small when compared to the effect of delay. For small delays (e.g., $T_d < 100$ ms), an increased DBP value leads to an increased impedance error. This is especially observable for delay of zero, which conforms to the conclusion of [66]: "a larger DBP value in the absence of communication delay reduces system transparency".

Figure 3.14(b) shows the measured average packet rate as a function of the DBP for different delays. As expected, higher DBPs lead to a lower packet rate. The DBP has a dominant effect on the packet rate. Moreover, the packet rate curves for different communication delays deviate only slightly from each other. Although the communication delay cannot directly affect the downsampling (packet reduction) of the haptic signals, it has a direct influence on the damping of the PCs. The damping alters the velocity and force signals. The altered velocity and force signals will in turn affect the downsampling when using the PD approach; hence,

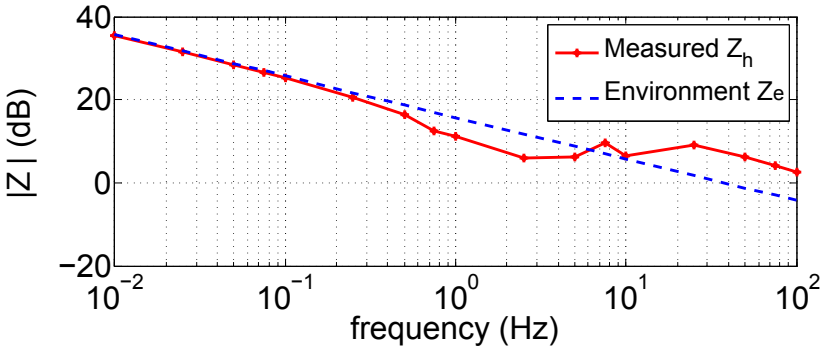

Figure 3.13: Bode plot of the displayed impedance in contact.

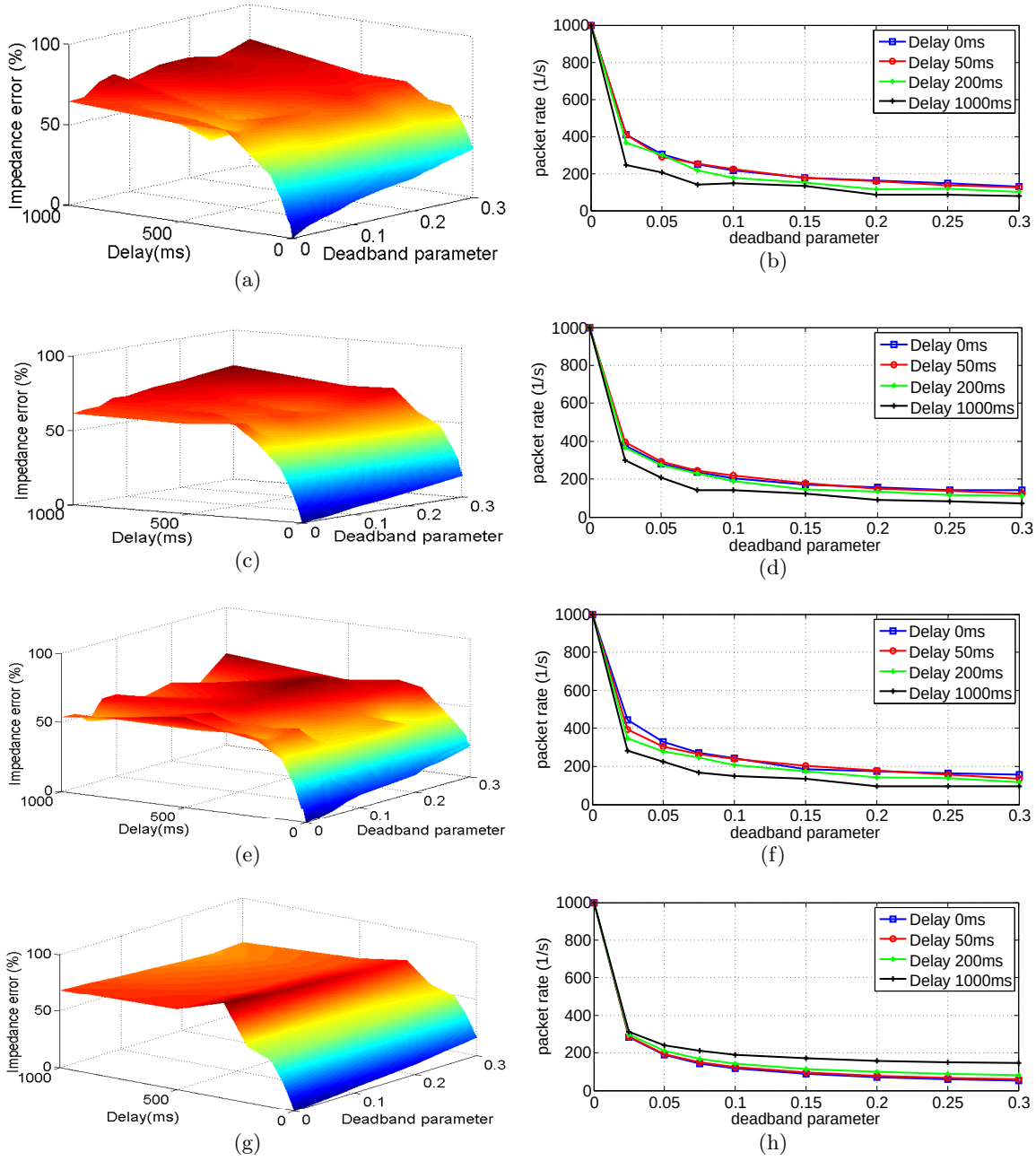

Figure 3.14: Simulation results of the average impedance errors and packet rates in different parameter settings. (a)(b) The PD+TDPA method. (c)(d) The PD+TDPA+EP method. (e)(f) The PD+TDPA+PDC method. (g)(h) The PD+WV method. Wave impedance is $b = 25$ Ns/m.

altering the packet rate. Therefore, the communication delays have an indirect influence on the packet rate, though this influence is small.

Figs. 3.14(c) and 3.14(d) illustrate the simulation results of the PD+TDPA+EP method. The results are very similar to the PD+TDPA method. For most tested parameters, the impedance errors of the PD+TDPA+EP method are lower than for the PD+TDPA method,

especially for small delays and large DBP values. As discussed in Sec. 3.1.3, larger DBP values lead to higher packet rate reduction, resulting in longer communication interruptions and more conservative behavior. Thus, the EP scheme works more efficiently for large DBP values. This indicates that the use of the EP scheme improves system transparency. On the other hand, the use of the EP scheme does not have significant influence on the packet rate compared to the PD+TDPA method.

Figs. 3.14(e) and 3.14(f) illustrate the results for the combination of the TDPA and the PD approach without the use of the EP scheme, but with the use of the PDC scheme (PD+TDPA+PDC). System transparency is better (lower average impedance errors) than in the PD+TDPA method. This is because the PDC scheme is able to minimize the position drift and inject energy into the system while guaranteeing passivity. The system using the PD+TDPA+PDC method is less conservative and more transparent than that using the PD+TDPA method. On the other hand, the impedance errors of the PD+TDPA+PDC method (Fig. 3.14(e)) are larger than for the PD+TDPA+EP method (Fig. 3.14(c)) for small delays. The reason for this is that the position drift is relatively small for small delays and the energy compensated for by the PDC scheme is smaller than that compensated for by the EP scheme. Thus, the PD+TDPA+PDC method is more conservative and less transparent. For large delays, however, the position drift is relatively large. The energy compensated for by the PDC scheme is larger than the energy compensated for by the EP scheme. This leads to less conservative control and less impedance errors for large delays, if the PDC scheme is applied.

Finally, the wave-variable-based haptic data reduction approach (PD+WV) proposed in [145] was simulated. The simulation results are shown in Fig. 3.14(g) and 3.14(h). The DBP values lead to a similar packet rate compared to Figs. 3.14(b),3.14(d), and 3.14(f). The impedance errors of the PD+WV method highly depend on the wave impedance (denoted as b). As discussed in [66], the displayed stiffness of a spring environment for the WV approach operated in low frequencies is a function of the environment stiffness k_e, the wave impedance b and the delay T_d:

$$\frac{1}{k_h} = \frac{1}{k_e} + \frac{T_d}{2b} \tag{3.26}$$

For a given delay, a larger value of b leads to higher transparency during contact. However, the wave impedance adds an additional inertia m_h while the slave moves in free space [66]:

$$m_h = \frac{bT_d}{2} \tag{3.27}$$

Higher additional inertia in free space motion leads to degraded system transparency. Obviously, increasing the transparency in both contact and free-space motion are conflicting objectives. In Fig. 3.14(g), the wave impedance is set to be $b = 25$ Ns/m, resulting in very similar average impedance errors compared to the PD+TDPA+EP method, especially for

small delays. However, $b = 25$ Ns/m adds an inertia of 1.25 kg for $T_d = 100$ ms, or 6.25 kg for $T_d = 500$ ms, to the slave's free-space motion. This discourages a quick and precise teleoperation in free space. On the other hand, decreasing the b value reduces the additional inertia; however, it also reduces the displayed stiffness while in contact, leading to higher impedance errors. From this point of view, the combination of the PD and the TDPA approaches, including its variations such as the PD+TDPA+EP and the PD+TDPA+PDC schemes, is more flexible for different teleoperation tasks.

In summary, from the simulation results the following conclusions can be drawn:

- Compared to the PD+TDPA method, the PD+TDP+EP scheme allows for less conservative control and thus improves system transparency, especially for small delays and large DBPs.
- The communication delay has a dominant influence on system transparency but limited influence on packet rate.
- The DBP has a dominant influence on packet rate but limited influence on system transparency.
- The use of the EP scheme, the PDC scheme, and different control schemes (TDPA or WV) do not have significant influence on the packet rate.

3.3.2 Subjective quality evaluation

3.3.2.1 Perceived transparency

Due to the communication delay and the use of the PD approach, the displayed impedance cannot exactly match the environment impedance. One of the major questions relates to the extent to which the displayed impedance can differ from the actual impedance such that the human user still perceives them to be the same. The concept of **perceived transparency** is introduced in [66] to take human perceptual limitations into account. A teleoperation system is perceived transparent if the displayed impedance lies within the range of the JND of the human perception:

$$Z_h(j\omega) \in [Z_e(j\omega) - \Delta Z_e(j\omega), Z_e(j\omega) + \Delta Z_e(j\omega)] \tag{3.28}$$

The JNDs for haptic stimuli are quite different for various physical properties. For example, the JND for forces is about 7% to 10% [81, 109], whereas the JND for stiffness is about 15% for soft contact and 23% for hard contact [82, 139]. Conservatively considering a perceptual threshold of 15% for stiffness discrimination, the sets of (T_d, DBP) pairs in Fig. 3.14(a), 3.14(c), 3.14(e), and 3.14(g) that lead to impedance errors of less than 15% are considered as the region of perceived transparency (RPT). The RPT boundaries of different

control and compensation methods are illustrated in Fig. 3.15. The areas below the boundary curves are the corresponding RPTs. The RPT of the PD+TDPA+EP method is larger than that of the PD+TDPA and PD+TDPA+PDC methods. This indicates that the use of the EP scheme improves the perceived transparency of the system for a linear spring environment. The RPT of the PD+WV method is very similar to that of the PD+TDPA+EP method when b is 25 Ns/m. Although the RPT will be larger for larger b values, system transparency is degraded in free-space motion due to the additional wave inertia. For $b = 3.5$ Ns/m, the wave inertia in free space is lower than for $b = 25$ Ns/m but according to Fig. 3.15, the RPT in contact becomes much smaller.

In summary, the RPT in the considered scenario denotes the parameter space for which the user cannot distinguish between the displayed stiffness and the environment stiffness.

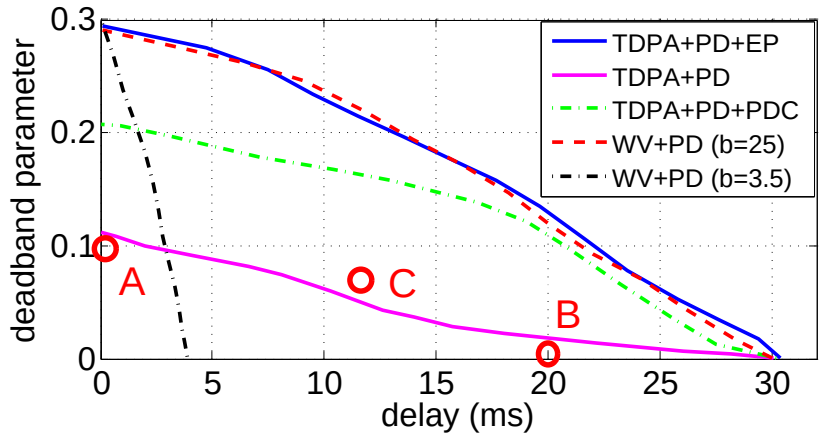

Figure 3.15: Boundaries of the region of perceived transparency for different control and compensation methods. The three tested parameter sets for Sec. 3.3.2.2 are A (0 ms, 0.1), B (20 ms, 0), and C (12 ms, 0.08).

3.3.2.2 Subjective transparency

Limitations of perceived transparency

The perceived transparency defines a perceptual quality metric from the point of view of the displayed impedance. Additionally, the force jumps caused by the TDPA and the step effects caused by the PD approach (see Figs. 3.6(d) and 3.8(d)) also lead to a distorted force signal and degraded subjective quality. These artifacts are potentially perceivable even if the current parameter set is in the RPT. For example, the experimental results presented in [61, 65] showed that the low-amplitude, high-frequency vibration is perceivable (though very small) when the DBP is 10% for negligible delays. This result corresponds to point A in Fig. 3.15. In addition, according to a series of tests using the PD+TDPA+EP method, the force signals corresponding to points B ($T_d = 20$ ms, DBP=0) and C ($T_d = 12$ ms, DBP=0.08)

in Fig. 3.15 are perceptually distorted compared to the reference force signal (original environment impedance) rendered for $T_d = 0$ and DBP=0. The perceived distortion mainly comes from the force jumps and vibrations. Therefore, besides the perceived transparency for the displayed impedance, the artifacts on the force signals, such as jumps and vibrations, should also be taken into account when evaluating the teleoperation quality.

Definition of subjective transparency

We present the concept of **subjective transparency**, which is different from the previously defined perceived transparency, to indicate that the user cannot perceive any difference between *the displayed signals* and *the reference signals* in terms of stiffness, force jumps, vibrations, etc. A subjectively transparent teleoperation system achieves the best subjective quality *with respect to the reference signals.*

Evaluation of subjective transparency

Subjective transparency defines the perceptual identity between the displayed haptic signal and the reference signal. The reference signals rendered under the conditions of $T_d = 0$ and DBP=0 (denoted as $\text{Ref}_{0,0}$) displays the original environment impedance. In the presence of communication delay, however, a subjectively transparent teleoperation system with respect to the original environment impedance cannot be achieved. This is because the delay is a network characteristic, which we cannot tune. If delay exists, the TDPA (or other control schemes) must be employed to ensure system stability. This leads to modified velocity and force signals, resulting in perceivable artifacts such as large deviation on displayed stiffness or force jumps.

One aim of the evaluation is to investigate how the use of the PD approach affects the subjective quality of time-delayed teleoperation when it is combined with the TDPA. For given communication delay T_d, signals rendered under the condition $T_d \neq 0$ and DBP=0 should be used as the reference (denoted as $\text{Ref}_{T_d,0}$). The reference $\text{Ref}_{T_d,0}$ represents the practically best possible haptic signals after controlling when no haptic data reduction schemes are used. Note that the reference $\text{Ref}_{T_d,0}$ varies according to different delays.

Figure 3.16 illustrates an example of the subjective quality as a function of packet rate for different delays. Low packet rates lead to degraded subjective quality. The increase of communication delay also degrades teleoperation quality. However, if delay exists, the practically best possible haptic signals are those obtained with a stability-ensuring control scheme when no haptic data reduction schemes are used, namely the reference points in Fig. 3.16. In the presence of delays, the use of haptic data reduction schemes can introduce distortion. However, at a certain level of packet rate reduction, due to the limitations of human haptic perception, these distortions are not necessarily perceivable. The thresholds

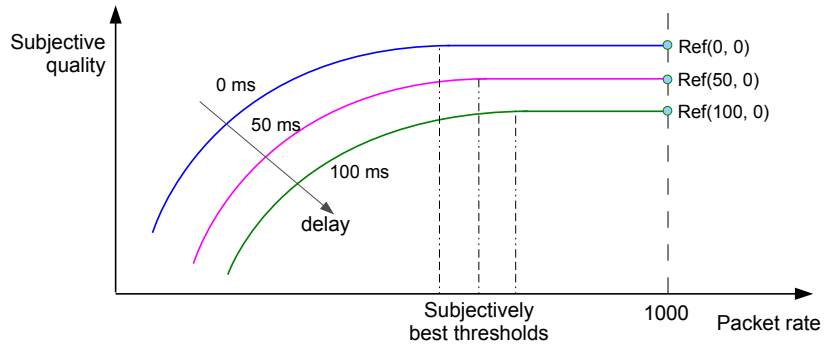

Figure 3.16: Hypothetical subjective quality measure as a function of communication delay and packet rate. The subjectively best thresholds represent the lowest possible packet rate, at which the system remains subjectively transparent with respect to the corresponding reference signals.

that allow for the highest data reduction without distorting user perception (subjectively transparent) for different delays are considered as the subjectively best thresholds.

Although the desired low packet rate and the targeted high subjective quality are conflicting objectives in teleoperation system design, considering the limits of human haptic perception, however, slight distortions introduced by the PD approach are not necessarily perceivable. With a proper DBP, a low packet rate and subjective transparency can be achieved simultaneously.

3.3.2.3 Experimental evaluation

In this section, the subjectively best thresholds (the best perceptual thresholds of the DBP) for given delays were determined experimentally, when the PD approach is combined with the TDPA. Choosing DBP values below these thresholds reduces the packet rate while achieving subjective transparency.

Results of two experiments are presented in this section. The first experiment aimed to determine the thresholds of the DBP to achieve subjective transparency. The second experiment compared the PD+TDPA+EP and PD+WV [145] methods in terms of subjective preference for the DBP thresholds found in the first experiment.

The Geomagic Touch haptic device was used as the master. In order to avoid measurement noise and control tremble of the slave robot, the slave and the remote environment were designed in a virtual environment (VE). The experimental setup is illustrated in Fig. 3.17. The VE was developed based on the Chai3D library (www.chai3d.org). A 1-DoF rigid wall with a stiffness of 10000N/m was placed in the middle of the VE as the remote object on the slave side. The controller and the dynamics of the virtual robot were designed as described in Section 3.3.1.2. The experiments were conducted on a PC with an Intel Core i7 CPU and 8 GB memory.

A. Experiment I: DBP thresholds

Setup and procedure:

The tested delays were time-varying with means of 0 ms, 25 ms, 50 ms, 100 ms, and 200 ms. The jitter was Gaussian distributed with standard deviations of 10% of the mean delays. For each delay condition, the methods PD+TDPA+EP, PD+TDPA, and PD+TDPA+PDC were tested. The DBP thresholds for each delay and each method were determined using the simple up-down staircase method [33] with ascending and descending trials. In each trial, the subjects tested two settings, one with the use of the PD approach (varying DBP values) and the other one without (i.e., $\text{Ref}_{T_d,0}$ with DBP=0). The subjects interacted with the virtual wall by pressing on the surface and slowly varying the applied force. They were asked whether they perceived the two settings to be the same or different. The orders of the two settings and the delays were randomly selected. The initial DBP was 0 for the ascending case and 0.3 for the descending case. The minimum step size of the change on the DBP was 0.01.

Twelve subjects participated in the experiment. They ranged in age from 25 to 45 and all were right handed. A headset with active noise cancellation was worn to isolate the subjects from ambient noise. The subjects were provided with a training session. The experiments started as soon as the subjects felt familiar with the setup and procedure.

Results:

The DBP thresholds for the three combination methods (PD+TDPA+EP, PD+TDPA, and PD+TDPA+PDC) are presented in Fig. 3.18. The mean and standard deviation of the thresholds across all subjects are listed in Table 3.1.

For a given delay and a certain combination of control and data reduction method, the

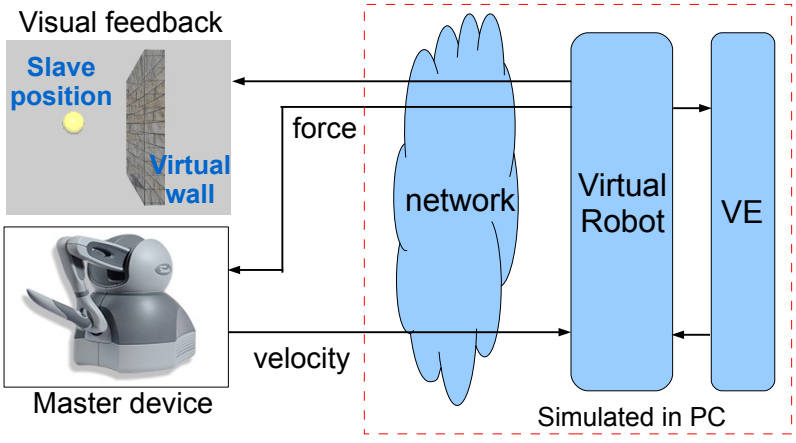

Figure 3.17: Experimental setup. The communication network, the slave (represented by a haptic interaction point), and the virtual environment are simulated on a PC using the CHAI3D library.

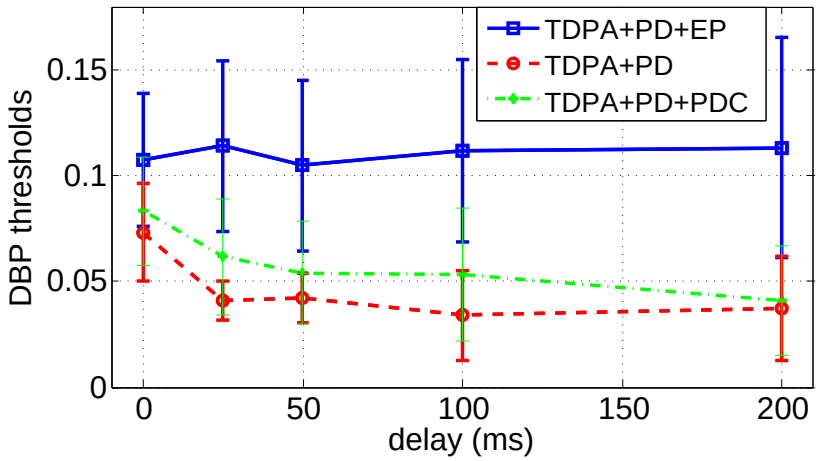

Figure 3.18: Detected DBP thresholds (mean and standard deviation) of the three tested methods across all subjects.

Table 3.1: Determined thresholds for the three tested methods across all subjects.

method / delay	PD+TDPA	PD+TDPA+PDC	PD+TDPA+EP
0 ms	0.073 ± 0.023	0.083 ± 0.020	$\mathbf{0.107} \pm 0.032$
25 ms	0.041 ± 0.009	0.055 ± 0.021	$\mathbf{0.114} \pm 0.040$
50 ms	0.043 ± 0.012	0.054 ± 0.019	$\mathbf{0.105} \pm 0.040$
100 ms	0.034 ± 0.021	0.051 ± 0.026	$\mathbf{0.112} \pm 0.043$
200 ms	0.041 ± 0.030	0.038 ± 0.021	$\mathbf{0.113} \pm 0.051$

detected DBP thresholds of the 12 participants are not necessarily normally distributed, since DBP=0 defines the lower bound and the distributions are hardly symmetric. This was verified using the chi-squared goodness-of-fit test. Therefore, the Friedman test was performed on the three combination methods for each tested delay. At the level of $\alpha = 0.01$, a statistically significant difference in the determined DBP thresholds of the three combination methods can be reported for the tested non-zero delays: $F_{25\text{ ms}} = 9.54$, $p_{25\text{ ms}} = 0.008$; $F_{50\text{ ms}} = 11.29$, $p_{50\text{ ms}} = 0.002$; $F_{100\text{ ms}} = 10.79$, $p_{100\text{ ms}} = 0.004$; and $F_{200\text{ ms}} = 10.17$, $p_{200\text{ ms}} = 0.005$. In addition, a post-hoc multiple comparison test was conducted to enable pairwise comparisons among the three combination methods. The results show that the determined DBP thresholds of the PD+TDPA+EP method are significantly different from the other two methods for the tested non-zero delays. Between the DBP thresholds of the PD+TDPA and PD+TDPA+PDC methods, no significant difference is found.

The statistical analysis above indicates that the PD+TDPA+EP method significantly increases the DBP thresholds compared with the other two methods. Since higher DBPs lead to a lower packet rate, the PD+TDPA+EP method is able to achieve higher data reduction rates

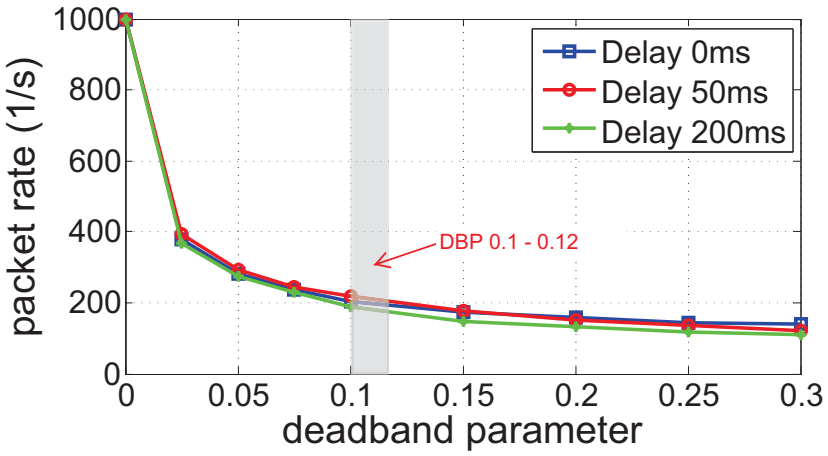

Figure 3.19: Packet rates vs. deadband parameters for different delays in Fig. 3.14(d). The packet rate in the gray area can be achieved using the determined mean DBPs of the PD+TDPA+EP method for the tested delay.

compared to the other two methods. The data reduction rate is of about 80% as illustrated in Fig. 3.19 by summarizing Fig. 3.14(d) and 3.18). Meanwhile, subjective transparency is guaranteed. According to Fig. 3.14(b), 3.14(f), and 3.18, using the DBP thresholds of the PD+TDPA or PD+TDPA+PDC methods, the data reduction can hardly achieve 80%.

B. Experiment II: Comparison

Setup and procedure:

One advantage of the PD+TDPA+EP method compared with the PD+WV method [145] is the ability to deal with time-varying delays. In this experiment, we aimed to determine the user preference between these two methods for the same DBPs. The wave impedance was set to $b = 3.5\ Ns/m$, as a compromise between the free-space motion and the contact.

The tested delays were the same as in the first experiment. The DBP thresholds determined in the first experiment were used for comparison. For each delay, the subjects tested three conditions: the PD+TDPA+EP method, the PD+WV method (both with the same DBP), and the zero delay reference with zero DBP ($\text{Ref}_{0,0}$). Comparisons were made between the first two methods in term of subjective preference, and they were also made between the reference and the PD+TDPA+EP method and between the reference and the PD+WV method in term of displayed impedance.

After each comparison, the subjects had to answer the following two questions: 1) which method shows more similar impedance (stiffness) to the reference? and 2) which method do you prefer considering both the free-space motion and the contact? Each comparison was repeated four times by each subject. The same subjects as in the first experiment participated in this experiment.

Results:

The results of the two questionnaires are shown in Tab. 3.2. For all tested delays, most of the subjects responded that the PD+TDPA+EP method showed a more similar stiffness to the reference if a delay exists. The PD+TDPA+EP method was preferred over the PD+WV method. Most subjects suggested that even though the PD+TDPA+EP method introduces irregular distortions (occasional force changes), the PD+WV method shows a larger inertia and oscillation in free-space motion and a softer environment in contact. This is more significant for large delays; therefore, all subjects voted for the PD+TDPA+EP method for $T_d = 200$ ms.

Similar to the first experiment, the packet rate highly depends on the user behavior. According to Fig. 3.14(d) and Fig. 3.14(h), the same DBP values lead to a similar packet rate for both methods. Nevertheless, the PD+TDPA+EP method is able to adaptively deal with unknown delays and to gain better subjective quality and higher user preference.

Table 3.2: Results of the questionnaires for the second experiment. The remaining answers in Q1 are "both methods show similar impedance".

Q1: impedance similarity					
delay (ms)	0	25	50	100	200
PD+TDPA+EP	22%	**69%**	**69%**	**79%**	**79%**
PD+WV	**27%**	10%	22%	15%	8%
Q2: subjective preference					
delay (ms)	0	25	50	100	200
PD+TDPA+EP	**52%**	**86%**	**83%**	**96%**	**100%**
PD+WV	48%	14%	17%	4%	0%

3.4 Discussion

Using the PD+TDPA+EP method, a major packet rate reduction is achieved without noticeably distorting the user perception. Compared to the PD+TDPA method, the EP scheme allows for larger DBP thresholds and thus results in lower packet rates (Fig. 3.18). It is also able to increase the output energy and improve teleoperation quality (Figs. 3.8, 3.14 and 3.15). This result, obtained from the numerical transparency analysis, is validated in the experimental user study. There are a number of factors that additionally play a role for both the teleoperation quality and packet rate reduction.

Delay variation and packet loss. As discussed in Sec. 3.2.2, packet loss or suddenly increased communication delay leads to energy overestimation and potentially results in active behavior. The main reason for this is that the increased delay or packet loss enlarges the

duration of the prediction period and thus introduces overestimation of the energy. For low packet rates, each transmitted packet is more important than that for high packet rates. This means that the system more easily tends to non-passive behavior in the presence of time-varying delay and packet loss, if it is operated at a low packet rate. In Sec. 3.2.2, we introduce a scheme to limit the EP activation time. It is able to bound the overestimated energy, reduce the probability of active behavior, and avoid the accumulation of the energy overestimation. Experimental results show that this scheme can control the overestimated energy and the active behavior into a limited range. System passivity, however, is not fully guaranteed. More knowledge about the network characteristics can be helpful for further improving the performance of the EP scheme.

Adaptive joint solutions. This work combines the PD and TDPA approaches to present a joint solution for haptic data reduction in time-delayed teleoperation systems. This is not the only joint solution, since other stability-ensuring control schemes such as the input-to-state stability (ISS) method [79], the 4-channel TDPA [116], the power-based TDPA [153] can be also combined with different haptic data reduction schemes such as the linear prediction and reconstruction approach [62]. In general, high-quality teleoperation requires the joint orchestration of control and communication approaches to cope with limitations such as restricted transmission capacity, time-varying delay and random or burst packet losses. Having adaptive control and communication approaches to implement teleoperation systems is important, as they vary in their robustness towards certain network characteristics.

3.5 Chapter Summary

This chapter presents the combination of the PD approach with the TDPA to reduce the packet rate over the communication network for time-delayed teleoperation. This approach allows for a reduction of the haptic data using the original zero-order-hold deadband reconstruction approach, while preserving system stability in the presence of time-varying (unknown) communication delays. The simple combination method (PD+TDPA, Section 3.1), however, leads to conservative control behavior during communication interruptions due to haptic data reduction. To address this issue, Sec. 3.2 proposes a novel energy prediction (EP) scheme to adaptively predict the energy during communication interruptions and thus compensate for the conservative control behaviors in the presence of haptic data reduction. Both objective and subjective evaluation verify the feasibility of the combination methods. The evaluation also compares the performance of different combination methods in terms of system transparency, perceived transparency, and subjective transparency including the subjectively best deadband parameters.

Here is a summary of the main conclusions:

- The combination of the PD and TDPA scheme significantly reduces the haptic packet rate while guaranteeing system stability. The EP scheme can additionally compensate for the conservative behavior and improve teleoperation quality (both objectively and subjectively) during communication interruptions for constant delay or time-varying delay with small delay jitter.

- Independent of the combination methods, the deadband parameter has a dominant influence on the packet rate, but limited influence on the system transparency. In turn, the communication delay has a dominant influence on system transparency but limited influence on packet rate.

- The use of the PD+TDPA+EP method is able to achieve an average data reduction of about 80% while guaranteeing subjective transparency. The PD+TDPA+EP method is preferred by subjects in the experiments compared to the PD+WV method from literature.

- There are some open topics left for improving the performance of the proposed joint solution. 1) The EP scheme can lead to energy overestimation and active behavior in the presence of time-varying delays and packet loss. Although the active behavior is limited, system stability is no longer guaranteed. 2) The EP scheme does not work well when combined with the position drift compensation scheme for the two-channel TDPA architecture. A 4-channel TDPA structure should be tested in this context. 3) More joint solutions by combing different control and communication schemes need to be studied (see Chapter 5). This is important to have adaptive control and communication approaches for dealing with various network characteristics.

Chapter 4

Point Cloud-based Model-mediated Teleoperation

In Chapter 2, model-mediated teleoperation (MMT) was identified as a promising approach to simultaneously guarantee system stability and transparency for time-delayed teleoperation. Due to the use of the local model, the dynamics of the slave and the deficiencies of the communication channel do not influence the displayed impedance on the master side in contrast to the passivity-based control schemes. MMT systems are able to fully and consistently display the slave environment to the operator on the master side in the presence of arbitrary communication delays. In addition, a frequent update of the local model is unnecessary for static or slowly varying environments. This means that the MMT system in principle does not require the high packet rate (e.g. 1000 packets/s) explained in the previous chapters. Therefore, the MMT approach has gained increasing interest in the recent years.

To ensure the superiority of the MMT approach over the passivity-based control schemes, fast and precise environment modeling methods are required. The modeling methods need to be applicable for complex environments and a variety of different tasks. In the literature, most related work on MMT approximates the environment with a simple geometry for rigid objects (e.g. a planar surface [103, 148]) or with simple physical models for deformable objects which allow for non-frictional interaction only (e.g. the Hunt-Crossley model [56]). In most cases, however, the geometric or physical properties of the remote objects are complex. A simplified approximation is not sufficient for performing various tasks in complex environments, since it leads to large deviations from the real environment and thus results in frequent model updates and incorrect haptic rendering.

This chapter extends the state-of-the-art MMT approach to deal with complex environments in the presence of arbitrary communication delays, while guaranteeing system stability and improved teleoperation quality. To this end, a point cloud-based model-mediated teleoperation (pcbMMT) approach is presented in Sec. 4.1. A point cloud of the object surface is captured to represent the surface geometry. The model mediation and force rendering are

purely based on point clouds without using any explicit geometric model or 3D meshes. For modeling deformable objects with frictional interaction, a radial function-based deformation (RFBD) method is proposed in Sec. 4.2. This approach allows for real-time modeling of deformable objects using point clouds. A dynamic and perception-based model update scheme is proposed in Sec. 4.3 to adaptively control the updating of the point cloud model and the physical properties of the object by exploiting known limitations of human haptic perception. As a result, perceptually irrelevant transmissions are avoided, and thus the packet rate in the communication channel is substantially reduced. In Sec. 4.4, a passivity-based model update scheme is developed to ensure the system stability during the model update on the master side.

4.1 System Design

An overview of the proposed pcbMMT system is shown in Fig. 4.1. The depth images captured by a 3D sensor are used to estimate the environment geometry. The corresponding physical properties (impedance parameters) are estimated after the slave comes into contact with the environment. Once the model parameters are obtained, they are transmitted to the master side. An update controller dynamically controls the packet transmissions on both the slave and the master side. On the master side, a local model is reconstructed based on the received model parameters (environment impedance and point cloud data). The force feedback signal is generated locally based on the point cloud model without noticeable delays.

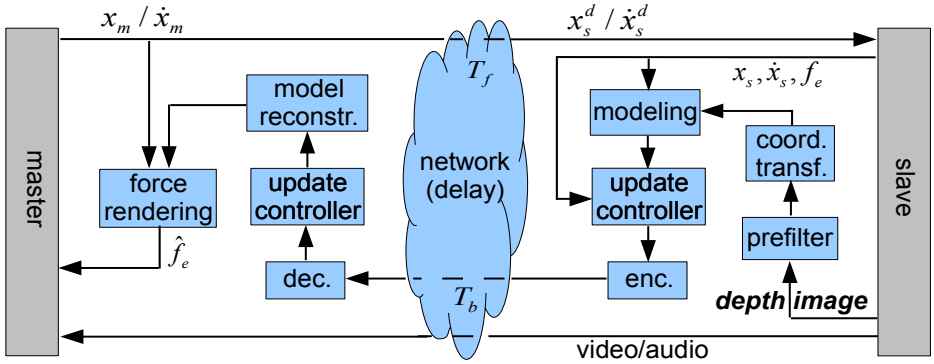

Figure 4.1: Overview of a point cloud-based model-mediated teleoperation system using a 3D sensor.

4.1.1 Pre-processing

4.1.1.1 The 3D sensor and depth maps

To obtain the point cloud model, a 3D sensor is employed. For complex environments there are always areas that cannot be scanned during approaching the objects because of occlusion

and the limited field of view. Thus, the 3D sensor needs to capture the point cloud of the object surface continuously during teleoperation.

The employed 3D sensor is a time-of-flight (ToF) camera (Argos®3D-P100), which captures at a high frame rate (up to 160 fps) and operates at a more flexible work range (10 cm to 5 m) compared to other 3D sensors, such as Microsoft's Kinect and ASUS' Xtion (about 50 cm to 3 m). The captured point clouds are organized and stored in matrices (depth maps) with a size of 120x160 pixels. The captured depth maps are considered as gray-scale images and thus image processing algorithms can be directly applied on the depth maps for noise reduction, image inpainting, and compression.

4.1.1.2 Pre-filtering

The raw depth maps captured by the 3D camera are normally quite noisy, sometimes even with missing parts (holes) due to an invalid work range or wrong reflection (see Fig. 4.2 left). Therefore, pre-filtering is necessary for noise reduction and hole filling. In order to reduce the computational complexity for the real-time environment modeling, simple standard image filters are employed. Firstly, a 5 by 5 median filter is applied on each depth image to remove outlier depth values. Then, a temporal per pixel average filter for every N frames is employed to reduce the noise of the depth image (see Sec. 4.1.2.1 for more details about the value N). In addition, an image inpainting method is employed to fill the holes in the depth image. Since the purpose of using image inpainting techniques is to recover the missing parts rather than providing a good visual quality, the simple and fast image inpainting algorithm described in [107] is adopted. In this hole-filling algorithm, the missing regions in the depth image are first extracted and marked. Then isotropic diffusion (convolution with matrices A and B) based on the neighborhoods of the hole regions is applied inside the hole regions for several rounds. The diffusion kernels suggested by [107] are as follows:

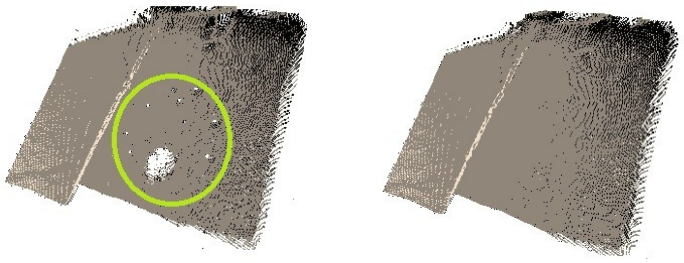

Figure 4.2: A depth image before filtering (left) and after filtering (right). The holes are filled by the median, average and inpainting filters.

$$A = \begin{pmatrix} a & b & a \\ b & 0 & b \\ a & b & a \end{pmatrix} \quad and \quad B = \begin{pmatrix} c & c & c \\ c & 0 & c \\ c & c & c \end{pmatrix} \tag{4.1}$$

where $a = 0.073235$, $b = 0.176765$ and $c = 0.125$. After filtering, a low-noise depth image is obtained without holes (Fig. 4.2 right).

Note that if there is a real hole on the object surface, the inpainting algorithm will fill it by mistake. This is because we do not apply any detectors to distinguish between a real hole and the missing part. To address this issue, more information such as the edge shape of the hole should be collected and analyzed in order to make a correct decision.

4.1.1.3 Coordinate transformation

The acquired depth maps are expressed in local pixel coordinates. In order to build the 3D point cloud model in world coordinates from the depth maps, 3D coordinate transformation is employed. As illustrated in Fig. 4.3(a), the coordinate transformation is composed of three steps: 1) from pixel coordinates to camera coordinates, 2) from camera coordinates to robot tool coordinates ($\mathbf{R_1}$ and $\mathbf{t_1}$) and 3) from robot tool coordinates to world coordinates ($\mathbf{R_2}$ and $\mathbf{t_2}$).

In the first step, every pixel in the depth map described by the vector $(u, v, d)^T$ is transformed into camera coordinates $(x_c, y_c, z_c)^T$, where u and v are the pixel coordinates in rows and columns and d is the depth value. An ideal pinhole camera model is adopted to apply this transformation. As illustrated in Fig. 4.3(b), the transformation can be described as follows:

$$x_c = (o_x - v) \cdot z_c / f_x, \quad y_c = (u - o_y) \cdot z_c / f_y, \quad z_c = d \tag{4.2}$$

where f_x and f_y are the camera focal lengths in x and y directions, o_x and o_y are the pixel shifts from the camera center.

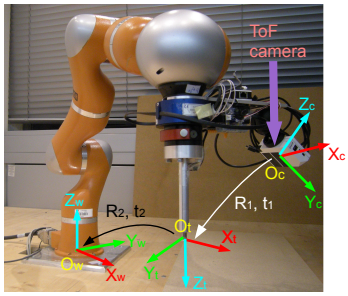

(a)

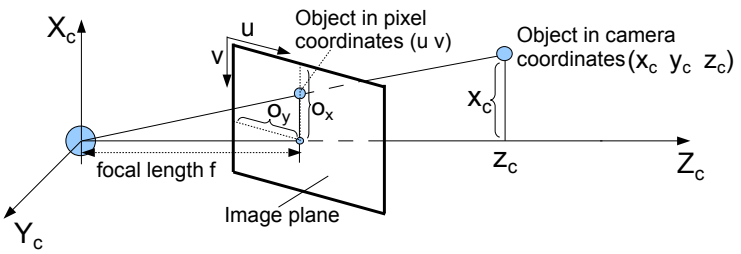

(b)

For the remaining steps from camera coordinates $(x_c, y_c, z_c)^T$ to robot tool coordinates $(x_t, y_t, z_t)^T$ and then to world coordinates $(x_w, y_w, z_w)^T$, 3D rotations and translations are applied as follows:

$$\begin{aligned}(x_w, y_w, z_w)^T &= \mathbf{R_2} \cdot (x_t, y_t, z_t)^T + \mathbf{t_2} \\ &= \mathbf{R_2} \cdot (\mathbf{R_1}(x_c, y_c, z_c)^T + \mathbf{t_1}) + \mathbf{t_2}\end{aligned} \tag{4.3}$$

4.1.2 Environment modeling

This is to estimate the geometry and physical properties for the remote object. The captured point cloud can be directly used for describing the object surface geometry. For static and rigid bodies with friction, the friction coefficient μ between the object surface and the robot end-effector is the first important parameter to be estimated. Additionally, an estimation of the stiffness value k is necessary. For rigid objects, k can be a very high value and represents the stiffness coupling between the slave robot and the environment. Due to the communication delay, initial values for k and μ are needed to be able to render the force signals on the master side before the first estimated physical properties are received.

For deformable objects, the dynamics model of the surface deformation must be also estimated in addition to the geometry and physical properties. The widely used multi-DoF Mass-Spring Models (MSM) or Finite Element Models (FEM) are quite time consuming and thus challenging for a real-time estimation. The RFBD method presented in Sec. 4.2 allows for an online modeling of deformable surfaces described by point clouds.

4.1.2.1 Geometry modeling

The object geometry is continuously updated and transmitted to the master side, while the slave is in free space. Thus, the master system can reconstruct a stable and precise 3D point cloud model before the slave gets in contact with the remote environment. The update rate of the object geometry is adaptively changed according to the slave velocity. For accuracy reasons, higher slave velocity results in higher update rate. As the frame rate of the 3D sensor is set to be 50 fps in our system, in order to balance the estimation accuracy and the computational time, the maximal and minimal update rates of the object geometry are set to be 25 Hz and 2 Hz, respectively. The update rate r as a function of the slave velocity $\mathbf{v_s}$ is selected as follows:

$$r = min\{2 + ||\mathbf{v_s}||, \quad 25\} \tag{4.4}$$

where $||\mathbf{v_s}||$ represents the value of the slave velocity (cm/s) but without unit.

According to Eq.(4.4), the update rate of the object geometry (point cloud) increases with increasing slave velocity. The adaptive length N of the temporal averaging filter in

Sec. 4.1.1.2 is computed as $N = round(50/r)$, which means that N continuous frames are taken to compute the surface geometry.

4.1.2.2 Physical properties

Friction coefficient (FC) μ

Three assumptions are made before the estimation:

1. The static FC is assumed to be the same as the dynamic FC.
2. The estimation is activated only when the robot velocity in the tangent direction of the object surface $\mathbf{v_s^t}$ is larger than a pre-defined threshold.
3. The FC value is the ratio of the measured tangential force f_s^t and the normal force f_s^n on the slave side:

$$\mu = f_s^t / f_s^n, \quad f_s^n = \langle \mathbf{f_s}, \mathbf{n} \rangle, \quad f_s^t = ||\mathbf{f_s} - f_s^n \cdot \mathbf{n}|| \tag{4.5}$$

Where $\langle , \rangle$ denotes the vector inner product, $\mathbf{f_s}$ is the measured slave contact force and $\mathbf{n}$ is the estimated surface normal at the contact position (see Sec. 4.1.4 for more details about surface normal estimation).

When the estimation is activated, the measured tangential and normal slave forces (sampling rate 1 kHz) are recorded as an effective force-pair sample. The FC is computed based on the last 100 effective force-pairs: $\bar{\mu} = \frac{\sum_{i=1}^{100} \mu_i}{100}$.

Stiffness k

While interacting with a rigid object, the slave end-effector stays on the surface of the object. The commanded (desired) slave position $\mathbf{x_s^d}$, however, can penetrate into the object due to limited force that can be displayed through the master device. The position difference between the slave end-effector $\mathbf{x_s}$ and the desired slave position $\mathbf{x_s^d}$ in the direction of the surface normal is regarded as the penetration depth:

$$\Delta d = || \left\langle \mathbf{x_s} - \mathbf{x_s^d}, \mathbf{n} \right\rangle || \tag{4.6}$$

With the help of Hooke's law, the stiffness k is computed as

$$k = f_s^n / \Delta d \tag{4.7}$$

Similar to the FC estimation, the last 100 effective $(f_s^n, \Delta d)$ samples are collected to estimate the k value. The stiffness estimation is activated if the normal force on the slave side is larger than a pre-defined threshold, which implies a stable contact between the slave end-effector and the environment.

The RFBD method for modeling the dynamics of deformable surfaces using point cloud is introduced in Sec. 4.2.

4.1.3 Model update

The two update controllers on the slave and master side play different roles.

On the slave side, it controls the transmission of the estimated model parameters (geometry and physical properties) and thus avoids excessive updating of model parameters. Instead of sending every estimate, only those resulting in a significant difference in perception are transmitted to the master. In the initial phase, the packet rate can be very high, since the estimates vary rapidly. Once the estimates converge to the true values, there will be no updates required. Thus, the system achieves zero transmission in the backward communication channel. For real teleoperation systems, however, the estimates can vary over time due to measurement error, natural tremble of human arm movement, etc. The designed updating scheme should be robust to the parameter changes due to measurement error and should be able to distinguish between the parameter changes due to noise and due to environment changes. A dynamic and perception-based transmission controller for reducing packet rate in the backward channel is presented in Sec. 4.3.

On the master side, the update controller is dedicated to provide a smooth and stable updating from the currently applied model parameters to newly received ones. A sudden change in the geometry or physical properties leads to system instabilities [149]. Thus, stability-ensuring update schemes are required. A gradual update method, such as the IIR low-pass filter method proposed in [149], is able to avoid sudden changes in the parameter updating process. It cannot, however, guarantee stability during the model updates. Sec. 4.4 introduces a passivity-based model update scheme to address this issue.

4.1.4 Point cloud-based force rendering

In order to render the interaction force based on the received point cloud model on the master side, a point cloud-based haptic rendering (pcbHR) method is employed. Compared to the traditional mesh-based rendering process, the pcbHR method can directly compute the force signals without converting the point cloud into meshes, which reduces the computational complexity. Previously proposed pcbHR approaches for rigid objects are described in [41, 91, 117, 118]. In order to apply a low-cost pcbHR method including friction rendering, this thesis extends the pcbHR method by combining the approach in [117, 118] and the friction cone method in [60]. As illustrated in Fig. 4.3, a proxy-HIP (haptic interaction point) method is used to estimate the surface normal and render the force.

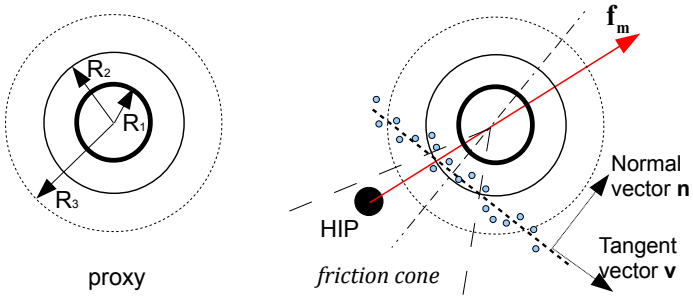

Figure 4.3: The definition of the proxy (left) and the estimation of the surface normal as well as master force (right).

4.1.4.1 Proxy states

Similar to [117], the proxy has three different radius ranges R_1, R_2 and R_3. R_1 and R_2 are used to detect collision while R_3 is used for surface normal estimation. The gap between the proxy radius R_1 and R_2 is chosen to be 5mm, which is just larger than the noise level of the point clouds captured by the ToF camera. R_3 is chosen sufficiently large to get a good surface normal estimation. Three different proxy states are defined as follows:

- Free space: no points within R_2
- In contact: there are points between R_1 and R_2, but no points within R_1
- Entrenched: points within R_1

4.1.4.2 Surface normal estimation

As suggested in [118], the surface normal is obtained by averaging all vectors which start from the contact point and point towards the center of the proxy $\mathbf{x_p}$. Every time before the proxy moves, the surface normal $\mathbf{n}$ is computed as follows:

$$\mathbf{n}' = \frac{1}{K}\sum_{i=1}^{K}\frac{\mathbf{x_p} - \mathbf{x_i}}{||\mathbf{x_p} - \mathbf{x_i}||}, \quad \mathbf{n} = \mathbf{n}'/||\mathbf{n}'|| \tag{4.8}$$

where $\mathbf{x_i}$ is the position vector of the point between the spheres defined by R_1 and R_3 (inside of R_3 but outside of R_1).

4.1.4.3 Proxy movement

A modified proxy movement algorithm based on [117] is employed to enable friction rendering. In the following, we define $\mathbf{s}$ as the proxy movement vector, d as the step size, and $\mathbf{x_m}$ and $\mathbf{x_p}$ as the master HIP and proxy position, respectively. $\mathbf{u} = \mathbf{x_m} - \mathbf{x_p}$ denotes the vector

which points towards the master HIP position from the proxy center and $\mathbf{v} = \frac{\mathbf{u}-\langle \mathbf{u},\mathbf{n} \rangle}{||\mathbf{u}-\langle \mathbf{u},\mathbf{n} \rangle||}$ is the surface tangent vector.

The proposed algorithm proceeds as follows:

- If the proxy is in free space, move it one step $\mathbf{s} = d \cdot \mathbf{u}$. Direction: from the proxy to the master HIP.
- If the proxy is entrenched, move it one step in the direction of $\mathbf{n}$: $\mathbf{s} = d \cdot \mathbf{n}$
- If the proxy is in contact with the object, a friction cone is computed based on the estimated friction coefficient. Then (1) If the HIP is inside of the friction cone, the proxy stays still ($\mathbf{s} = 0$); (2) If the HIP is outside of the friction cone, move the proxy one step $\mathbf{s}$ in the direction of $\mathbf{v}$. The step size of $\mathbf{s}$ is computed such that after the proxy movement the HIP stays just at the boundary of the friction cone [60].

4.1.4.4 Force rendering

The haptic signal is simply rendered at 1 kHz with a spring model between the proxy and the HIP based on Hooke's law:

$$\mathbf{f_m} = k \cdot (\mathbf{x_p} - \mathbf{x_m}) \tag{4.9}$$

4.1.5 Point cloud compression

In the pcbMMT system, the captured 3D point clouds are transmitted to the master side to reconstruct a local virtual model. The transmission of the 3D point clouds, however, requires a large data rate in the communication channel. To reduce the data rate, we transmit the filtered depth map in the camera view (similar to a gray-scale image) along with the coordinate rotation and translation parameters. Thus, the 3D model can be reconstructed in a lossless manner on the master side with reduced data. However, directly transmitting the depth images still requires a large bit rate. Considering a depth map of size 120x160 pixels and the maximum update rate of 25 fps, the maximum required bit rate is $120 \cdot 160 pixel/frame \cdot 8bit/pixel \cdot 25 frame/s = 3.84 Mb/s$, which is still a quite large rate requirement. Therefore, lossless H.264/AVC compression is employed to compress the depth maps.

,

4.2 Radial function-based deformation method for real-time modeling of deformable objects using point clouds

In the MMT approach, an object model with unknown parameters is first selected to approximate the remote environment. Then, these unknown parameters are estimated on the slave

side and transmitted to the master in real time during the slave's interaction with the remote environment. On the master side, a local object model can be built according to the received model parameters, and the force feedback signals are generated based on this local model without noticeable delay.

Obtaining a precise model for complex deformable objects is a big challenge for the MMT approach. Fortunately, it is not necessary to obtain the whole environment model. It is sufficient to estimate a local model to approximate the area which the slave currently has contact with. Once the local model no longer matches the remote object, the slave computes a new model according to the current contact information, and a model update is triggered.

Online modeling of simple deformable objects for MMT systems is widely studied in the literature. In [92], a single degree of freedom damper-spring model is employed to approximate the environment. In [12, 56], a non-linear Hunt-Crossley model was employed to approximate the remote soft object. The models used to describe the object's surface deformation in these work, however, are too simple. Deformation in their work is assumed only along the surface normal vector without friction (no tangential deformation). For the modeling of complex deformable objects, the multi-degrees of freedom Mass-Spring Models (MSM) [138] or the Finite Element Models (FEM) [35] are considered as the most popular methods, which are widely investigated in soft tissue simulations [35, 36, 95]. However, an online parameter identification for MSM and FEM methods is challenging due to the huge computational complexity [35, 36].

The challenge of real-time modeling for deformable objects is to balance the model accuracy with the computational time for the parameter identification. This section presents a radial function-based deformation (RFBD) method that allows for real-time modeling in pcbMMT systems, while preserving the important properties of the deformable objects, i.e. allowing for tangential deformation under frictional contact.

4.2.1 A model of deformable objects

The parameters of the object (deformable) model can be categorized into three parts: the surface geometry, the physical properties and the dynamics of the surface deformation. The choice of the object model is based on the following assumptions about the environment and the pcbMMT system:

- The surface geometry is described by a 3D point cloud which is captured by a 3D sensor. The point cloud contains no other information except its spatial position. All the points are massless, rigid, and independent units without any spring connection (see Fig. 4.4).

- The physical properties of the object model are considered isotropic, including the stiffness, damping factor, and surface friction. The static and dynamic friction coefficients are considered to be identical.

- The dynamics of the surface deformation are chosen based on the theory of elasticity (Sec. 4.2.2), which should be sufficiently simple to enable online parameter identification, but not so simple that model accuracy is significantly sacrificed.

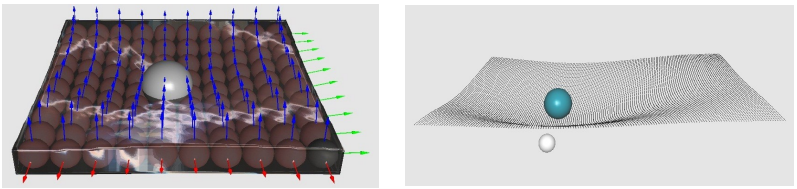

Figure 4.4: Comparison of the membrane deformation between the MSM and the proposed approach. Both models use the proxy-HIP haptic rendering method. (a) The MSM model developed by CHAI3D (www.chai3d.org) with 100 mass balls and 180 springs. (b) The proposed RFBD model with 150×150 points.

Note that the object model does not necessarily need to exactly match the real object in the remote environment, since the slave will update the estimated model parameters once a model mismatch is detected. In addition, the quality of haptic signals is more important than the quality of the visual deformation of the object model. This is because the visual information displayed to the user comes from the live video, not from the virtual object model. Thus, compared to the deviation of haptic signals, we have more tolerance for visual deviation between the real object and the virtual model.

4.2.2 Radial function-based deformation

In the theory of elasticity, the surface deformation of soft objects under external pressure is simply modelled as a contact problem between a rigid end-effector and an elastic half-space [89]. According to the geometry of the contact area, the surface deformation can be described by different radial functions with an infinite deformation area. Fig. 4.5(a) shows the deformation of an infinite elastic half-space with a force applied to it at a single point. The precise analytical solution of this problem given in [89] shows that the longitudinal displacement z is proportional to the inverse of the radial distance r. According to this solution, the deformation at the contact position becomes infinite, which is impossible in our teleoperation system, since the contact area between the slave end-effector and the object surface is more than a single point. In addition, the deformation area on the object surface is infinite, which is too complicated for the object modeling. Thus, we use a sixth-order polynomial radial function with a finite deformation area to approximate the surface deformation of the object model. As illustrated in Fig. 4.5(b), the longitudinal displacement of the object surface z as a function

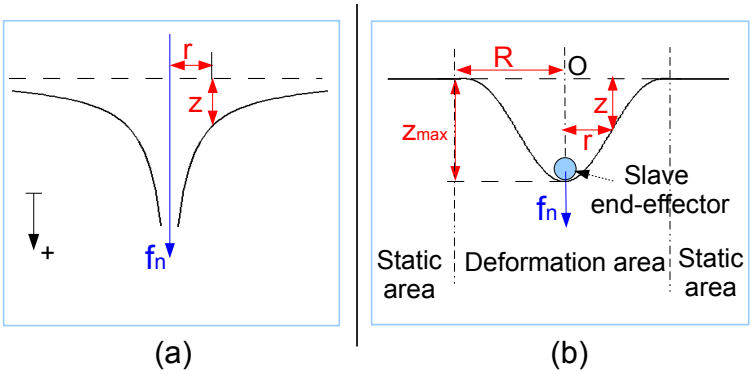

Figure 4.5: Longitudinal deformation of an elastic half-space with a force applied to a small region. (a) The precise analytic solution ($z \sim 1/r$), and (b) the sixth-order polynomial approximation with finite deformation area. O denotes the collision position and x_s is the current slave position.

of the radial distance r can be described as:

$$z(r) = \begin{cases} c \cdot (R^2 - r^2)^3 & , r \leq R \\ 0 & , r > R \end{cases} \tag{4.10}$$

where R is the radius of the deformation area depending on the material of the object. To reduce the number of unknown parameters, we define that R is proportional to the maximal longitudinal displacement z_{max}, described as $R = n \cdot z_{max}$ ($n \in \mathbb{R}^+$). c represents the parameter of the model dynamics depending on the object materials, the force inputs, and the value of R. Although there is a visible difference in the surface deformation between the real and approximated models, it is acceptable if the haptic rendering is accurate, since the visual information displayed to the user comes from the live video, and not from the virtual object model.

4.2.2.1 Longitudinal deformation

The object stiffness, damping factor and dynamics parameter c can be estimated according to the longitudinal deformation of the object surface. Normally, when a force is applied to the surface of a deformable object, the relationship between the normal force f^n and the maximal displacement z_{max} at the contact point can be described as $f^n \sim (z_{max})^p$, where p is a factor with a value between 1 and 2 in most cases [89, 114]. Thus, we use a second-order spring-damper model to approximate the force-displacement relationship on the slave side:

$$\hat{f_s^n} = k_1 \cdot z_{max} + k_2 \cdot z_{max}^2 + b \cdot v_s^n \tag{4.11}$$

where $\hat{f_s^n}$ is the computed slave normal force based on this spring-damper model. v_s^n are the measured slave velocity in the normal direction. b denotes the damping factor. k_1 and k_2 are the stiffnesses for the first and second order.

A least-squares approach is employed to estimate the model parameters $(k_1, k_2, b)^T$ based on the known samples $(z_{max}, v_s^n, f_s^n)^T$,

$$(k_1, k_2, b) = \arg \min_{(k_1,k_2,b)} \left\| f_s^n - \hat{f}_s^n \right\|_2^2 \tag{4.12}$$

where f_s^n is the real slave normal force measured by the slave robot. The velocity v_s^n can also be obtained by the slave robot. Meanwhile, we define a collision position O as the point where a collision is detected on the object surface before deformation. Then, the displacement z_{max} can be computed as the distance between the current slave position x_s and the collision position O: $z_{max} = x_s - O$ as illustrated in Fig. 4.5(b).

In addition, according to (4.10), the displacement at the contact position can also be expressed as $z_{max} = z(0) = c \cdot R^6$. Suppose a perfect model match as $\hat{f}_s^n = f_s^n$, and combined with (4.11) we have

$$c = \frac{-k_1 + \sqrt{k_1^2 + 4k_2(f_s^n - bv_s^n)}}{2k_2 R^6} \tag{4.13}$$

Thus, the surface deformation of the object model can be uniquely determined using the estimated physical properties and the applied contact force. On the master side, the deformation of the object surface can be computed based on the master normal force f_m^n and velocity v_m^n.

4.2.2.2 Tangential deformation

Due to the surface friction, lateral motions of the slave end-effector on the object surface cause tangential deformations [114]. Applying a lateral force that is smaller than the maximal static friction results in local dragging. This means that the tangential deformation of the object surface is limited to a local area, while the contact point is stretched tangentially without

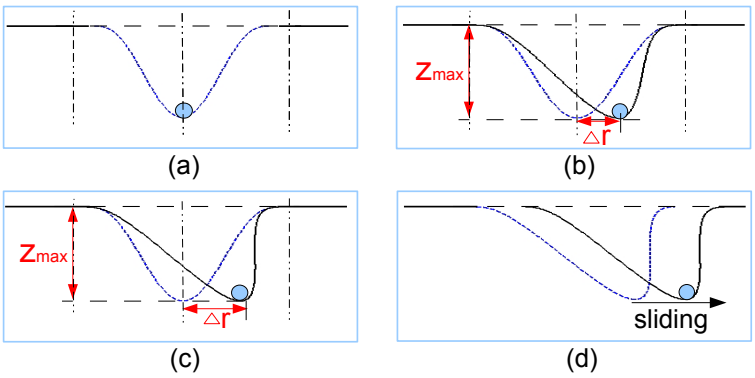

Figure 4.6: The tangential deformation of the object surface approximated by shearing algorithms. The blue and black lines represent the object surfaces before and after the corresponding tangential deformations. (a) Surface without tangential deformation. (b) Small local dragging. (c) Critical local dragging. (d) Global sliding.

sliding relative to the slave end-effector (Fig. 4.6(b)(c)). If the lateral force is larger than the maximal static friction, the contact point between the end-effector and the object surface is released, and a relative sliding occurs [114]. As illustrated in Fig. 4.6(d), we use a global sliding of the deformation area to approximate this effect. This means that the deformation area as a whole follows the end-effector's motion on the object surface without further local dragging. For the local dragging, we use a shearing algorithm to approximate it, which is described as follows:

$$\begin{pmatrix} x' \\ y' \\ z' \end{pmatrix} = \begin{pmatrix} 1 & 0 & s \\ 0 & 1 & s \\ 0 & 0 & 1 \end{pmatrix} \begin{pmatrix} x \\ y \\ z \end{pmatrix} \tag{4.14}$$

where $(x, y, z)^T$ and $(x', y', z')^T$ are the same point in the deformation area on the object surface before and after the local dragging. s is the shearing factor, which depends on the applied tangential force and the physical properties of the object. Given the aforementioned assumption of isotropic physical properties, the slave lateral force can be approximated as:

$$\hat{f}_s^t = k_1 \cdot \Delta r + k_2 \cdot (\Delta r)^2 + b \cdot v_s^t \tag{4.15}$$

where $\hat{f}_s^t$ is the approximated slave lateral force based on the force model. Δr is the dragging distance of the contact point. According to (4.14), Δr can be expressed as:

$$\begin{aligned} \Delta r \mid_{z=z_{max}} &= \sqrt{(\Delta x)^2 + (\Delta y)^2} \mid_{z=z_{max}} \\ &= \sqrt{(x' - x)^2 + (y' - y)^2} \mid_{z=z_{max}} \\ &= \sqrt{2} s z_{max} \end{aligned} \tag{4.16}$$

Suppose a perfect model match as $\hat{f}_s^t = f_s^t$, combined with (4.15) and (4.16) we have:

$$s = \frac{-\sqrt{2} k_1 z_{max} + \sqrt{2 k_1^2 z_{max}^2 + 8 k_2 z_{max}^2 (f_s^t - b v_s^t)}}{4 k_2 z_{max}^2} \tag{4.17}$$

Thus, using the estimated physical properties and the applied lateral forces, the tangential deformation can be determined. On the master side, instead of f_s^t and v_s^t, we use the master lateral force f_m^t and velocity v_m^t to simulate the surface deformation of the object model.

Note that the surface friction coefficient $\mu = f_s^t / f_s^n$ can only be estimated when there is a relative sliding between the slave end-effector and the object surface.

4.2.2.3 Haptic rendering

The pcbHR method as introduced in Sec. 4.1.4 is employed to render the force feedback signals on the master side. Due to the simplicity of the object dynamics model, the haptic rendering

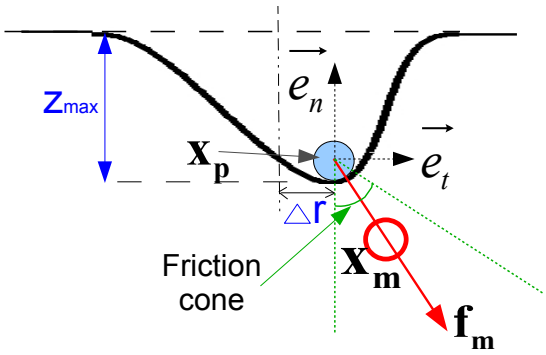

Figure 4.7: Overview of the force rendering approach on the master side.

can run at 1 kHz while the deformation simulation can run at 100 Hz or even higher. As illustrated in Fig. 4.7, the force generated on the master side can be expressed as:

$$f_m^t = k_p(\mathbf{x_m} - \mathbf{x_p}) \cdot \vec{e_t} \quad , and \quad f_m^n = k_p(\mathbf{x_m} - \mathbf{x_p}) \cdot \vec{e_n} \tag{4.18}$$

where k_p is the virtual stiffness between the master proxy and HIP. $\mathbf{x_p}$ and $\mathbf{x_m}$ are the positions of the master proxy and HIP. $\vec{e_t}$ and $\vec{e_n}$ denote the tangential and normal vectors of the contact surface computed by the point cloud. If the master HIP is in the friction cone determined by the position of the master proxy and the surface normal, the tangential deformation of the object surface is limited to a local dragging. Otherwise, it becomes a global sliding.

4.2.3 Feasibility Evaluation

The RFBD method was evaluated for different interactions. The SensAble PHANTOM Omni haptic device with CHAI3D library was used for the evaluation. The simulated environment contained a simple 3D membrane composed of 150 by 150 points placed in the $z = -0.1$ plane with a surface normal of $(0, 0, 1)^T$. All the programs ran on a 3.33GHz Intel® Core(TM) i5 desktop PC with 4GB RAM.

The results of the longitudinal and tangential deformations are shown in Fig. 4.8. We assume that a proper online parameter estimation scheme is adopted and the physical properties of the virtual membrane are already known (set as fixed values). Changing the ratio between the deformation radius R and the maximal longitudinal displacement z_{max} leads to different visual deformations of the object surface. Fig. 4.8 shows the surface deformation in side and top views for the values of $R : z_{max} = 3 : 1$ and $R : z_{max} = 6 : 1$.

During the interaction, the master position and force signals were recorded. As illustrated in Fig. 4.9, at time t_1 the master HIP makes contact with the membrane, leading to an increasing z-directional force. At t_2, a lateral motion starts, resulting in a tangential deformation and an increasing x/y-directional force in amplitude. At t_3, the lateral force reaches the maximal

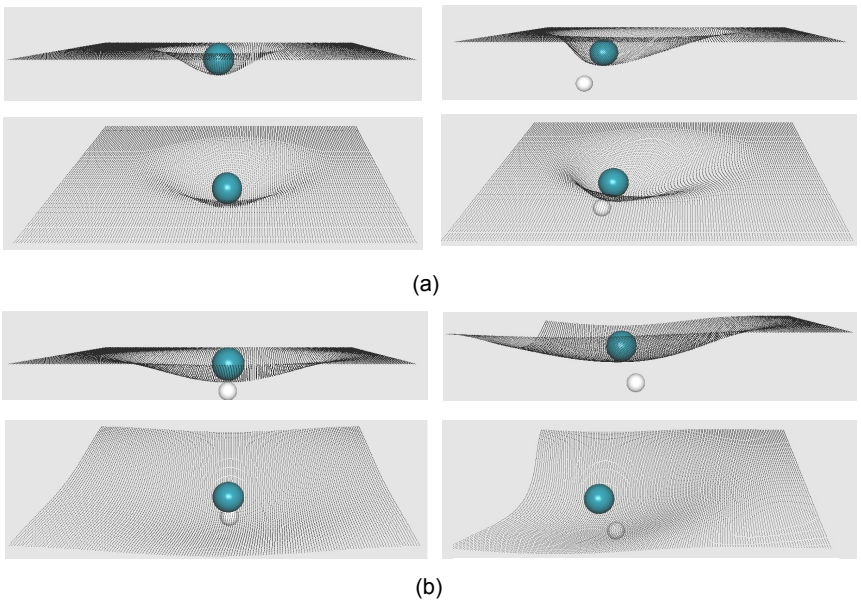

Figure 4.8: Side and top views of the surface deformation. The blue and white spheres represent the master proxy and HIP. (a) $R : z_{max} = 3 : 1$. (b) $R : z_{max} = 6 : 1$. Please refer to http://www.lmt.ei.tum.de/forschung/projekte/prohaptics.html#demos/videos for more video demos.

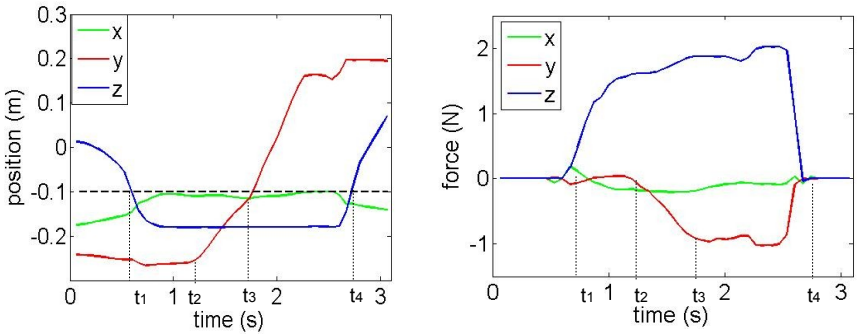

Figure 4.9: Position and locally rendered force signals of the master HIP during its interaction with the membrane.

static friction of the object surface. Thus, a global sliding occurs, and the lateral force stays equal to the surface dynamic friction. After t_4, the contact is released.

In addition, the online parameter identification described by (4.12) is tested with the help of the GSL linear algebra library (http://www.gnu.org/software/gsl/). The computational time for estimating the physical properties $(k_1, k_2, b)^T$ with 100 samples $(z_{max}, v_s^n, f_s^n)^T$ is less than 1 ms, which achieves the requirement of real-time estimation.

The evaluation results show that the RFBD method is able to approximate the surface dynamics of deformable objects under frictional contact. The model parameters can be estimated in real time. With convergent and precise estimation, the RFBD method provides

stable force rendering. Note that the radius of the deformation area (denoted as R) is manually chosen in our experiment. However, this value represents a certain physical property of the object material, which could couple with other physical properties such as stiffness, tension applied to the surface, etc.

4.3 Slave update controller: dynamic and perception-based model update

A model update on the slave side includes the transmission of object geometry and impedance parameters (physical properties). During teleoperation, a continuous updating of the model parameters (object geometry and physical properties) is necessary to ensure high system transparency. For each update, the latest estimated parameters are transmitted back to the master side and the local model on the master side is updated accordingly. Although the packet rate in the backward channel is not necessarily 1 kHz for slowly varying or static environments, excessive updating of model parameters also leads to high packet rate and increases communication load. As discussed in Sec. 2.3.2.2, both the reduction of the estimation rate and the selected transmissions can reduce the packet rate in the backward communication channel. This section presents a perception-based update scheme to selectively transmit the estimated model parameters.

4.3.1 Updating the object geometry

The geometry parameters are updated when a significant geometry mismatch, e.g., a position difference, is detected. The geometry parameters depend on the adopted environment model. For example, if a plane model is employed, the geometry parameters are the plane normal and the plane position. If a spherical model is employed, the geometry parameters are the sphere center and the radius [7]. However, a simple geometry model cannot accurately approximate complex environments. This leads to a large model mismatch and results in frequent model updating.

The use of point clouds in the pcbMMT system avoids frequent model mismatch in geometry parameters. The update of the environment geometry is activated while the slave is in free space. The captured object geometry (point cloud) is directly encoded and transmitted to the master. The geometry updates are deactivated once the slave is in contact with the environment. This is to avoid sudden geometry model changes during the slave's interaction with the environment and to thus ensure a stable exploration. The switch signal is triggered by the measured environment force. If the measured environment force is larger than a pre-defined threshold, the slave is considered to be in contact state. Otherwise, it is in free space.

If the local model is accurate for the current interaction area, the proposed geometry updating scheme allows for stable exploration. However, the slave could try to touch the environment where no point cloud model is available. This happens for instance if the workspace of the master/slave is larger than the field of view of the 3D sensor. This leads to a model mismatch between the slave and master and results in unpredictable distortion. On the master side, as there is no valid point cloud model, the force feedback is zero, while on the slave side the slave end-effector could be still in contact with the object. Extrapolation of the current model across the model boundaries can be a solution. However, once a large force/position difference is detected or the position command exceeds the model boundary too much, the user is asked to stop the exploration and command the slave back to free space. Thus, the geometry updating is activated again and new point cloud data is captured according to the current sensor view.

The captured object surface geometry can be also described and transmitted using triangular meshes. Point clouds are preferred over the triangular meshes for two reasons. First, the pcbHR method, compared with the mesh-based rendering [158], can provide similarly high quality haptic feedback using a simpler and faster collision detection scheme [117, 118]. In addition, if the surface point cloud is captured and streamed in real time, the use of point cloud-based transmission and haptic rendering saves computation time for meshing and collision tree (bounding box) creation.

To verify this, an experiment is conducted to test the time needed for meshing and bounding-box creation for a spherical model. The fast meshing algorithm proposed in [101] (source code from pointclouds.org/documentation/tutorials) and the axis-aligned bounding box (AABB) algorithm (source code from www.chai3d.org) are adopted for this test. This test is run on a PC with Intel(R) Core(TM) i5 CPU, 3.33GHz, 4G RAM. The results are shown in Table 4.1.

Dataset	points	mesh	time for meshing	time for AABB
Sphere 1	4034	7288	75 ms ± 20 ms	ca. 1 ms
Sphere 2	16258	31652	400 ms ± 110 ms	ca. 30 ms

Table 4.1: Computational time of meshing and bounding-box creation for a spherical model with two different resolutions.

According to Table 4.1, real-time meshing of geometry is challenging. The maximum update rate of the meshes is only $1000ms/75ms \approx 13.3$ frames/s for the low resolution spherical model, and $1000ms/400ms \approx 2.5$ frames/s for the high resolution spherical model. However, the resolution of a normal 3D sensor can be even higher than that of the tested model, e.g., 120×160 points as discussed in Sec. 4.1.1.1. The 3D sensor captures many more points than

the tested model and consequently results in more time for meshing and AABB creation. Therefore, transmitting meshes for describing environment geometry is quite difficult.

4.3.2 Updating the physical properties of the objects

For a typical teleoperation system, the haptic signals in the backward channel are transmitted at a rate of 1 kHz. This packet rate can be significantly reduced by applying the PD approach as proposed in [62–64, 69, 134, 135]. For the pcbMMT system, the same approach can be employed to reduce the packet rate in the forward channel where the velocity signals are transmitted. For the transmission of the estimated physical properties in the backward channel, a similar concept can be adopted. Instead of sending every new estimate of the physical properties, only the values which could result in significantly different perception during the user's exploration will be transmitted back to the master. Based on the PD approach, an update is triggered if the difference between the locally rendered master force and the measured slave force is larger than the JND. Triggering updates based on the force JND have some drawbacks, since there are only two choices to obtain the master force on the slave side: (1) Transmit the master force to the slave in the forward channel. (2) Render the force from a local model on the slave side based on the physical properties of the object transmitted to the master. The former method works poorly with increasing communication delay, as the slave receives the master force only after a round-trip delay (T_d). During the round-trip period, the measured slave force and the received master force on the slave side, however, are still mismatching. This results in unnecessary updates and leads to high packet rate in the backward communication channel. The latter method does not suffer from this effect. Yet, it is resource consuming. The whole force rendering algorithm needs to be run at 1 kHz on the slave side in order to simulate the local master force without delay.

An alternative way to selectively transmit the model parameters is to apply JNDs directly to the estimated impedance parameters. If the difference between the current estimate and the most recently sent one is larger than the JND defined by Tab. 2.2, an update is triggered. The difference can be in terms of stiffness, damping, friction coefficient, etc. Compared with the use of only the force JND, this method requires more JNDs for the update decision. However, force rendering is not needed on the slave side, which saves computational resources of the slave system.

If the physical properties of the object are perfectly estimated by the modeling algorithm, there will be no updates required and thus the system achieves zero transmission in the backward communication channel after the initial model transfer. For a real teleoperation system, however, this is impossible. Various factors like noise, human behavior, field of view etc., affect the model completeness and accuracy. Therefore, we expect a certain but not extremely high packet rate reduction while the pcbMMT method is employed.

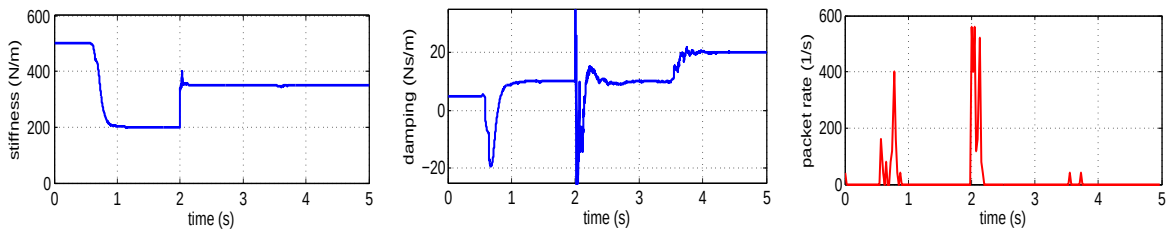

(a) (b) (c)

Figure 4.10: (a) Estimated stiffness values. (b) Estimated damping values. (c) Packet rate vs. time.

An experiment is conducted in simulation to evaluate the feasibility of the perception-based packet rate reduction scheme in the presence of measurement noise and environment changes. The environment is a 1D spring-damper model with an initial stiffness of 200 N/m and an initial damping of 10 Ns/m. A sinusoidal excitation with a frequency of 0.1Hz is used as the input position signal. The self-perturbing recursive least squares (SPRLS) method [110] is used to estimate the impedance parameters (stiffness and damping). At time $t = 2s$, the environment stiffness changes to 350 N/m. At time $t = 3.5s$, the environment damping changes to 20 Ns/m. The updating scheme based on the changes of the impedance parameters is employed to control the data transmission. The JNDs for stiffness and damping are set to be 23% and 34%, respectively, according to Tab. 2.2. In order to show the feasibility of the selective transmission approach, the estimation rate is set to be 1 kHz. This means that the environment impedance parameters are estimated every 1 ms. In practice, it is unnecessary to apply such a high estimation rate for slowly varying environments.

The simulation results are shown in Fig. 4.10. The estimates converge quickly at the initial contact and at the time when the environment changes. High packet rates are also observed at these time periods (see Fig. 4.10(c)). After the estimates converge to the true values, JNDs are not violated and thus no further updates are triggered.

4.4 Master update controller: passivity-based model update

The main task of the update controller on the master side (see Fig. 4.1) is to ensure system stability during the model updating phase. In the MMT systems, the local model must be updated when the environment changes or novel, previously unseen parts are encountered. During the model update, a sudden change of the model parameters leads to model-jump effects and results in unpredictable motion and force. As an example, assume that a simple spring model is used to approximate the remote environment. The model parameters are the object stiffness and initial position. If the slave sends a stiffness update which is larger than the previous one used by the master, and the local model is updated accordingly, a

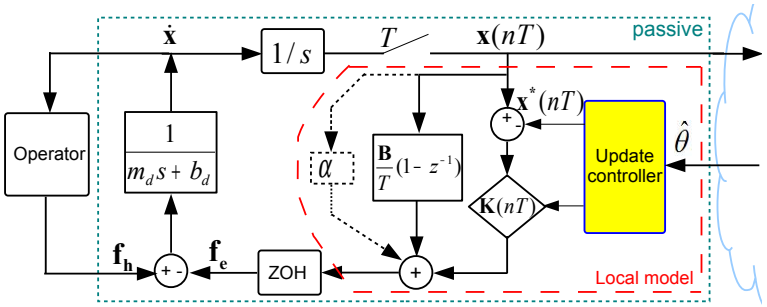

Figure 4.11: A sampled-data master system with a spring-damper model. $\hat{\theta}$ represents the received model parameters, T is the sample period, and ZOH denotes zero-order hold.

suddenly increased force is displayed to the human user. If the user cannot adjust her/his arm impedance quickly enough to follow (stabilize) this force change, an unexpected motion occurs, which can cause dangerous slave behavior. Therefore, a smooth and stable model update is required to mitigate this effect.

This section presents a passivity-based model update (PMU) method for a 3D spring-damper environment model. System stability is guaranteed during the model update if the PMU method is employed. Energy generated due to the changes of the model parameters is dissipated through an adaptive damper element. The sampling effect of the haptic device is also taken into account. The feasibility and performance of the proposed passivity-based model update scheme is evaluated through simulations and subjective experiments.

4.4.1 Overview of master system with environment model

The human operator, the haptic device and the local model on the master side of the MMT system composes the master system. The position/velocity signal of the haptic device is sampled with a constant sampling period T (typically 1 ms), while the force feedback is converted back to the continuous-time domain using a Zero-order Hold (ZOH) element. Figure 4.11 illustrates this sampled-date master system.

The received model parameters on the master side are applied to update the local model. The local model should reflect the most important parameters of the remote environment, but at the same time should not be too complex, otherwise the parameter estimation in real time on the slave side becomes challenging. Since the object position, stiffness, and damping are the most important parameters, in the following of this section we assume that a 3D spring-damper model is adopted to approximate the environment. The model parameters that need to be estimated and transmitted are the stiffness $\mathbf{K} = diag(k_x, k_y, k_z)$, damping $\mathbf{B} = diag(b_x, b_y, b_z)$, and initial position $\mathbf{x}^*$.

The block diagram of the master system with a spring-damper model is illustrated in Fig. 4.11. The haptic device is modeled as a mass-damper system ([11, 32]) with mass m_d

and damping $\mathbf{B_d} = b_d\mathbf{I_3}$. The virtual environment (VE) is a spring-damper model, where $\mathbf{K}$, $\mathbf{B}$ and $\mathbf{x}^*$ denote the object stiffness, damping, and initial position, respectively. All three parameters could change during the model update phase. The effect of the human arm on the system passivity is not taken into account, since it is unknown how the human operator changes her/his arm impedance during the model update phase. Thus, the passivity is only enforced in the part marked by the dotted green rectangle in Fig. 4.11. In addition, low frequency inputs are also assumed, similar to [11, 59, 99]. This means that the sampling rate of the system is substantially faster than the dynamics of the haptic device, human operator, and virtual environment, so that the changes in force and velocity between two samples are small.

4.4.2 Passivity condition

The system is passive if the energy storage W_s is smaller than the work input by the human operator (denoted as W_h) between two samples from $t = 0$ to $t = T$, as shown in [11], where the passivity condition for a 1D spring model with unchanging model parameters is derived. Considering a spring-damper model with varying model parameters (stiffness, damping, and initial position) in 3D space, the passivity condition can be derived in our case as follows.

The input work W_h within a sample period T is:

$$W_h = \mathbf{f_h^T}(\mathbf{x_1} - \mathbf{x_0}) = \mathbf{f_e^T}(\mathbf{x_1} - \mathbf{x_0}) + E_k + \int_0^T \dot{\mathbf{x}}^\mathbf{T}\mathbf{B_d}\dot{\mathbf{x}}dt \tag{4.19}$$

where $E_k = \frac{1}{2}m_d(||\dot{\mathbf{x}}_\mathbf{1}||^\mathbf{2} - ||\dot{\mathbf{x}}_\mathbf{0}||^\mathbf{2})$ denotes the change of the kinetic energy within a sample period. The vector $\mathbf{f_e}$ is the environment force in 3D Cartesian coordinates. $\mathbf{x_0}$ and $\mathbf{x_1}$ are the device position vectors at the time $t_0 = 0$ and $t_1 = T$. The energy storage within a sample period T is:

$$W_s = E_k + E_e = E_k + \frac{1}{2}(\mathbf{x_1} - \mathbf{x_1^*})^\mathbf{T}\mathbf{K_1}(\mathbf{x_1} - \mathbf{x_1^*}) - \frac{1}{2}(\mathbf{x_0} - \mathbf{x_0^*})^\mathbf{T}\mathbf{K_0}(\mathbf{x_0} - \mathbf{x_0^*}) \tag{4.20}$$

where E_e denotes the change of the elastic potential energy within a sample period. $\mathbf{x}^*$ is the object's initial position. $\mathbf{K}$ is the object stiffness matrix. The subscripts of $\mathbf{K}$ and $\mathbf{x}^*$ denote the corresponding time instants $t_0 = 0$ and $t_1 = T$.

The system is passive if $W_h \geq W_s$. By eliminating the terms of the kinetic energy and substituting the rendered environment force $\mathbf{f_e} = \mathbf{K_0}(\mathbf{x_0} - \mathbf{x_0^*}) + \mathbf{B_0}\dot{\mathbf{x}}_\mathbf{0}$ into (4.19):

$$[\mathbf{K_0}(\mathbf{x_0} - \mathbf{x_0^*}) + \mathbf{B_0}\dot{\mathbf{x}}_\mathbf{0}]^\mathbf{T} \cdot (\mathbf{x_1} - \mathbf{x_0}) + \int_0^T \dot{\mathbf{x}}^\mathbf{T}\mathbf{B_d}\dot{\mathbf{x}}dt \geq E_e \tag{4.21}$$

where $\mathbf{B_0}$ is the object damping matrix at $t = 0$. The Cauchy-Schwarz inequality $T\int_0^T \dot{x}^2(t)dt \geqslant (\int_0^T \dot{x}(t)dt)^2$ and the assumption of low frequency inputs ($\mathbf{x_1} = \mathbf{x_0} + \dot{\mathbf{x}}_\mathbf{0}T$) are used to simplify

(4.21):

$$\begin{aligned}&[\mathbf{K_0}(\mathbf{x_0}-\mathbf{x_0^*})+(\mathbf{B_d}+\mathbf{B_0})\dot{\mathbf{x}}_\mathbf{0}]^\mathbf{T}(\mathbf{x_1}-\mathbf{x_0})\\ \geq\ &\frac{1}{2}[(\mathbf{x_1}-\mathbf{x_1^*})^\mathbf{T}\mathbf{K_0}(\mathbf{x_1}-\mathbf{x_1^*})-(\mathbf{x_0}-\mathbf{x_0^*})^\mathbf{T}\mathbf{K_0}(\mathbf{x_0}-\mathbf{x_0^*})]+\frac{1}{2}(\mathbf{x_1}-\mathbf{x_1^*})^\mathbf{T}\Delta\mathbf{K}(\mathbf{x_1}-\mathbf{x_1^*})\end{aligned} \tag{4.22}$$

where $\Delta\mathbf{K}=\mathbf{K_1}-\mathbf{K_0}$. Eq. (4.22) is the passivity condition for the model update. According to (4.22), the change rate of the damping does not affect the system passivity. Thus, we do not consider damping changes in the following analysis, and assume that $\mathbf{B_0}=\mathbf{B}=b\mathbf{I_3}$ is constant. To simplify the analysis, we discuss the change of stiffness and the change of the initial position separately.

4.4.2.1 Stiffness update

Considering only stiffness changes, we assume that $\mathbf{x_0^*}=\mathbf{x_1^*}=\mathbf{0}$. Substituting this into (4.22) leads to

$$\dot{\mathbf{x}}_\mathbf{0}^\mathbf{T}(\mathbf{B_d}+\mathbf{B})\dot{\mathbf{x}}_\mathbf{0}\geq\frac{T}{2}\dot{\mathbf{x}}_\mathbf{0}^\mathbf{T}\mathbf{K_0}\dot{\mathbf{x}}_\mathbf{0}+\frac{1}{2T}\dot{\mathbf{x}}_\mathbf{1}^\mathbf{T}\Delta\mathbf{K}\dot{\mathbf{x}}_\mathbf{1} \tag{4.23}$$

A more conservative condition by applying the passivity condition to each axis independently (1D condition) can be derived as

$$b_d+b\geq\frac{k_0T}{2}+\frac{1}{2}(\frac{\Delta k}{T})\frac{x_1^2}{\dot{x_0}^2} \tag{4.24}$$

Comparing (4.24) to the passivity conditions derived in [11, 32], the term $\frac{1}{2}(\frac{\Delta k}{T})\frac{x_1^2}{\dot{x_0}^2}$ is the additional damping required to achieve system passivity following the increase in stiffness, while low frequency inputs are assumed.

Note that the damping of the haptic device and the environment are fixed during the model update. We manually add an adaptive virtual damper α in the VE to keep the system passive if the device and environment damping b_d+b are not large enough (see Fig. 4.11). Using an adaptive damping element to guarantee the system passivity is also adopted in [59] for an environment with unchanging model parameters.

Rewrite (4.24) by considering α:

$$\alpha\geq\frac{k_0T}{2}+\frac{1}{2}(\frac{\Delta k}{T})\frac{x_T^2}{\dot{x_0}^2}-b_d-b,\quad or \tag{4.25}$$

$$\dot{k}=\frac{\Delta k}{T}\leq 2(\alpha+b_d+b-\frac{k_0T}{2})\cdot(\frac{\dot{x_0}}{x_T})^2 \tag{4.26}$$

Eq. (4.25) shows the lower bound of the extra damper α when the change rate of the stiffness $\dot{k}$ is known. Eq. (4.26) shows the upper bound of the stiffness change rate if the damper α is known. Note that increasing the stiffness has a negative effect on the system passivity. For decreasing stiffness, this is not a problem. The reason is that when increasing the stiffness, energy is generated in the system. If the generated energy cannot be dissipated

by the system damping during the model update phase, the system becomes non-passive. Decreasing the stiffness reduces the energy stored in the system, and thus gains energy budget for the system passivity.

To avoid an infinite damping design in Eq. (4.25) when $\dot{x_0} \to 0$, the adaptive damping α should be upper bounded. This leads to the system being non-passive when the device velocity is close to zero. However, when considering the impedance of human arms, which have a flexible and wide range of damping [71], the operator (human) contributes to make the system more stable because of its own damping [50]. In other words, depending on how the operator holds the device, energy that is generated during the parameter updates can be dissipated by the additional damping of the human arm. Hence, the whole system including the human operator is most likely still passive. A similar assumption, a small non-passive behavior can be compensated by the additional damping of the human operator and the haptic device, is also adopted in [59] for designing an adaptive damping element in an one-dimensional unchanging environment.

4.4.2.2 Position update

A change of the initial position $\mathbf{x}^*$ usually happens when the slave first gets in contact with a new environment (object). Before the first contact, the object position can only be estimated using vision sensors [148] or 3D sensors as presented in Sec. 4.1.2.1. After the contact, the first contact position is regarded as the correct initial object position. The object surface model can be represented by point clouds in a pcbMMT system. The position error of the point cloud surface in the depth direction, which is supposed to be the slave's approaching direction, has a main influence on the contact force and system energy.

Considering only the change of the initial object position in the depth direction (slave's approaching direction), Eq. (4.22) degenerates to be one dimensional, where $\mathbf{x}^* \to x^*$, $\Delta\mathbf{K} \to \Delta k = 0$ and $\mathbf{K} \to k$:

$$\frac{2T\dot{x}_0}{k}[k(x_0 - x_0^*) + (b_d + b + \alpha)\dot{x}_0] + (x_0 - x_0^*)^2 \geq (x_1 - x_0^* - \Delta x^*)^2 \tag{4.27}$$

where $\Delta x^* = x_1^* - x_0^*$. If we suppose that the penetration is in the positive direction, which means $x_1 - x_0^* \geq 0$, then a change of the initial position in the negative direction increases the right part of (4.27) (energy generation), and thus jeopardizes the system passivity. An upper bound of the position change Δx^* in each sample period in the direction of the negative penetration is defined by (4.27), if α is known.

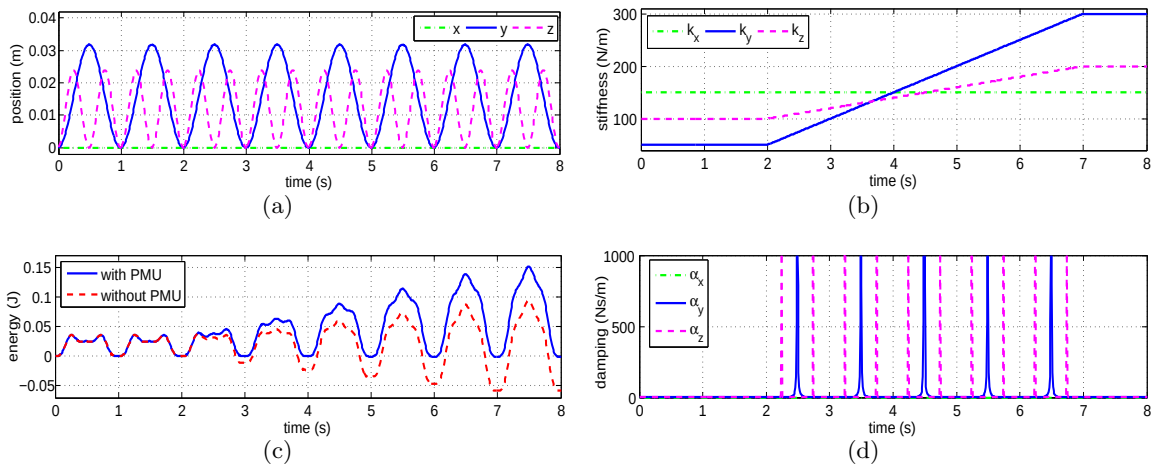

Figure 4.12: Simulation results for a linear stiffness increase. (a) Device position. (b) Object stiffness as a function of time. (c) The net energy output with and without the PMU method. (d) Adaptive damping for system passivity.

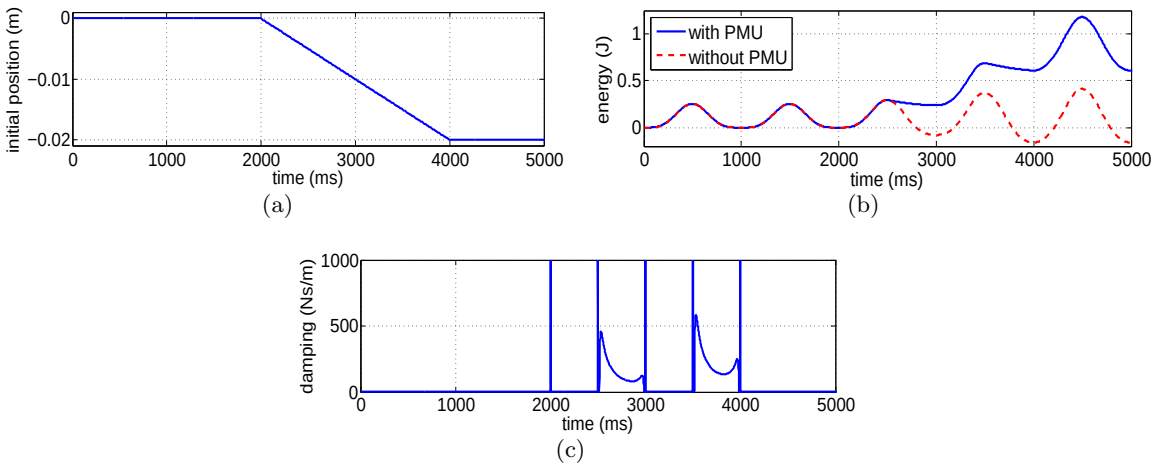

Figure 4.13: Simulation results for the initial position change in the slave's approaching direction. (a) The change of the initial position. (b) The net energy output w/ and w/o the proposed PMU method. (c) Adaptive damping for system passivity.

4.4.3 Evaluation

4.4.3.1 Simulation Study

The proposed PMU scheme was first evaluated using simulation. The local environment was a 3D spring-damper model with an initial stiffness of $\mathbf{K}_{init} = diag(150, 50, 100)N/m$ and an initial damping of $\mathbf{B} = diag(1, 1, 1)Ns/m$. The initial position of the object model was at $\mathbf{x}^* = \mathbf{0}$, and the penetration was in positive direction. The device mass and damping were set to be $m_d = 0.2$ kg and $b_d = 0.5$ Ns/m. During the simulation, the master received new model parameters from the slave side and applied the update accordingly with or without the PMU

scheme.

First only the stiffness changes were taken into account. The stiffness started to increase at time $t = 2$ s with a fixed change rate $\frac{\Delta \mathbf{K}}{T} = diag(0, 50, 20)$ N/(m·s), where $T = 1$ ms was the sampling period. The final stiffness was set to be $\mathbf{K}_{final} = diag(150, 300, 200)$ N/m. In addition, the value of the adaptive damping $\vec{\alpha} = (\alpha_x, \alpha_y, \alpha_z)^T$ was unlimited.

Simulation results are illustrated in Fig. 4.12. The simulated human force $\mathbf{f_h}$ is designed to drive the device position being a sine wave in y and z directions (Fig. 4.12(a)). The net energy output with and without using the proposed PMU method is computed as $E = \int_0^t \mathbf{f_h^T}(\tau)\dot{\mathbf{x}}(\tau)d\tau$, and shown in Fig. 4.12(c). For the case when using the PMU method, the damping $\vec{\alpha}$ is computed according to (4.25), and hence the net energy output stays non-negative. For the case without using the PMU method, $\vec{\alpha}$ is set to be $\mathbf{0}$. Obviously, without using the PMU scheme, the net energy output quickly decreases to negative values (the system is active) due to the stiffness increase.

The results of only updating the initial position are shown in Fig. 4.13. As discussed in Sec. 4.4.2.2, the most important update of the initial position is in the slave's approaching direction. Thus, we design a change of the model's initial position against the slave's approaching direction (Fig. 4.13(a)), which generates energy in the system, and thus leads to negative net energy output if the PMU method is not used (Fig. 4.13(b)). The device has a sine-wave motion in the y-direction as in Fig. 4.12(a), and keeps still in the other two directions. An observation in Fig. 4.13(b) is that with the PMU method, the net energy output does not reduce back exactly to zero. This is because the object position is changed towards the negative direction, while we only control the device position back to zero, which leads to energy storage in the system.

Note that the damping α in both the stiffness and position updates increases to a quite large value once the device velocity is close to zero as illustrated in Fig. 4.12(d) and Fig. 4.13(c). This is not feasible in a real MMT system. Therefore, the adaptive damping should be upper bounded.

4.4.3.2 Subjective evaluation

A subjective experiment was conducted to evaluate the subjective quality of the two cases: using or without using the PMU scheme. The experimental setup is shown in Fig. 4.14. The local model on the master side was implemented in a virtual environment (VE) which was developed based on the Chai3D library (www.chai3d.org). A Geomagic Touch (Phantom Omni) was used as the haptic device. The local environment was a 3D dolphin with isotropic physical properties. Its position, surface friction, and damping stayed constant during the experiment, while its stiffness could change according to the received model parameters.

During the experiment, the subjects were asked to interact with the virtual dolphin in

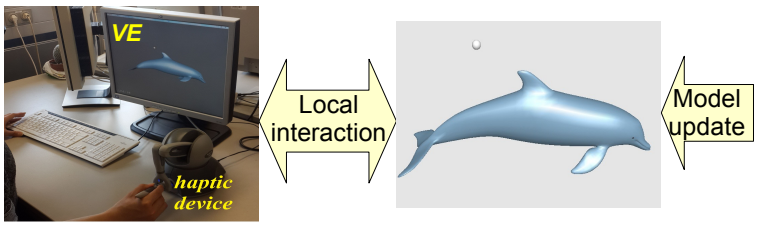

Figure 4.14: Experimental setup.

different ways: pressing, slow tapping, fast tapping. The interaction was repeated several times for both cases: with or without the PMU scheme. One second after the first contact, the VE received an update and the stiffness of the dolphin increases from initially 100N/m to finally 500 N/m. With the PMU scheme, the adaptive damping was fixed to 5 Ns/m. The stiffness update was thus based on (4.26) in each axis. Without the PMU scheme, the stiffness increased linearly from 100 N/m to 500 N/m in 700 ms.

10 subjects participated in the experiment. Two questions were asked after the experiment: 1) Do you feel the stiffness change? 2) Only being concerned about the stiffness change, which case feels more comfortable, with or without the PMU? Meanwhile, the stiffness update times are recorded.

The experimental results are shown in Table 4.2. For question 1), all the participants perceive the stiffness change. For question 2), 60% of the answers vote for the method "with PMU", and 10% of them prefer the scheme "without PMU", while 30% vote for "no difference". In addition, with the PMU scheme enabled, the average update time is $t_{update} = 546ms \pm 91ms$, which has a comparable (average reduction of 22%) update time compared to the method without the PMU. Subjects who prefer "with PMU" are mostly satisfied with the moderate force change during the model update. This is the benefit of using the adaptive damper. Thus, we conclude that the proposed PMU scheme on the one hand guarantees the system stability, on the other hand leads to a more comfortable model update within a comparable update time, compared to the method without using the PMU method.

Table 4.2: Results of the subjective test.

	with PMU	without PMU
Preference	60%	10%
Average t_{update}	546ms ± 91ms	700ms

Note that according to (4.26) the stiffness is not updated when the interaction velocity is zero. Therefore, the update time of the PMU scheme strongly depends on the interaction behavior. In this subjective test, the subjects keep moving the device during their interaction with the environment, leading to a comparable update time, compared to the linear update

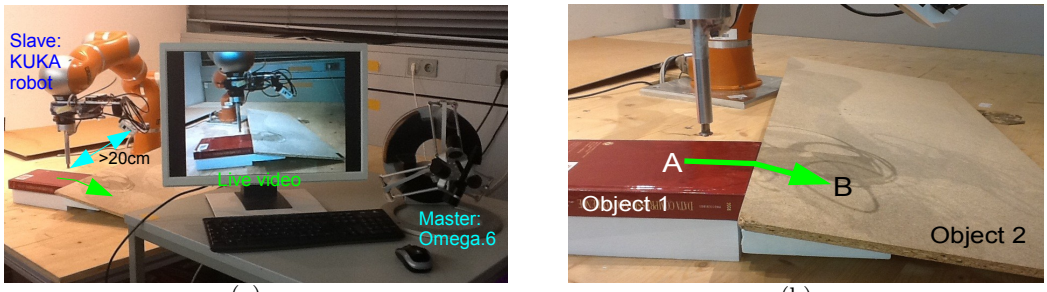

(a) (b)

Figure 4.15: (a) The setup of the teleoperation system. (b) The tested remote environment, which consists of two objects, one is a horizontally placed book with a smooth hard cover and the other one is a declining wooden plank. The green arrow from point A to point B denotes the trajectory of the slave motion during the test.

method. Much longer update time are possible for other interaction behavior with the PMU method. To avoid this issue, it is necessary to set a non-zero lower bound of the stiffness update rate in addition to (4.26).

4.5 Evaluation of the pcbMMT system

This section presents experiments that evaluate the performance of the entire pcbMMT system in terms of position/force tracking, packet rate reduction, and subjective experience*.

4.5.1 Setup

A Force Dimension® Omega.6 and a KUKA Lightweight arm were used as the master and slave devices (Fig. 4.15(a)). A JR3 force sensor (6 DOF force/torque sensor) was mounted at the end-effector of the slave robot to measure the contact force. The measured force was automatically calibrated and decoupled by the sensor SDK. Gravity, inertial forces were also compensated in the force measurement. The Argos®3D-P100 ToF camera was used to capture the depth images. The measurement errors of the 3D sensor have been already compensated by using a look-up table during the camera calibration procedure. Besides, a RGB camera was used on the slave side to capture the video signals of the slave robot. The software environment was based on ROS (www.ros.org), the FRI library (cs.stanford.edu/people/tkr/fri/html) and the SDK of Force Dimension.

As illustrated in Fig. 4.15(b), the remote environment is composed of two objects: a hardcover book with a smooth surface (object 1) and a plank with a relatively rough surface (object 2). Object 1 is placed horizontally on a hard base while object 2 is arranged with a small slope and supported by foam boards. Therefore, during the experiment different stiffness

*Please refer to http://www.lmt.ei.tum.de/forschung/projekte/prohaptics.html#demos/videos for more video demos.

values and surface friction coefficients for the two objects are expected. The exploration trajectory is illustrated in Fig. 4.15(b) with a green arrow. The slave robot is first commanded to touch the point A, after the contact is stable, it is controlled to move across the two object surfaces along the trajectory. At point B, the slave end-effector leaves the object surface. During the exploration, the system estimates the object stiffness k as well as the friction coefficient μ and triggers updates according to the changes of the estimates. The packet rate in the communication channel is also recorded. The forward and backward communication delays are set to be constant with $T_f = T_b = 500ms$.

4.5.2 Results

4.5.2.1 Position and force tracking

Figure 4.16 shows the measured position and force signals on both the master and the slave side in world coordinates. The master position and force signals are shifted by the forward communication delay T_f for easier comparison. Table 4.3 shows a summary of the slave status based on its motion. Before t_1, the slave is in free space and commanded to approach the object 1. At t_1, the slave gets in contact with object 1. Between t_1 and t_2, the slave end-effector stays in contact with object 1 without moving. At t_3, the slave reaches the boundary of the two objects, which leads to a disturbed slave force, especially in Fig. 4.16(f). Between t_4 and t_5, the slave stays on the surface of object 2 without moving. After t_5 the slave is controlled to leave object 2 and returns to free space again. Between t_2 and t_3, since the slave is moving on the surface of a horizontally placed object, the force in z-direction is mainly affected by the penetration depth and the environment stiffness, while the forces in x-direction and y-direction are caused by surface friction. Between t_3 and t_4, the slave is in contact with a declining object. Therefore, the force signals in all three directions have influence on the estimation of the object stiffness and friction coefficient.

The estimated stiffness and friction coefficient values are shown in Fig. 4.17. The time period between t_1 and t_2 is considered to be a time buffer to enable a stable slave contact

Table 4.3: Slave status during the operation.

Time	Contact	Motion
$0 \sim t_1$	No	Yes
$t_1 \sim t_2$	object 1	No
$t_2 \sim t_3$	object 1	Yes
$t_3 \sim t_4$	object 2	Yes
$t_4 \sim t_5$	object 2	No
$t_5 \sim$	No	Yes

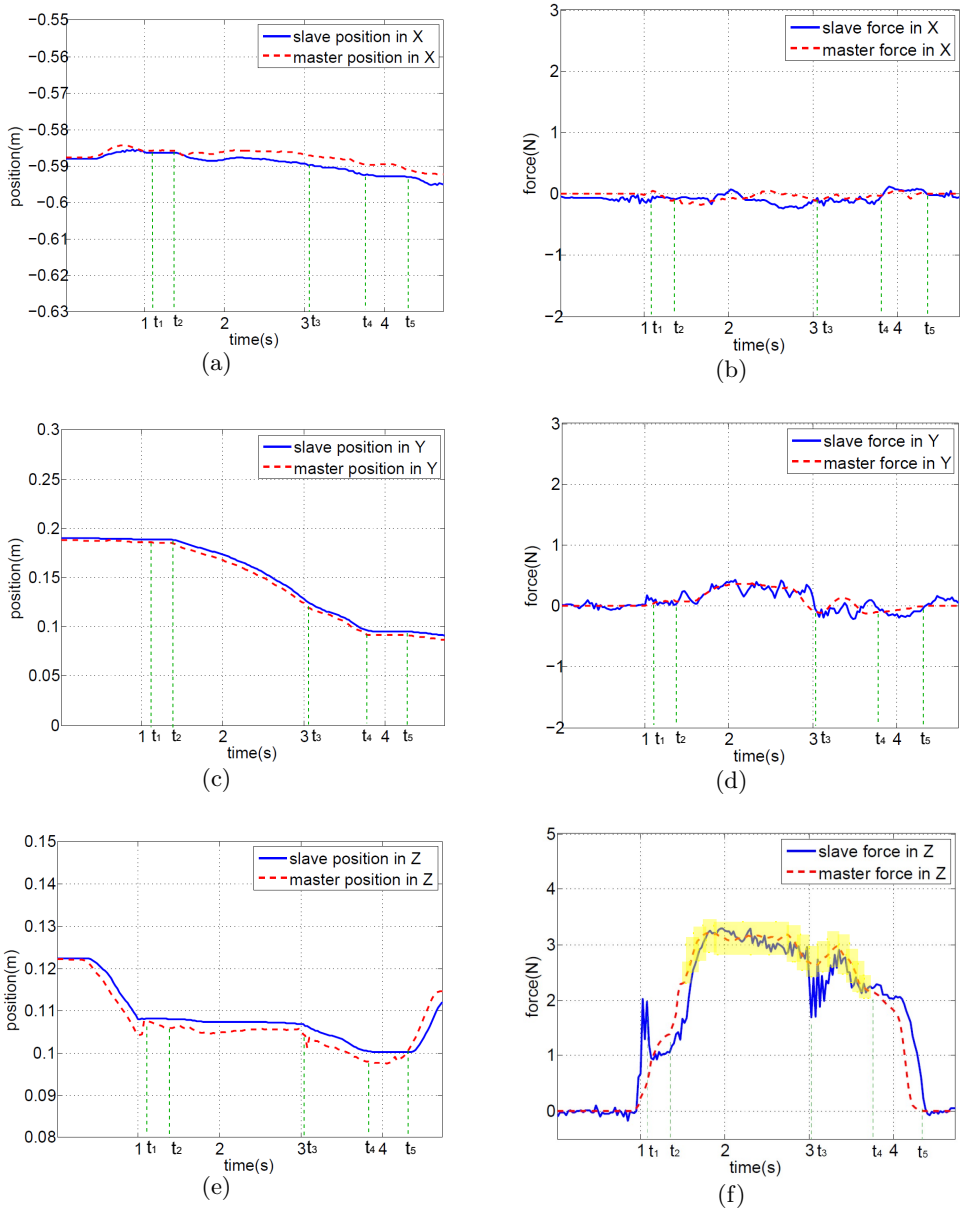

Figure 4.16: Experimental results. (a)(c)(e) the master and slave position in x, y and z directions, respectively. (b)(d)(f) the locally rendered master force and the remotely measured slave force in x, y, and z directions, respectively. The yellow region in (f) represents the 10% deadband with respect to the master force.

before obtaining the effective physical properties. In the periods $t_2 \sim t_3$ and $t_3 \sim t_4$ the system measures the stiffnesses k_1 and k_2, and friction coefficient μ_1 and μ_2 for the two objects. The mean and standard deviation (Std.) values of the estimated physical properties are shown in Tab. 4.4. Since object 2 is supported by foam boards, which are softer than the base of object 1, the estimated stiffness of object 2 is lower than for object 1. In addition, the estimated friction coefficients between the two objects are also different due to the different surface

smoothness of the two objects. A statistical analysis shows that significant differences exist for the estimated stiffnesses and friction coefficients (T-test $p < 0.01$, Ranksum test $p < 0.01$). Thus, the pcbMMT system successfully detects the different physical properties for the two objects. In addition, after time instant t_2 in Fig. 4.17(b), a peak for the friction coefficient is detected, which is caused by static friction before the end-effector's stable sliding over the surface (dynamic friction).

Note that between t_1 and t_2 the measured stiffness value changes rapidly, while the master force does not change as quickly. According to the master update controller (Sec. 4.4), the stiffness value on the master side is not immediately updated once a new update arrives. Instead, it is altered smoothly and gradually based on the master's motion. Between t_2 and t_4, the slave contacts with the objects stably (except at the time around t_3). Thus, the estimated model parameters (stiffness and friction coefficient) of the remote objects are stable too. From Fig. 4.16(f) we observe that once the contact is stable, the difference between the locally rendered master force and the remotely measured slave force are almost smaller than 10% (the yellow region in Fig. 4.16(f)). According to the limits of human haptic perception, the user can hardly distinguish the difference between the master force and the slave force, which implies that the estimated environment model is sufficiently accurate and the system is perceptually transparent.

Table 4.4: Mean and standard deviation of the estimated stiffness values and friction coefficients for the two objects.

	k_1	k_2	μ_1	μ_2
mean	1410 N/m	870 N/m	0.108	0.214
Std.	140 N/m	180 N/m	0.014	0.018

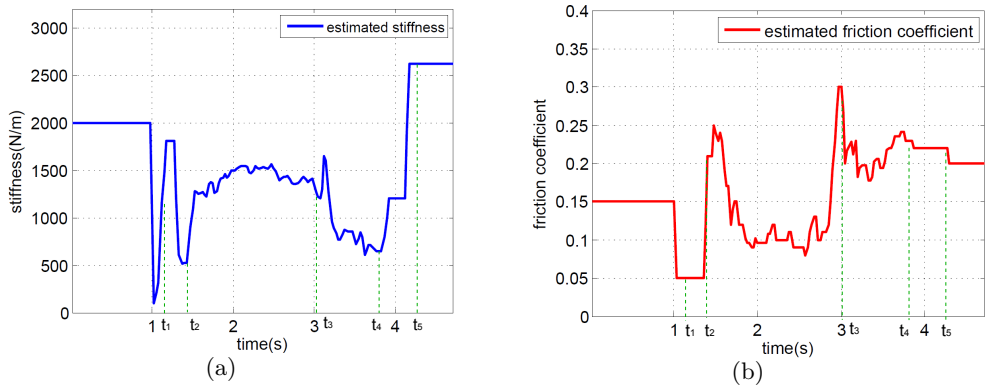

(a) (b)

Figure 4.17: (a) Estimated stiffness. (b) Estimated friction coefficient.

4.5.2.2 Data reduction

The achieved data reduction includes the compression of the point cloud model and the reduction of the update packet rate for the physical properties of the objects.

To evaluate the point cloud compression, a total of 40 filtered depth images are recorded during a 5-second slave movement in free space, which includes the slave statement of still, slow motion ($< 5cm/s$) and rapid motion (up to $20cm/s$). The lossless H.264/AVC compression algorithm with IPPP... GOP (group of pictures) structure is applied, where the I frame period is 10. The results are shown in Tab. 4.5. Due to the GPU acceleration, the compression time of the depth images is negligible compared to the communication delay. Even for the worst case (25 Hz update rate), the maximum required bitrate in the communication channel is still moderate ($3.85\ kB \cdot 8 \cdot 25\ Hz = 770\ kbps$).

The update packet rate vs. time is shown in Fig. 4.18. The DBP is 0.23 for the stiffness and 0.1 for the FC. High packet rates are observed at t_1, t_2, t_3 and after t_4. At t_1, the slave first gets in contact with object 1. The system starts to estimate the stiffness of object 1. Since the estimated stiffness is significantly different from the initial one, new updates are triggered. At t_2, the slave starts to slide across object 1, and thus, the friction estimation is activated and the estimated friction coefficients are transmitted to the master for updating the previous value. At t_3, the slave is moving across the boundary between object 1 and object 2. Due to the disturbed slave force (Fig. 12(f)), the estimated physical properties are varying intensely, resulting in a large number of updates. After t_4, the slave starts to leave object 2. The drastic change of the estimated stiffness results in a high packet rate.

During the contact time period ($t_1 \sim t_5$), the total average packet rate is 103 packets/s, which shows a packet rate reduction of about 90% in the backward communication channel compared to the uncompressed rate (1000 packets/s).

4.5.3 Subjective test

A subjective experiment was conducted to additionally evaluate the system transparency. Before the experiment, the live video of a 10-second-teleoperation was recorded. During teleoperation, the slave and master force signals were also recorded after the system estimates a stable environment model. During the experiment, the recorded video along with the slave/master force signals were replayed to the subjects. The subjects were asked to focus on

Table 4.5: Frame size and compression time for the depth images of the point cloud model.

	Mean	max.	min.
frame size	3.36kB	3.85kB	2.74kB
compression time	1.7ms	3ms	1ms

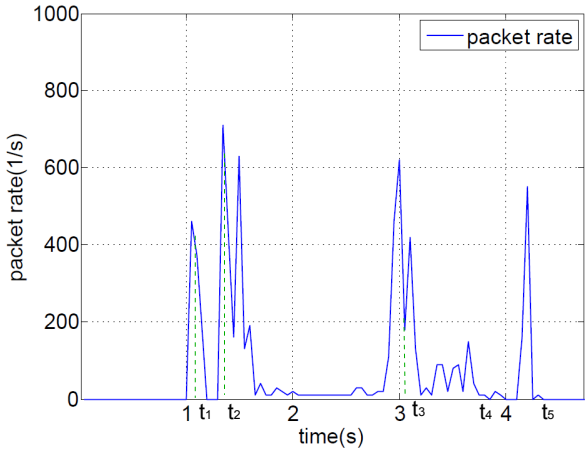

Figure 4.18: Packet rate for transmitting the physical properties in the backward channel during the teleoperation.

the force feedback while watching the replayed video. All subjects were trained until they felt comfortable with the experimental setup and the task.

The experiment was composed of 6 trials. In each trial, two force signals (either slave-slave force, slave-master force, or master-master force) were displayed to the subjects and the subjects needed to answer whether they feel any difference in the quality of the two force signals. In four of the total six trials the slave-master force signals were displayed, while in the remaining two trials the slave-slave forces and master-master forces were displayed. A subject was considered to fail to distinguish between the slave and master force signals, if she/he gave the answer "no difference" more than twice in the four trials where the slave-master force signals are displayed.

10 subjects participated in the experiment, ranging in age from 25-44, all right-handed. The experimental results for each subject are illustrated in Fig. 4.19.

Nine out of ten subjects give the answers "no difference" more than twice when the slave-master force signals are displayed, which means 90% of the subjects fail to distinguish between the remotely measured slave and locally rendered master force. Therefore, we conclude that the slave force is perceptually identical to the master force and the pcbMMT system is thus perceptually transparent for the tested scenario.

4.6 Discussion

As discussed in Chapter 2, the design of a reliable MMT system encounters three challenges: environment modeling, data transmission, and system stability in the transition states. The pcbMMT system presented in this chapter extends the state-of-the-art MMT method to be able to deal with complex environment geometry. Corresponding perception-based data trans-

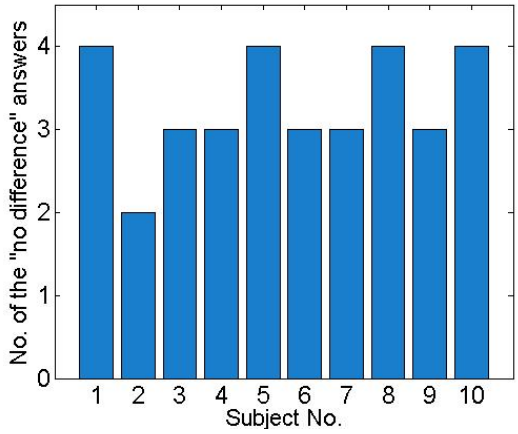

Figure 4.19: Results of the subjective experiment. We only count the numbers of the "no difference" answers when the slave-master force signals are displayed.

mission and passivity-based model update schemes were developed to guarantee the efficiency and stability of the pcbMMT system in the transition states. These schemes address some of the MMT challenges for special scenarios and teleoperation settings. To adapt for different environments, network conditions, and teleoperation tasks, the pcbMMT system needs to be further studied.

4.6.1 Modeling of complex environments

The current pcbMMT method is not capable of dealing with movable objects in a 3D environment. For modeling movable objects, the complete model dynamics, including the object mass, friction, free motion, rotation behaviors, etc., need to be taken into account. This is too complex to be described and modeled in real time. One of the major questions relates to the extent to which the applied model can differ from the actual environment such that the MMT system is still operated stably and efficiently. In other words, either simple or complex models can be adopted to approximate the environment. The former one is easy to apply online but leads to large model mismatch and frequent model update (high packet rate), while the latter one provides a precise approximation (less frequent update) but is challenging for real-time estimation. The RFBD method presented in Sec. 4.2 studies the possible trade-off between model accuracy and model complexity. In general, the RFBD method enables online parameter estimation for deformable models by means of degraded physical accuracy. However, it is still unknown to which extent the employed model can be physically inaccurate but perceptually plausible. Future studies in this direction should focus on developing low cost and perceptually plausible models for deformable and movable objects.

4.6.1.1 Model estimation on the master side

One issue of using precise but complex model for approximating the environment is the computational load on the slave side, since the model estimation is running in real time at the slave system. An alternative structure for MMT is to place the model estimator on the master side. Similar structures are employed in [30, 92, 146]. In this case, the data exchanged over the network are the haptic signals (motion and force), and not the environment parameters. This structure reduces the computational load on the slave side. However, the slave position, velocity and force signals need to be continuously transmitted to the master, to ensure the accuracy of the online parameter estimation. Even in the case of constant contact force, signals still need to be transmitted, as a constant slave contact force does not mean that the estimation on the master side already converges. This alternative MMT structure can be used for example for ground-space teleoperation systems in which the computational capacity of the slave computer is limited by weight or cost restrictions, but communication quality is guaranteed by sufficiently high communication priority and capacity.

4.6.1.2 Non-parametric modeling

One of the prior conditions for environment modeling is that the environment model needs to be approximately known. However, the environment model can be partially or completely unknown if the slave enters an environment that is either new, has been changed, or has been previously explored, but for which historical data is not fully available (e.g., due to memory limitations). Although the environment model can be learned during teleoperation, the learning duration is unpredictable. In this situation, it is difficult to employ any models to approximate the environment; hence, non-parametric environment modeling methods can be used. The task of non-parametric environment modeling is to directly identify the linear or nonlinear input-output mapping of the slave-environment behavior which is independent of the environment complexity. One of the non-parametric environment modeling methods is the neural network-based (NN-based) online estimation [93, 94, 131, 132]. This method uses the slave position, velocity and acceleration as the input, and the measured slave contact force as the output. The aim of this method is to online train the NN weights to provide a precise input-output mapping. The accuracy and convergence of the NN weights highly depend on the design and training algorithm of the neural network.

4.6.2 Modeling of human behavior

Just as the environment can be modeled on the slave side, human behavior can be modeled on the master side. The estimated model parameters of human behavior on the master side are transmitted to the slave to guide the slave's motion. The slave is thus not controlled by the delayed master motion commands, but performs specific tasks in complete autonomy based on

the received human behavior model. Similarly, if the model as well as the model parameters can accurately approximate the user's behavior, the slave can behave like a human user and a complete skill transfer can be realized.

Modeling human behavior for MMT systems has not been studied intensively so far, since human behavior is normally complicated (e.g., nonlinear) and time-varying during teleoperation. It is difficult to model such a behavior in real time. A compromise is to use fixed and predefined models to describe the motion of the human arm [115, 146], and to guide the slave motion during teleoperation.

4.6.3 Selective transmission of model parameters

The perception-based dynamic model update scheme presented in Sec. 4.3 is able to adaptively transmit the estimated model parameters to reduce the packet rate in the backward communication channel. There are two transmission schemes: model update is triggered 1) based on the force JND between the computed master local force and the measured slave force, or 2) based on the human JND of the impedance parameters. The former one is simple, but not adaptive to different teleoperation tasks and interaction. For example, in the experiment of stiffness discrimination, the subjects are normally asked to press the materials with varying forces and velocities. According to Table. 2.2, the force JND is only ca. 10%, while the stiffness JND is about 23% for hard contact with a linear spring. This means that a 20% stiffness difference is not perceivable, though this stiffness difference leads to a 20% force difference. In this case, transmitting model parameters based on the stiffness changes is preferable rather than based on the force JND. This indicates that the choice of the transmission scheme should adapt to the teleoperation tasks. For complex environments with multiple impedance parameters, the update scheme should consider not only the task, but also the effects of the combination of different impedance parameters on human perception. Therefore, model updates will be triggered according to the change of the model vector containing the most important impedance parameters.

4.6.4 System transparency

A comprehensive study on system transparency for MMT is not available in literature.

For MMT systems in the steady state, system transparency depends on the accuracy of the model estimation. The estimated model impedance Z_{est} will be directly transmitted to the master and displayed to the human user. Therefore, Equation (2.21) as discussed in Chapter 2.4 can be used to measure the steady-state transparency.

For MMT systems in the transition state, system transparency is affected mainly by the duration of the transition state. The duration T_{trans} can be defined as a sum of the round-trip delay T_R, the convergence time of the parameter estimation T_{conv} on the slave side, and the

duration of the model updating T_{update} on the master side:

$$T_{trans} = T_R + T_{conv} + T_{update} \tag{4.28}$$

The smaller T_{trans} is, the shorter the transition state lasts, and thus the less model mismatch the MMT system has. Ideally, the duration of the transition state should be zero; thus, the model mismatch in the transition state is avoided. However, this is impossible due to the communication delay and the non-zero convergence time of the model estimation algorithm. The use of a quickly converging estimation algorithm and a fast model updating scheme can improve system transparency. However, too short of an updating time leads to model jump effects and results in instability as discussed in Sec. 4.4. From this perspective, stability and transparency become conflicting objectives.

In the transition state, the parameters of the local model are time-varying, leading to time-varying displayed impedance. Frequency analysis of the displayed impedance cannot perfectly describe the time-varying impedance. The time-frequency analysis methods such as the short-time Fourier transform (STFT) can simultaneously analyze the time-frequency response. The total transparency of MMT systems should be a combination of the transparency error in the steady and transition states.

4.7 Chapter Summary

Environment modeling, data transmission, and system stability in the transition states are the main challenges for MMT systems, which were studied in this chapter.

For the first challenge, this chapter presented a pcbMMT system that extends the state-of-the-art MMT method for dealing with complex environments in the presence of communication delays. The environment model is no longer approximated by simple geometry, but by point clouds. The point cloud model is built with the help of a ToF 3D sensor (Sec. 4.1). During teleoperation, the environment parameters (geometry and physical properties) are estimated and transmitted back to the master side. The developed RFBD method allows for real-time modeling of deformable objects while preserving the important surface deformation dynamics (Sec. 4.2).

For the second challenge, a slave update controller was developed based on known human perception limits to reduce the packet rate and avoid excessive data transmission, while guaranteeing subjectively high teleoperation quality (Sec. 4.3).

For the third challenge, a master update controller (passivity-based model update scheme) was proposed to guarantee system stability during the model update on the master side.

Feasibility of the entire pcbMMT system was evaluated with a real teleoperation setup. By exploiting the limits of human haptic perception, the proposed pcbMMT achieves a significant haptic data reduction of about 90% for the tested scenario.

Strengths and further challenges of the pcbMMT system were discussed at the end. In summary, it can be stated that the pcbMMT approach has the benefit of being simultaneously stable and transparent for environments with complex geometry but relatively simple impedance parameters. To adaptively deal with different environments and teleoperation tasks, the pcbMMT system needs to be further studied. Here is a suggestion of future work for the pcbMMT method.

- develop a more realistic point cloud-based deformable model, which might be physically not accurate due to its low cost for online modeling, but is perceptually plausible for human users.
- develop a dynamic slave model update scheme, which triggers transmission from the slave to the master adaptively based on teleoperation tasks, environments, and the joint changes of the most important model parameters as well as force.
- analyze system transparency for pcbMMT systems in the steady and transition states and develop transparency metrics for measuring teleoperation quality.

Chapter 5

Toward Joint Optimization of Communication and Control for Networked Teleoperation

In Chapter 3 and 4, two different solutions for haptic data reduction in time-delayed teleoperation systems are presented. To achieve significant haptic data reduction without degrading system stability and transparency, the approach described in chapter 3 combines the TDPA (with energy prediction) with the state-of-the-art perceptual deadband-based haptic data reduction approach (PD+TDPA+EP), while the approach in chapter 4 is based on an extended MMT method using a 3D sensor (pcbMMT method) and combines it with the PD approach based on the human JND of the estimated impedance parameters (denoted as PD+MMT).

Different control and communication approaches introduce different types of artifacts into the system. Their performance varies between tasks (e.g. free space versus contact, soft objects versus rigid surface, etc.), and they also differ in their robustness towards different network quality of service (QoS) parameters. For example, the PD+TDPA method presented in Chapter 3 introduces sudden force changes and displays environment stiffness softer than it should be, when the delay is large. The pcbMMT system can provide high teleoperation quality for large delays, if the model estimation is accurate. However, it can introduce excessive model updates which require high packet rate and disturb the display of the actual environment impedance, especially, when the slave first interacts with the environment or the applied model on the master side strongly mismatches the real environment.

Thus, the implementation of teleoperation systems using realistic communication networks requires a more holistic view. Communication and control need to be optimized jointly to achieve the best possible trade-off between system performance and QoS requirements. In other words, the teleoperation system needs to adaptively switch between different control and communication schemes according to the current QoS parameters so that system performance is always guaranteed at the highest possible level. The system performance metrics can

represent the quality of control (QoC), the quality of experience (QoE), the quality of task (QoT) or QoS-related characteristics as illustrated in Fig. 5.1(a). Stability of the teleoperation system is required for any joint solution. Transparency, as the most important performance metric, can be described as the match between the impedance of the remote environment and the impedance displayed to the human users [90]. Additional quality measures can represent task dependent properties like position or force tracking errors, control and communication induced artifacts like sudden discontinuities in the displayed force signals or communication properties like the amount or burstiness of the generated traffic.

The system performance metrics are used to identify the best-suited control and communication approach and their joint parametrization for a given QoS support offered by the network. A hypothesis is that different joint solutions vary not only in their performance for a fixed set of QoS conditions, but also vary in their robustness towards individual QoS parameters (see Fig. 5.1(b)). Identifying the system performance for an offered QoS-level is important to realize adaptive teleoperation systems that can cope with varying network conditions, while still guaranteeing the best possible performance. To date, however, there is neither a common understanding about the preferred control/communication approaches for certain QoS parameters, nor generalizable results about the required QoS to achieve a certain teleoperation quality.

This chapter aims to verify the hypothesis of Fig. 5.1(b) using an experimental case study. System performance of the two joint solutions (PD+TDPA+EP and PD+MMT) is evaluated in the presence of different QoS parameters (communication delays). The environment is a simulated 1D non-linear soft object. The system performance is evaluated in terms of the perceived transparency, the quality of experience, and the packet rate over the communication channel. The experimental design and the analysis of the experimental results are presented in Sec. 5.1. Factors that affect system performance as well as further research work toward joint optimization of communication and control for networked teleoperation are discussed in Sec. 5.2.

5.1 Experimental Case Study

To jointly optimize communication and control for networked teleoperation, the main question should be answered first: whether an adaptive use of the joint solutions leads to better system performance compared to the use of any single joint solution?

Typically, a high-quality teleoperation system should have superior performance in terms of both objective quality (e.g. system control and system transparency) and subjective quality such as task performance, quality of user experience, etc. Various factors, such as the tasks the teleoperation system is performing, the QoS the network is offering, the local model that is

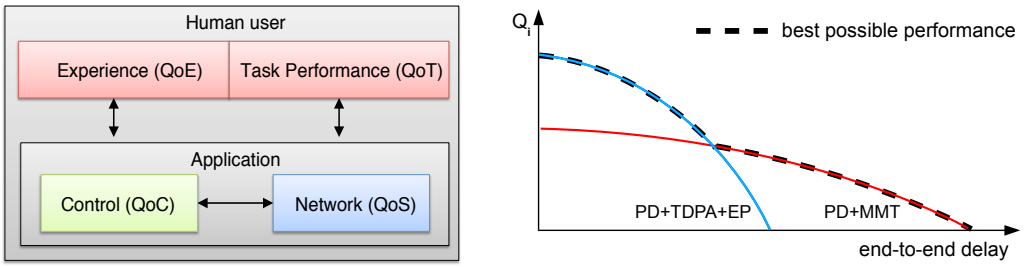

Figure 5.1: (a) Various system performance measures can be applied to objectively compare the quality of different control and communication approaches. (b) Hypothetical performance measure for the previously proposed two joint solutions as a function of the end-to-end delay.

used to approximate the remote environment, etc., have influence on the system performance. The influence is, however, quite different for various control schemes.

For example, as discussed in Chapter 3, the main artifacts of the PD+TDPA+EP method are the sudden force changes caused by the passivity controller and the reduced system transparency (softer displayed object stiffness) due to communication delay. Since communication delay always exists in geographically distributed teleoperation systems, the aforementioned artifacts are unavoidable if the TDPA is used as the control scheme. On the other hand, as discussed in Chapter 4, the main distortions of the PD+MMT method come from the model mismatch and the resulting model-jump effects. Note that the MMT method is able to guarantee very high system performance that is hardly affected by communication delay, if the applied local model perfectly matches the remote environment. In a real teleoperation system, however, a perfect match is challenging due to the high complexity of or the limited knowledge about the remote environments. Thus, the model mismatch in MMT systems is to a certain extent also inevitable.

The experimental study in this section focuses on the subjective teleoperation quality. The main artifacts and distortions of both joint solutions (PD+TDPA+EP and PD+MMT) were taken into account. The tested scenario was an interaction with a 1D soft object with non-linear properties. The performance of both joint solutions in the presence of difference communication delays were evaluated subjectively in terms of the perceived transparency and the quality of experience. The packet rate over the communication channel was recorded and analyzed.

5.1.1 Experimental setup

The experiments were conducted in a virtual environment (VE) developed based on the Chai3D library (www.chai3d.org). The Phantom Omni haptic device was used as the master, while the slave in the VE was designed as a single haptic interaction point (HIP) with negli-

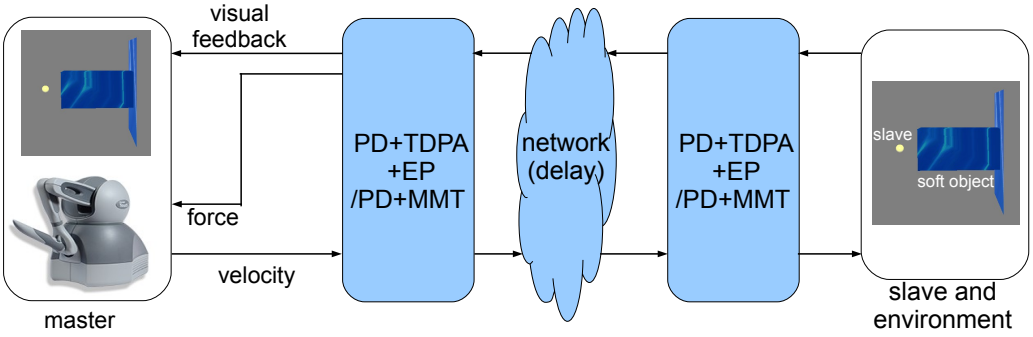

Figure 5.2: Experimental setup. The communication network, the slave (represented by a haptic interaction point), and the virtual environment are simulated on a PC using the CHAI3D library.

gible mass. The network was simulated in a local PC. The VE contained a 1D non-linear soft object, whose parameters were designed based on the Hunt-Crossley model [75]

$$f_e = \begin{cases} Kx^n + Bx^n\dot{x} + \Delta f & x \geq 0 \\ 0 & x < 0 \end{cases} \tag{5.1}$$

where f_e is the interaction force (environment force) and Δf is the Gaussian distributed measurement noise with a mean of 0 N and a standard deviation of 0.1 N. x denotes the penetration (compressed displacement). Corresponding parameters are set as: $K = 200$ N/m, $n = 1.5$, and $B = 0.5$ N/ms. For the PD+MMT method, a simple linear spring model ($\hat{f}_e = \hat{K}x$) was employed to approximate the environment. This leads to model mismatch and excessive changes in the estimated model stiffness $\hat{K}$ during interaction. The passivity-based model update scheme introduced in Chapter 4.4 was applied to ensure stable model update on the master side.

The whole experimental setup is illustrated in Fig. 5.2. The experiments were conducted on a PC with an Intel Core i7 CPU and 8 GB memory.

5.1.2 Experimental procedure

The tested round-trip delays were 0 ms, 10 ms, 25 ms, 50 ms, 100 ms, and 200 ms. For each delay, the subjects tested three conditions: the PD+TDPA+EP method, the PD+MMT method, and the zero delay reference without using any control scheme. For the former two tested methods (the two joint-solution methods), the DBPs for both the force and stiffness were set as 0.1, while for the last one (the reference) the DBP was zero. The reference can display the original environment impedance to the subjects and provides the best teleoperation performance (uncompressed, non-delayed) for this system setup.

A summary of the most important parameter settings for the experiment is listed in Tab. 5.1.

master	Phantom Omni
slave	virtual HIP with negligible mass
environment	non-linear spring-damper model (Hunt-Crossley mode)
tested methods	PD+TDPA+EP, PD+MMT, the reference
local model for PD+MMT	simple linear spring model
tested delays (ms)	0, 10, 25, 50, 100, 200 (0 for the reference)
DBP	0.1 (0 for the reference)

Table 5.1: Parameter settings for the experiment.

The subjects interacted with the virtual object by pressing on the surface and slowly varying the applied force (at about 0.3 Hz with a visual guide). Comparisons were made between the two joint-solution methods and the reference in term of perceived transparency and interaction quality. After each comparison, the subjects had to first answer the question "which combination method shows more similar impedance (stiffness) to the reference". To quantitatively understand the difference of the two joint solutions in terms of subjective quality, the subjects were asked to give a rating by comparing the interaction quality between the two joint-solution methods and the reference. They should take all perceivable distortions (e.g. the force vibration, the force jumps, the perceived stiffness jumps, etc.) into account when evaluating the interaction quality. The rating scheme is based on Table 2.7. The reference, designated level 5, is considered as the best performance. The reference signals can be recalled at any time during the experiment. Each delay case was repeated four times. The order of the tested delays as well as the order of the tested joint-solution methods were randomly selected.

Twelve subjects participated in the experiment. They ranged in age from 25 to 33 and all were right handed. A headset with active noise cancellation was worn to isolate the subjects from ambient noise. The subjects were provided with a training session. The experiments started as soon as the subjects felt familiar with the setup and procedure.

5.1.3 Results

5.1.3.1 Environment modeling for PD+MMT

Before discussing the results of the subjective evaluation, it is necessary to pay attention to the modeling results of the PD+MMT method. Different from the PD+TDPA+EP method, in which the communication delay has a dominant influence on system performance, the modeling accuracy is the key factor that affects system performance of the PD+MMT method. This means that once the applied model in the PD+MMT method is fixed for a static or slowly varying environment, the teleoperation quality degrades slowly with increasing delay.

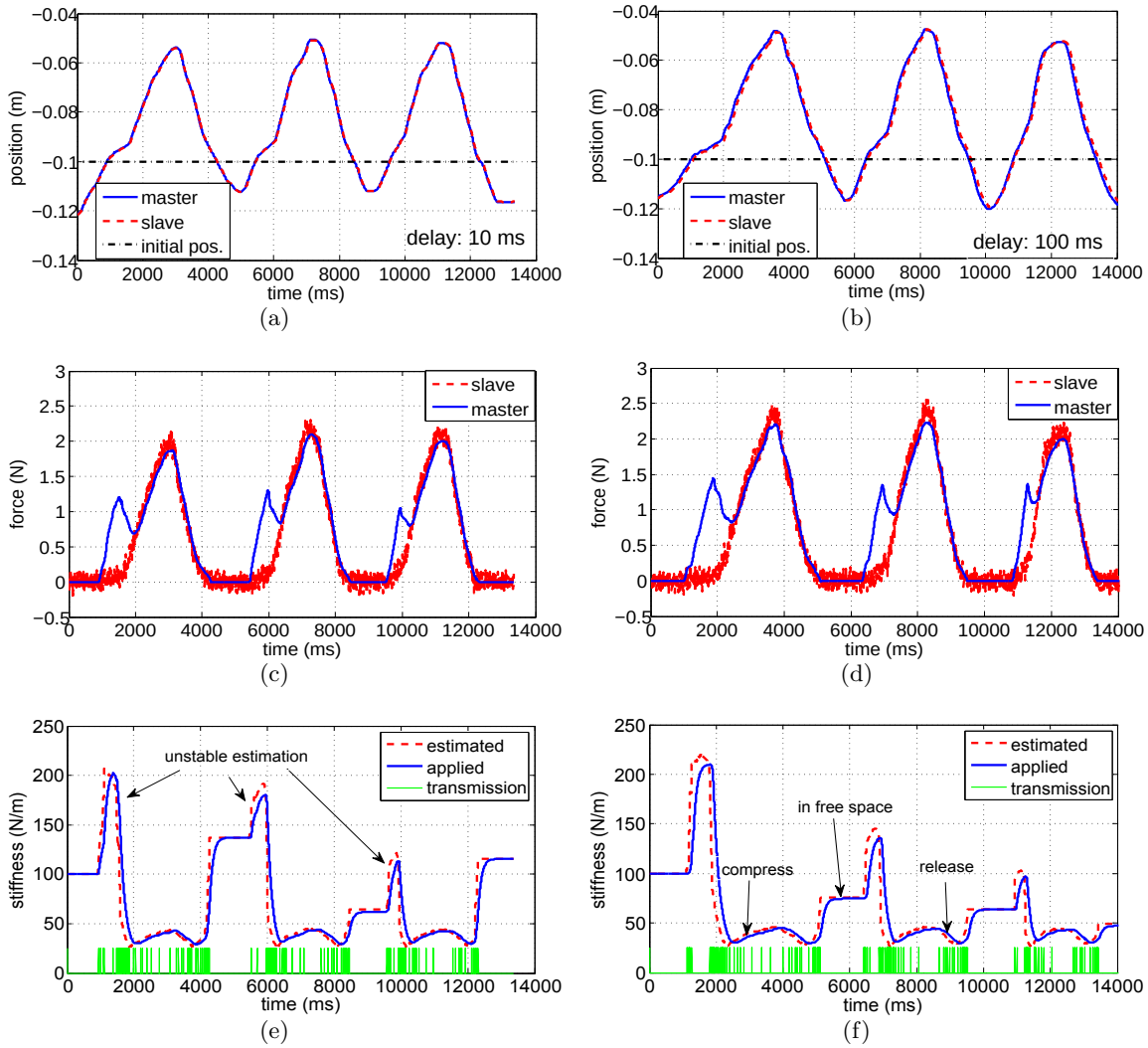

Figure 5.3: Measurements of the position and force signals and the estimated stiffness for the PD+MMT method. (a)(b) The master and slave position signals for 10 ms and 100 ms delays. (c)(d) The master and slave force signals for 10 ms and 100 ms delays. (e)(f) The estimated, transmitted, and applied stiffness values for 10 ms and 100 ms delays.

As an example, the measurements of the position, force, and estimated stiffness for delays of 10 ms and 100 ms are shown in Fig. 5.3. For both delays, similar master position inputs lead to similar force signals and parameter estimates. For the PD+TDPA+EP method, the force signals in the presence of 10 ms and 100 ms delays are illustrated in Fig. 5.4. Significant differences between the force of 10 ms delay and the force of 100 ms delay can be observed. This verifies that the communication delay in the tested range has only minor effects on system performance for the PD+MMT method.

According to Fig. 5.3(c) and 5.3(d), unexpected peaks are observed in the master force signals. This is because of the overshooting in the stiffness estimation (unstable estimation) at every initial contact instant. After the estimates converge to the correct values, the master

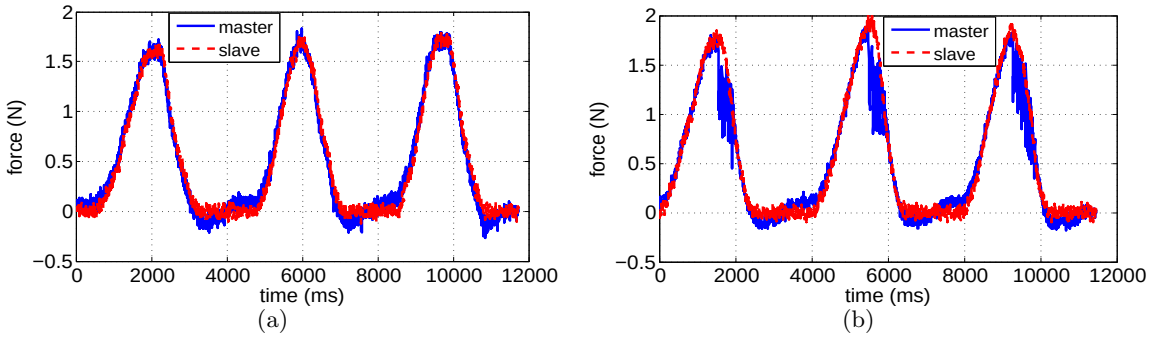

Figure 5.4: Measurements of the force signals for the PD+TDPA+EP method. (a) Delay of 10 ms. (b) Delay of 100 ms.

force, which is computed locally based on the applied linear spring model, follows the slave force without much deviation.

The estimated, transmitted, and applied stiffness values for 10 ms and 100 ms delays are shown in Fig. 5.3(e) and 5.3(f). The use of the PD approach avoids excessive transmission of the estimated stiffness data (see the green bars). The initial stiffness value for the local model is set to be 100 N/m before the slave's first contact with the object. Except the time periods of overshooting and free space motion, the estimates slightly vary during the compress and release phases, leading to frequent packet transmission. Since a linear spring model is used to approximate the non-linear soft object, the estimated stiffness cannot be a constant value during the interaction. The more the object is compressed, the higher is the estimated stiffness. In addition, the passivity-based model update scheme as introduced in Chapter 4.4 is employed to guarantee stable and smooth changes in the applied stiffness values on the master side (represented by the blue solid lines).

Note that the strongly varying estimated stiffness at each initial contact leads to a mismatch between the master and slave force. This can disturb the subjects' perception of the object stiffness and jeopardize the teleoperation quality.

5.1.3.2 System performance vs. communication delay

The result of the subjects' answers to the questionnaire (stiffness similarity to the reference) is shown in Fig. 5.5(a). The two joint solutions vary significantly in the subjects' choices for different communication delays. For small delays, most subjects believe that the PD+TDPA+EP method, compared to the PD+MMT method, shows a more similar stiffness to the reference. For large delays, in turn, the PD+MMT is perceptually more preferred. As discussed in Sec. 5.1.3.1 and shown in Fig. 5.3(e) and 5.3(f), the displayed environment stiffness of the PD+MMT method does not quickly decrease with increasing communication delay. However, it does when the PD+TDPA+EP method is used. This means that the perceived stiffness of

using the PD+MMT method is almost invariant with increasing delay and is mainly disturbed by the unstable estimation at each initial contact. On the other hand, the perceived stiffness of using the PD+TDPA+EP method can be close to the original environment stiffness (reference) when the delay is small, and it becomes very soft and deviates significantly from the reference when the delay is large. Therefore, the PD+TDPA+EP method receives most votes from the subjects for small delays, while the PD+MMT method is preferred for large delays.

The quality of the perceived stiffness is an important metric for system transparency. It is also relevant to the quality of task performance for teleoperation tasks such as tele-surgery and tele-palpation. For example, when a doctor palpates or examines the lesions of an organ or a tissue, the perceived stiffness is normally considered as one of the key factors. For a remote palpation using a teleoperation system, the ability of displaying the undistorted environment impedance to the operator can be the decisive factor. Fig. 5.5(a) implies that by using the PD+TDPA+EP method for small delays and the PD+MMT method for large delays the quality of perceived stiffness as well as the quality of task performance are improved.

Furthermore, a quantitative evaluation for the two joint solutions is illustrated in Fig. 5.5(b). The subjective rating for the PD+MMT varies only slightly with increasing delay. Especially, it is nearly constant between delays of 10 ms and 100 ms, since the force signals and the stiffness estimation for these delays are quite similar (see also Fig. 5.3). For the PD+TDPA+EP method, although it is able to provide relatively higher subjective quality for small delays, the subjective rating decreases quickly with increasing delay. This is because the subjects perceived more vibrations and force jumps when the delay is large. The overall rating result indicates that the subjective quality of the PD+MMT method is not mainly affected by communication delay. Thus, using the PD+TDPA+EP method for low delays and the PD+MMT method for large delay can gain higher subjective quality than the use of any single joint solution.

In conclusion, the hypothesis in Fig. 5.1(b) is verified subjectively for the tested teleoperation task and communication delays. The answer to the question raised at the beginning of this section is affirmative.

Note that the subjective quality of the PD+MMT method can also strongly degrade when the delay further increases, e.g. to more than 1 s. In this case, the parameters of the local model cannot quickly follow the latest estimates of the environment due to the large delay. This leads to a long duration of the transition state (model mismatch), and can be misleading in the perceived environment impedance. However, for teleoperation under quite large communication delays, operators should be experienced and well trained. A good training can to a certain extent compensate for this potential distortion in the operator's perception.

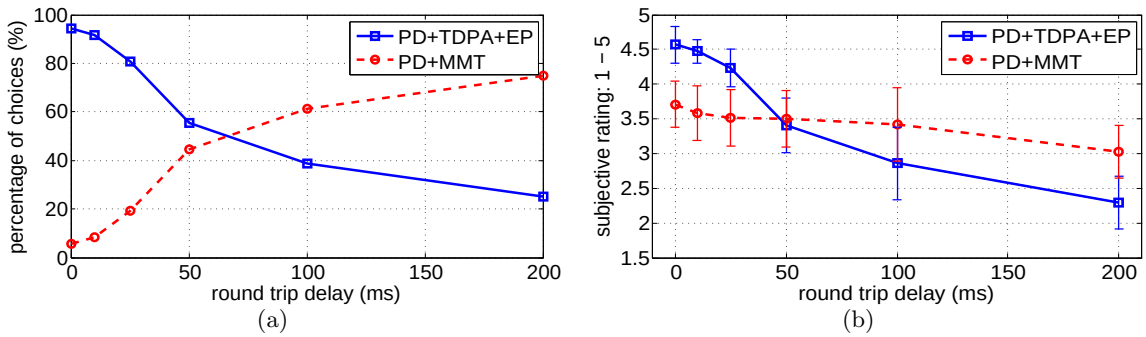

Figure 5.5: Experimental results. (a) The proportion of the subjects' choices in the two joint solutions based on the perceived stiffness similarity compared to the reference. (b) The average and standard deviation of the subjective ratings on the quality of experience for the two joint solutions.

5.1.3.3 Packet rate reduction

Packet rate reduction over the network without introducing significant distortion is an important system capability to adaptively deal with different network QoS. It can be achieved using a proper DBP for the PD+TDPA+EP method as discussed in Chapter 3.3.2. Furthermore, the MMT method does not require a high update rate, especially for static or slowly varying environments. Model parameters are updated only when significant model mismatch is detected. For the PD+MMT method, the stiffness is estimated every 1 ms based on the most recent 100 samples (position and force). The DBP in this experiment is set to be 0.1 for both joint solutions, indicating that a packet transmission is triggered when the change in force or estimated stiffness value is larger than 10%.

The average packet rates of the two joint solutions over all subjects during their interaction with the soft object are shown in Fig. 5.6. Although the applied local model mismatches the environment model, the average packet rates of the PD+MMT method is still much lower than for the PD+TDPA+EP method. This is one of the strengths of the PD+MMT method compared to the PD+TDPA+EP method. For the PD+MMT method, triggering of packet transmission is concentrated in the periods of unstable estimation (e.g. at initial contact and during release). For the PD+TDPA+EP method, the average packet rates over the tested delay range are smaller than 50 packets/s, which are quite lower than the simulation results shown in Fig. 3.14(d) (about 200 packets/s). This is mainly because of the interaction frequency. In Fig. 3.14(d), the tested interaction frequencies range from 0.01 Hz to 100 Hz, and the packet rate is averaged over all tested frequencies. Obviously, larger interaction frequency leads to more quickly varying velocity and force signals, resulting in higher packet rate. In this experiment, the subjects controlled their interaction frequency to be lower than 1 Hz with the help of a visual guide. Therefore, the experimental result in Fig. 5.6 does not conflict with the simulation result in Fig. 3.14(d).

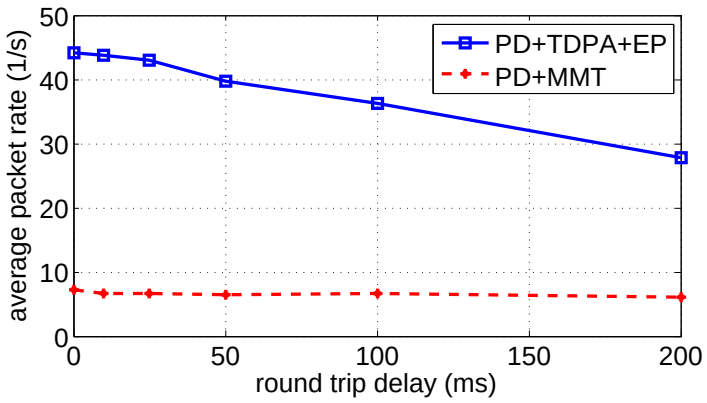

Figure 5.6: Average packet rate over all subjects during the interaction with the soft object.

In summary, both joint solutions are able to strongly reduce the packet rate for the tested interaction task. However, if the applied local model for the PD+MMT method is more accurate, the packet rate during the interaction can be additionally reduced.

5.1.4 Conclusions

According to the discussion in Sec. 5.1.3, the following conclusions can be drawn:

- System performance of the PD+MMT method mainly depends on the accuracy of the applied local model. Once the local model is fixed, communication delay has only limited influence on the force quality as well as the estimation behavior. In the tested delay range, the PD+MMT method can provide nearly constant interaction quality. The displayed stiffness also less depends on the communication delay.

- The quality of interaction and the displayed stiffness in the PD+TDPA+EP method, in turn, quickly degrades with increasing delays. For small delays, this method is able to provide better subjective quality than the PD+MMT method.

- The PD+MMT method generates fewer packet updates even for a significant model mismatch. However, it requires more computational resources for environment modeling and parameter estimation.

- An adaptive use of the two joint solutions can improve the overall subjective quality for different communication delays and thus achieve better system performance. This implies the necessity of jointly optimizing communication and control in teleoperation systems for different network QoS.

5.2 Discussion and Open Research Questions

The communication delay is considered as one of the main QoS factors. Our experiments show a gain in subjective quality when adaptively using the two joint solutions for different communication delays. Other QoS factors, such as delay variation, packet loss rate, and transmission capacity, can also have a strong influence on the system performance. A comprehensive evaluation should take all possible QoS parameters into account. Besides this, the cost for environment modeling in the PD+MMT method is also unignorable. Teleoperation systems need to determine whether it is worthy to spend system computational resources for MMT to gain potential performance improvement for the current network QoS. This is especially challenging when the environment is complex. For example, the processing and transmission of the surface point cloud for the pcbMMT system as discussed in Chapter 4 is resource-demanding, but it improves the modeling accuracy in geometry. Furthermore, if teleoperation systems have sufficient knowledge about the remote environment or a pre-scanning procedure as well as an offline modeling is acceptable, such as tele-surgery with the help of medical Magnetic Resonance Imaging (MRI), it is preferred to use the PD+MMT method that guarantees higher system performance for a large range of QoS parameters.

The necessity of adaptively using the joint solutions is verified by this experiment. The next question following the experimental results is when to switch between different joint solutions according to varying QoS parameters. In other words, the relationship between system performance and the offered QoS needs to be quantitatively determined. This includes two open questions: 1) achievable system performance for a given QoS, and 2) required QoS for a desired system performance.

Achievable system performance for a given QoS

For the first question, future work could focus on defining system performance metrics, which will allow us to analyze and to compare different control and communication approaches for bilateral teleoperation systems. The goal is to derive relationships that map the QoS support offered by the communication network, the stability-ensuring control schemes, and different data communication/reduction approaches to various system performance measures:

$$Q_i = \mathcal{F}_{\mathbf{i}}(\vec{p}, C, D) \tag{5.2}$$

where $\vec{p}$ denotes the QoS parameters. $C \in \{C_1, ..., C_M\}$ is the set of control schemes, $D \in \{D_1, ..., D_N\}$ represents the haptic data communication and reduction schemes, and Q_i denotes the i^{th} system performance metric. The system performance metrics Q_i can represent both the objective and subjective teleoperation quality, e.g. system transparency, subjective transparency, the QoC, QoT, etc. The control schemes can be the TDPA, the MMT, the WV, or the input-to-state stability [79] method, while the communication schemes can be various

haptic data reduction methods introduced in Chapter 2.2.1.

Required QoS for a desired system performance

This is to establish models to quantitatively identify the required QoS to achieve a desired performance of the teleoperation system. Intuitively, low-latency communication is a desirable property for a highly-immersive teleoperation session. The communication network, however, cannot always provide the desired conditions, especially for long-distance teleoperation across continents, where communication delay is lower bounded by the speed of light. A well-defined and robust control and communication architecture can cope with deteriorated QoS conditions, which, however, also affect the system performance. At the same time, the system can tolerate a certain performance degradation while still being able to successfully complete a task. Furthermore, certain system performance demands might be impossible to satisfy with certain QoS while still guaranteeing stability. In these cases, a compromise needs to be made to satisfy at least the most important performance measures for a certain task.

5.3 Chapter Summary

Joint optimization of control and communication is important to realize adaptive teleoperation systems that can cope with varying network conditions, while still guaranteeing the best possible interaction performance. This requires an adaptive switching between different control and haptic communication schemes for various QoS offered by the network. This chapter presents first results in this direction, which experimentally verify that an adaptive use of different control/communication schemes for various communication delays is able to subjectively improve system performance.

The performance of the PD+TDPA+EP method is mainly influenced by communication delay. The larger the delay, the softer is the displayed impedance (stiffness), and the stronger the distortion in the force signals. On the other hand, the performance of the PD+MMT method depends to a large extent on the model accuracy. The distortion introduced by the modeling error is almost constant for a certain delay range. Even when the delay is small, the system performance or interaction quality can still be low due to the modeling error and frequently updated model parameters. Hence, the PD+TDPA+EP method is more suitable for small delays, while the PD+MMT method is more preferred for large delays. The adaptive use of these two methods is able to avoid the drawbacks of each method and thus to improve the overall system performance.

Future work could focus on the quantitative evaluation of system performance for various QoS parameters. This requires a mapping from the known QoS, control and communication schemes to the various performance measurements, including QoC, QoT, QoE, etc. Further investigation would be in the methodology of an inverse mapping, which is able to provide a

suggestion of required QoS for a desired system performance. Considering the tolerance of the human user in operation and perception as well as the tolerance of the control in teleoperation systems, the required QoS can be within a range.

Chapter 6

Conclusion and Future Work

The work presented in this thesis focuses on haptic data communication and reduction for time-delayed teleoperation over packet-switched networks. Teleoperation systems with haptic feedback allow a human user to immerse into a distant or inaccessible environment to perform complex tasks. High packet rate (typically 1 kHz) and system stability in the presence of communication delay are the two main issues for haptic communication in time-delayed teleoperation systems. Teleoperation across communication networks, hence, requires a tight integration of communication and control with the involved robotic systems at the operator and the remote side. Perceptual deadband coding approaches for kinesthetic data reduction and various stability-ensuring control schemes for dealing with time delay have been individually researched upon over the past decades. Joint solutions combining haptic data reduction and stability-ensuring control schemes have not yet received much attention.

In Chapter 3 and 4, two joint solutions are presented, which combine the perceptual deadband-based haptic data reduction approach (PD approach) with the time domain passivity approach (TDPA) and the model-mediated teleoperation (MMT) method. The presented joint solutions achieve a strong packet rate reduction while guaranteeing system stability for time-delayed teleoperation systems in real life challenging scenarios. In Chapter 5, an experimental case study for the development of adaptive teleoperation systems was presented. It aimed to jointly optimize the communication and control schemes, thus to achieve the best possible system performance for various quality of service (QoS) provided by the network. A summary of the main contributions for each part of this thesis is given below, along with ideas for future research.

6.1 Haptic Data Reduction using the Time Domain Passivity Approach

In Section 3.1, the PD approach was combined with the TDPA (PD+TDPA). The TDPA was able to guarantee system passivity regardless of the used data reduction scheme. This

joint solution allowed for a reduction of the haptic packet rate of up to 80% in the presence of unknown and time-varying communication delays, without significantly degrading subjective quality during teleoperation.

The simple combination method (PD+TDPA) introduced a more conservative control behavior compared to the original TDPA during communication interruptions due to haptic data reduction. This led to stronger force jumps and vibrations in the force signals. To address this issue, Section 3.2 proposed a novel energy prediction (EP) scheme to adaptively predict the energy during communication interruptions and thus compensate for the conservative control behaviors (PD+TDPA+EP). Objective and subjective teleoperation quality were evaluated and compared with other joint solutions from literature. Results showed that the PD+TDPA+EP scheme can improve the objective and subjective quality, while achieving higher data reduction compared to other combination methods.

Limitations and Future work

The EP scheme cannot guarantee full passivity in the presence of time-varying delay and packet loss. System energy can be overestimated, which leads to active behavior. With the help of a forced-transmission scheme (Sec. 3.2.2), the active behavior can be limited and the overestimated energy is upper bounded. However, the system is no longer guaranteed to be passive. In extreme cases such as high packet loss rate, the active behavior is unpredictable. In addition, position drift is an important challenge for the two-channel TDPA structure. This leads to workspace mismatch and can result in task failure.

More knowledge about the network characteristics is helpful for further improving the performance of the EP scheme. Real-time estimated network parameters can be used to compute an upper bound of the energy estimation, thus allows the EP scheme to adaptively adjust the predicted energy to fulfill different network conditions. With the help of additional force sensors on the master and slave sides, a 4-channel TDPA structure can be developed as suggested in [116], which is able to avoid position drift and to compensate for the master/slave dynamics in the force feedback signals. However, the TDPA, as a passivity-based control scheme, has the main drawback that system transparency quickly degrades with increasing communication delay. A typical effect is that the displayed object is much softer than it should be. Therefore, having other control and communication approaches to implement teleoperation systems is important, as different control schemes could vary in their performance towards certain network characteristics.

6.2 Point Cloud-based Model-mediated Teleoperation

The model-mediated teleoperation approach is identified as a promising scheme to simultaneously guarantee system stability and transparency. It is possible to realize a fully transparent

teleoperation system in the presence of unknown and varying delay using MMT. To this end, the following challenges must be addressed: 1) to precisely estimate the models of remote environments, 2) to efficiently transmit the estimated model parameters from the slave to the master, 3) to ensure system stability, especially to guarantee a stable local haptic rendering on the master side during the transition states. Current studies on MMT focus on addressing the first challenge, however, for simple environment geometry (e.g. 2D planar surface) and simple physical models (e.g. rigid object model or deformable objects without frictional contact).

Chapter 4 presents a point cloud-based model-mediated teleoperation (pcbMMT) structure, which extends the state-of-the-art MMT technique for dealing with complex environments using a depth sensor. The focus of this chapter is to address the three MMT-challenges for certain scenarios. Section 4.1 introduces an overview of the pcbMMT system design. Section 4.2 proposes a radial function-based deformation method toward real-time modeling of deformable objects including frictional contact. Section 4.3 combines the PD approach with the pcbMMT method to avoid excessive transmission of the model parameters. Section 4.4 presents a passivity-based model update scheme to guarantee system stability during model update. Evaluation in a real teleoperation system showed the feasibility of the designed system. The packet rate over the backward communication channel was reduced by up to 80% thanks to the PD approach.

Limitations and Future work

The MMT approach has the benefit of being simultaneously stable and transparent for relatively simple environments. However, due to the limitations of existing online model-estimation algorithms, the MMT approach cannot work efficiently in complex or completely unknown environments. The current pcbMMT method is still not capable of dealing with complex deformable or movable objects in a 3D environment for arbitrary interaction. Using a simple but imprecise model to approximate the environment leads to strong model mismatch and frequent model update. This jeopardizes system performance, or even causes task failure. On the other hand, position/velocity signals are transmitted in the forward channel. During the transition states, the master's motion commands can lead to dangerous slave behavior such as undesirably deep penetration into an object or improperly large force acting on the environment. Therefore, the slave must be controlled to ignore improper master commands during the transition states.

For future extension of the pcbMMT method, one idea is to develop online modeling algorithms for deformable or movable objects. This requires a sufficiently simple model whose parameters can be identified online. To be sufficiently simple, this model can be physically inaccurate, but should be able to provide a perceptually realistic haptic feedback. On the

other hand, the use of additional external sensors (e.g. ultrasonic sensors) can improve the estimation accuracy of the model parameters and identify the object physical properties even before the slave gets into contact with the environment.

Different from the TDPA, the main factor that affects system stability and transparency for MMT is the modeling accuracy, not the communication delay. It is questionable that whether the MMT method is more efficient than the TDPA for small delays, since the MMT consumes much more computational resources than the TDPA, and the transparency degradation of the TDPA for small delays can be still acceptable for certain scenarios and teleoperation tasks. Thus, an adaptive system design for time-delayed teleoperation is necessary. This aims to jointly optimize communication and control according to different tasks and various QoS of the network, and thus achieve the best possible teleoperation performance.

6.3 Toward Joint Optimization of Communication and Control for Networked Teleoperation

Different communication and control approaches introduce different types of artifacts. Their performance varies between tasks and also differs in their robustness towards different network QoS parameters. Section 5.1 presented an experimental case study toward realizing adaptive teleoperation systems. It clearly showed that an adaptive use of different control/communication schemes for various communication delays was able to subjectively improve system performance for the tested scenario. Experimental results also showed that the performance of the PD+TDPA+EP method was mainly influenced by communication delay, while the performance of the PD+MMT method depended on the model accuracy. Distortions introduced by the modeling error were almost constant for a certain range of delay. Consider the modeling error, the PD+TDPA+EP method is more suitable for small delays, while the PD+MMT method is more preferred by the subjects for large delays. Therefore, Chapter 5 concluded that a joint optimization of communication and control is able to mitigate the drawbacks of each individual control method and thus to improve the overall system performance.

Limitations and Future work

The necessity of adaptively switching between the joint solutions is verified by the experiment. The next task is to quantitatively evaluate the relationship between system performance and the offered QoS. This requires a mapping from the known QoS, control and communication schemes to the various performance metrics, including QoC, QoT, QoE, etc. This is important to determine the optimal communication and control schemes under different network conditions, and to answer the question when the system needs to switch to another communication

and control scheme. In Chapter 5, only communication delay is considered. Other QoS factors, such as delay variation, packet loss rate, bandwidth, etc., can also have strong influence on system performance. In addition, system performance can also vary in different teleoperation scenarios and tasks. To investigate a comprehensive evaluation is challenging. However, it is necessary to study the two open questions in future work: 1) achievable system performance for given QoS, and 2) required QoS for a desired system performance. Considering the tolerance of the human user in operation and perception as well as the tolerance of the control in teleoperation systems, the achieved system performance or the required QoS can be in a range.

The main ideas of this thesis on haptic communication will motivate further developments towards communication-oriented design of teleoperation systems. This would force a joint understanding of the human haptic perception and the control of teleoperation, thus achieve a fully transparent haptic communication over the current networks and the emerging tactile Internet [45, 46, 129].

Appendix A

A Summary of Relevant Studies on Model-mediated Teleoperation

Paper /Year	Environment modeling				Data transmission		Model updating in transition state	Slave control in transition state
	Adopted model	Model parameters		Estimation method	Data type (f: forward b: backward)	Data reduction scheme		
		Geometry	*Physical properties*					
[58] /1989	1D, two-port model	-	H-matrix	analytical analysis	Torque & impedance (f,b)	-	-	-
[96] /1995	Multi-DoF, mass-spring-damper	-	M, B, K	RLS	-	-	-	-
[47] /2003	1D, spring model	-	K	adaptation method (master side)	pos (f,b), force (b)	-	-	-
[155] /2004	3D, compliance model	-	compliance gains	pre-defined parameters	pos (f)	-	-	reference force
[131,132] /2005	3D, unknown model	neuron weights		online-trained neural network	pos (f), weights (b)	-	-	-
[104] /2006	1D, mass-spring-damper	P	I, B, K	laser rangefinder & SPRLS	vel (f), model data (b)	-	-	waiting strategy
[92] /2007	1D, mass-spring-damper	P	M, B, K	stereo camera & SALS (master side)	pos (f,b), force (b)	time-triggered estimation	-	-
[103] /2008	1D, rigid wall	P	-	force-based on-off contact detector	pos, vel, force (f) model data (b)	-	zero-energy injection	force-controlled while in contact
[141]/2008	1D, spring model	P	K	adaptation method	pos (f), model data (b)	-	-	-
[144]/2008	2D, plane	P, n	K, μ	Kalman filter-based	pos (f), model data (b)	event-triggered	-	-
[146] /2009	1D, spring model & human-trajectory model	-	K, T	RLS (master and slave sides)	pos (f,b), force (b)	-	-	-
[7] /2011	3D, smooth plane/sphere	P, n, R	K	block least square (master side)	pos (f), force (b)	perceptual deadband	-	-
[149] /2012	1D, rigid wall	P	-	force-based on-off contact detector	pos, vel, force (f) model data (b)	-	1st-order low-pass filter	force-controlled while in contact
[148] /2012	2D, rough plane	P, n	-	stereo camera & force trajectory	pos, vel, force (f) model data (b)	-	-	force-controlled (in normal direction)
[1] /2014	3D, complex surface	point cloud	K, μ	3D sensor & block least squares	pos, vel, force (f) model data (b)	perceptual deadband	linear interpolation	relative tracking

1D: one-dimensional. P: position. n: surface normal. R: sphere radius. M: mass. B: damping. K: stiffness. I: inertial.
μ: friction coefficient. T: movement duration. RLS: recursive least squares. SPRLS: self-perturbing recursive least squares. SALS: sliding-average least squares.

Bibliography

Publications by the author

Journal publications

[1] X. Xu, B. Cizmeci, A. Al-Nuaimi, and E. Steinbach, "Point cloud-based model-mediated teleoperation with dynamic and perception-based model updating," *IEEE Transactions on Instrumentation and Measurement*, vol. 63, no. 11, pp. 2558–2569, 2014.

[2] X. Xu, B. Cizmeci, C. Schuwerk, and E. Steinbach, "Model-mediated teleoperation: Toward stable and transparent teleoperation systems," *IEEE Access*, vol. 4, pp. 425–449, 2016.

[3] X. Xu, C. Schuwerk, B. Cizmeci, and E. Steinbach, "Energy prediction for teleoperation systems that combine the time domain passivity approach with perceptual deadband-based haptic data reduction," *IEEE Transactions on Haptics*, 2016.

Conference publications

[4] X. Xu, S. Chen, and E. Steinbach, "Model-mediated teleoperation for movable objects: Dynamics modeling and packet rate reduction," in *14th IEEE International Symposium on Haptic Audio-Visual Environments and Games*, Ottawa, Canada, 2015.

[5] X. Xu, B. Cizmeci, C. Schuwerk, and E. Steinbach, "Haptic data reduction for time-delayed teleoperation using the time domain passivity approach," in *IEEE World Haptics Conference, Chicago, USA*, 2015.

[6] X. Xu, B. Cizmeci, and E. Steinbach, "Point-cloud-based model-mediated teleoperation," in *Proc. of IEEE Int. Symposium on Haptic Audio-Visual Environments and Games (HAVE)*, Istanbul, Turkey, 2013.

[7] X. Xu, J. Kammerl, R. Chaudhari, and E. Steinbach, "Hybrid signal-based and geometry-based prediction for haptic data reduction," in *IEEE International Symposium on Haptic Audio Visual Environments and Games*, Qinhuangdao, Hebei, China, 2011.

[8] X. Xu, G. Paggetti, and E. Steinbach, "Dynamic model displacement for model-mediated teleoperation," in *IEEE World Haptics Conference 2013*, Daejeon, Korea, 2013.

[9] X. Xu, C. Schuwerk, and E. Steinbach, "Passivity-based model update for model-mediated teleoperation," in *6th IEEE International Workshop on Hot Topics in 3D - Hot3D, Proc. of IEEE International Conference on Multimedia Expo*, Turin, Italy, 2015.

[10] X. Xu and E. Steinbach, "Towards real-time modeling and haptic rendering of deformable objects for point cloud-based model-mediated teleoperation," in *5th IEEE International Workshop on Hot Topics in 3D - Hot3D, Proc. of IEEE International Conference on Multimedia and Expo*, Chengdu, China, 2014.

General publications

[11] J. Abbott and A. Okamura, "Effects of position quantization and sampling rate on virtual-wall passivity," *IEEE Transaction on Robotics*, vol. 21, no. 5, pp. 952-964, October 2005.

[12] A. Achhammer, C. Weber, A. Peer, and M. Buss, "Improvement of model-mediated teleoperation using a new hybrid environment estimation technique," in *Proceedings of the IEEE International Conference on Robotics and Automation*, Anchorage, USA, 2010.

[13] M. Aiple and A. Schiele, "Pushing the limits of the cybergrasp for haptic rendering," in *IEEE International Conference on Robotics and Automation*, Karlsruhe, Germany, 2013.

[14] A. Alfi and M. Farrokhi, "A simple structure for bilateral transparent teleoperation systems with time delay," *ASME Journal of Dynamic Systems, Measurement, and Control*, vol. 130, no. 4, pp. 22-43, Juen 2008.

[15] ——, "Force reflecting bilateral control of master-slave systems in teleoperation," *Journal of Intelligent and Robotic Systems*, vol. 52, no. 2, pp. 209-232, March 2008.

[16] R. Anderson and M. Spong, "Bilateral control of teleoperators with time delay," *IEEE Transaction on Automatic Control*, vol. 34, no. 5, pp. 494-501, May 1989.

[17] P. Arcara and C. Melchiorri, "Control schemes for teleoperation with time delay: A comparative study," *Journal of Robotics and Autonomous Systems*, vol. 38, no. 1, pp. 49-64, January 2002.

[18] J. Artigas, J.-H. Ryu, C. Preusche, and G. Hirzinger, "Network representation and passivity of delayed teleoperation systems," in *IEEE/RSJ International Conference on Intelligent Robots and Systems*, San Francisco, CA, USA, 2011.

[19] C. Basdogan and M. A. Srinivasan, "Haptic rendering in virtual environments," in *in Stanney, K. (Ed.), Handbook of Virtual Environments*, Lawrence Erlbaum, Inc., London, 2002.

[20] A. Bejczy and W. Kim, "Predictive displays and shared compliance control for time-delayed telemanipulation," in *Proceeding of the IEEE International Conference on Intelligent Robots and Systems*, Ibaraki, Japan, 1990.

[21] A. Bejczy, W. Kim, and S. Venema, "The phantom robot: Predictive displays for teleoperation with time delay," in *Proceeding of the IEEE International Conference on Robotics and Automation*, Cincinnati, USA, 1990.

[22] C. J. Bovy, H. T. Mertodimedjo, G. Hooghiemstra, H. Uijterwaal, and P. V. Mieghem, "Analysis of end-to-end delay measurements in internet," in *Passive and Active Measurement Workshop*, Pisa, 2002.

[23] F. Brandi and E. Steinbach, "Prediction techniques for haptic communication and their vulnerability to packet losses," in *Proceedings of IEEE International Symposium on Haptic Audio Visual Environments and Games*, Istanbul, Turkey, 2013.

[24] H. Brandtstädter, J. Schneider, and F. Freyberger, "Hardware and software components for a new internet-based multimodal tele-control experiment with haptic sensation," in *EuroHaptics Conference*, Munich, Germany, 2004.

[25] T. Burkert, J. Leupold, and G. Passig, "A photo-realistic predictive display," *Presence: Teleoperators and Virtual Environments*, vol. 13, no. 1, pp. 22-43, February 2004.

[26] M. Buss and G. Schmidt, "Control problems in multi-modal telepresence systems," in *Advances in Control: Highlights of the 5th European Control Conference, P. Frank, Ed. Berlin, Germany: Springer-Verlag*, Karlsruhe, Germany, 1999, pp. 65–101.

[27] F. Buzan and T. Sheridan, "A model-based predictive operator aid for telemanipulators with time delay," in *Proceeding of the IEEE International Conference on Systems, Man and Cybernetics*, Cambridge, UK, 1989.

[28] V. Chawda, H. V. Quang, M. O Malley, and J.-H. Ryu, "Compensating position drift in time domain passivity approach based teleoperation," in *Proceedings of Haptics Symposium*, Houston, USA, February 2014.

[29] B. Cizmeci, R. Chaudhari, X. Xu, N. Alt, and E. Steinbach, "A visual-haptic multiplexing scheme for teleoperation over constant-bitrate communication links," in *Proceedings of EuroHaptics Conference*, Versailles, France, 2014.

[30] S. Clarke, G. Schillhuber, M. Zaeh, and H. Ulbrich, "Prediction-based methods for teleoperation across delayed networks," *Multimedia Systems*, vol. 13, no. 4, pp. 253-261, January 2008.

[31] J. Colgate and J. Brown, "Factors affecting the z-width of a haptic display," in *Proceedings of IEEE International Conference on Robotics and Automation*, San Diego, USA, May 1994.

[32] J. Colgate and G. Schenkel, "Passivity of a class of sampled-data systems: Application to haptic interfaces," *Journal of Field Robotics*, vol. 14, no. 1, pp. 37-47, January 1997.

[33] T. Cornsweet, "The staircase-method in psychophysics," *The American Journal of Psychology*, vol. 75, no. 3, pp. 485-491, September 1962.

[34] R. Daniel and P. McAree, "Fundamental limits of performance for force reflecting teleoperation," *The International Journal of Robotics Research*, vol. 17, no. 8, pp. 811-830, August 1998.

[35] H. Delingette, "Toward realistic soft-tissue modeling in medical simulation," *Proceedings of the IEEE*, vol. 86, no. 3, pp. 512-523, March 1998.

[36] H. Delingette and N. Ayache, "Soft tissue modeling for surgery simulation," *Computational Models for the Human Body, Handbook of Numerical Analysis, P. Ciarlet and N. Ayache, eds., Elsevier*, pp. 453–550, 2004.

[37] N. Diolaiti, C. Melchiorri, and S. Stramigioli, "Contact impedance estimation for robotic systems," *IEEE Transactions on Robotics*, vol. 21, no. 5, pp. 925-935, October 2005.

[38] N. Diolaiti, G. Niemeyer, F. Barbagli, and J. Salisbury, "Stability of haptic rendering: Discretization, quantization, time delay, and coulomb effects," *IEEE Transaction on Robotics*, vol. 22, no. 2, pp. 256-268, April 2006.

[39] M. Eid, J. Cha, and A. Saddik, "Admux: An adaptive multiplexer for haptic audio visual data communication," *IEEE Transaction on Instrumentation and Measurement*, vol. 60, no. 1, pp. 21-31, February 2011.

[40] M. Eid, A. Lssawi, and A. Saddik, "Slingshot 3d: A synchronous haptic-audio-video game," *Journal of Multimedia Tools and Applications*, vol. 71, no. 3, pp. 1635-1649, November 2012.

[41] N. El-Far, N. Georganas, and A. E. Saddik, "An algorithm for haptically rendering objects described by point clouds," in *Proceedings of Canadian Conference on Electrical and Computer Engineering*, Niagara Falls, May 2008.

[42] D. Erickson, M. Weber, and I. Sharf, "Contact stiffness and damping estimation for robotic systems," *International Journal of Robotics Research*, vol. 22, no. 1, pp. 41-57, January 2003.

[43] W. Ferrell and T. Sheridan, "Supervisory control of remote manipulation," *IEEE Spectrum*, vol. 4, no. 10, pp. 81-88, October 1967.

[44] D. Feth, A. Peer, and M. Buss, "Incorporating human haptic interaction models into teleoperation systems," in *IEEE/RSJ International Conference on Intelligent Robots and Systems*, Taipei, China, 2010.

[45] G. Fettweis, H. Boche, T. Wiegand, E. Zielinski, H. Schotten, P. Merz, S. Hirche, A. Festag, W. Häffner, M. Meyer, E. Steinbach, R. Kraemer, R. Steinmetz, F. Hofmann, P. Eisert, R. Scholl, F. Ellinger, E. Weiß, and I. Riedel, "The tactile internet," *ITU-T Technology Watch Report*, August 2014.

[46] G. P. Fettweis, "The tactile internet: Applications and challenges," *IEEE Vehicular Technology Magazine*, vol. 9, no. 1, pp. 64-70, March 2014.

[47] K. Fite, M. Goldfarb, and A. Rubio, "Transparent telemanipulation in the presence of time delay," in *Proceeding of IEEE/ASME International Conference on Advanced Intelligent Mechatronics*, Ibaraki, Japan, 2003.

[48] M. Fujimoto and Y. Ishibashi, "Packetization interval of haptic media in networked virtual environments," in *Proceedings of 4th ACM Workshop on Network and System Support for Games*, Portland, Oregon, USA, October 2005.

[49] G. A. Gescheider, "Psychophysics: The fundamentals," in *Psychology Press*, 1997.

[50] J. Gil, A. Avello, A. Rubio, and J. Florez, "Stability analysis of a 1 dof haptic interface using the routh-hurwitz criterion," *IEEE Transaction on Control Systems Technology*, vol. 12, no. 4, pp. 583-588, July 2004.

[51] J. D. Greenspan and S. J. Bolanowski, "The psychophysics of tactile perception and its peripheral physiological basis," Academic Press Inc., 1996.

[52] F. Guo, C. Zhang, and Y. He, "Haptic data compression based on a linear prediction model and quadratic curve reconstruction," in *Proceedings of IEEE International Conference on Multimedia and Expo*, Beijing, China, 2007.

[53] ——, "Haptic data compression based on a linear prediction model and quadratic curve reconstruction," *Journal of Software*, vol. 9, no. 11, pp. 2796-2803, November 2014.

[54] G. Guthart and J. Salisbury, "The intuitive telesurgery system: Overview and application," in *Proceedings of IEEE International Conference on Robotics and Automation*, San Francisco, CA, USA, 2000.

[55] A. Haddadi and K. Hashtrudi-Zaad, "On-line identification of contact dynamics in the presence of geometric uncertainties," in *IEEE/RSJ International Conference on Intelligent Robots and Systems*, Nice, France, 2008.

[56] ——, "Online contact impedance identification for robotic systems," in *Proceeding of the IEEE International Conference on Intelligent Robots and Systems*, Nice, France, 2008.

[57] A. Hamam, M. Eid, and A. Saddik, "Effect of kinesthetic and tactile haptic feedback on the quality of experience of edutainment applications," *Journal of Multimedia Tools and Applications*, vol. 67, no. 2, pp. 455-472, November 2013.

[58] B. Hannaford, "A design framework for teleoperators with kinesthetic feedback," *IEEE Transaction on Robotics and Automation*, vol. 5, no. 4, pp. 426-434, August 1989.

[59] B. Hannaford and J. H. Ryu, "Time-domain passivity control of haptic interfaces," *IEEE Transaction on Robotics and Automation*, vol. 18, no. 1, pp. 1-10, February 2002.

[60] W. Harwin and N. Melder, "Improved haptic rendering for multi-finger manipulation using friction cone based god-objects," in *Proceedings of EuroHaptics*, Edinburgh, UK, July 2002.

[61] P. Hinterseer, S. Hirche, S. Chaudhuri, and E. Steinbach, "Perception-based data reduction and transmission of haptic data in telepresence and teleaction systems," *IEEE Transaction on Signal Processing*, vol. 56, no. 2, pp. 588-597, February 2008.

[62] P. Hinterseer, E. Steibach, and S. Chaudhuri, "Model-based data compression for 3d virtual haptic teleinteraction," in *International Conference on Consumer Electronics, Digest of Technical Papers*, 2006.

[63] ——, "Perception-based compression of haptic data streams using kalman filters," in *Proceedings of IEEE International Conference on Acoustics, Speech and Signal Processing*, 2006.

[64] P. Hinterseer and E. Steinbach, "A psychophysically motivated compression approach for 3d haptic data," in *14th Symposium on Haptic Interfaces for Virtual Environment and Teleoperator Systems*, 2006.

[65] P. Hinterseer, E. Steinbach, S. Hirche, and M. Buss, "A novel, psychophysically motivated transmission approach for haptic data streams in telepresence and teleaction systems," in *Proceedings of IEEE International Conference on Acoustics, Speech, and Signal Processing*, Philadelphia, PA, USA, March 2005.

[66] S. Hirche and M. Buss, "Human-oriented control for haptic teleoperation," *Proceedings of the IEEE*, vol. 100, no. 3, pp. 623-647, January 2012.

[67] ——, "Packet loss effects in passive telepresence systems," in *IEEE International Conference on Decision and Control*, Atlantis, Bahamas, 2004.

[68] ——, "Transparent data reduction in networked telepresence and teleaction systems. part ii: Time-delayed communication," *Presence: Teleoperators and Virtual Environments*, vol. 16, no. 5, pp. 532-542, January 2007.

[69] S. Hirche, P. Hinterseer, E. Steinbach, and M. Buss, "Transparent data reduction in networked telepresence and teleaction systems. part i: Communication without time delay," *Presence: Teleoperators and Virtual Environments*, vol. 16, no. 5, pp. 523-531, January 2007.

[70] G. Hirzinger, B. Brunner, J. Dietrich, and J. Heindl, "Rotex-the first remotely controlled robot in space," in *Proceedings of International Conference on Robotics and Automation*, San Diego, CA, USA, 1994.

[71] N. Hogan, "Controlling impedance at the man/machine interface," in *Proceedings of IEEE International Conference on Robotics and Automation*, Scottsdale, 1989.

[72] ——, "Impedance control: An approach to manipulation," in *American Control Conference*, San Diego, USA, 1984.

[73] P. F. Hokayem and M. W. Spong, "Bilateral teleoperation: An historical survey," *Automatica*, vol. 42, no. 12, pp. 2035-2057, December 2006.

[74] J.-Q. Huang and F. L. Lewis, "Neural-network predictive control for nonlinear dynamic systems with time-delay," *IEEE Transactions on Neural Networks*, vol. 14, no. 2, pp. 377-389, February 2003.

[75] K. Hunt and F. Crossley, "Coefficient of restitution interpreted as damping in vibroimpact," *ASME Journal of Applied Mechanics*, vol. 42, no. 2, pp. 440-445, June 1975.

[76] W. Ijsselsteijn, H. de Ridder, J. Freeman, and S. E. Avons, "Presence: Concept, determinants and measurement," in *Proceedings of the International Society for Optics and Photonics*, Bellingham, USA, 2000.

[77] R. Isermann and M. Münchhof, "Identification of dynamic systems: An introduction with applications," Springer-Verlag Berlin Heidelberg, 2011, pp. 131–132.

[78] J. A. J. Ryu and C. Preusche, "A passive bilateral control scheme for a teleoperator with time-varying communication delay," *Elsevier Journal of Mechatronics*, vol. 20, no. 7, pp. 812-823, October 1994.

[79] A. Jafari, M. Nabeel, and J. Ryu, "Stable and transparent teleoperation over communication time-delay: Observer-based input-to-state stable approach," in *IEEE Haptics Symposium*, Philadelphia, 2016.

[80] A. Jazayeri and M. Tavakoli, "A passivity criterion for sampled-data bilateral teleoperation systems," in *IEEE World Haptics Conference*, Istanbul, Turkey, 2011.

[81] L. Jones, "Matching forces: Constant errors and differential thresholds," *Perception*, vol. 18, no. 5, pp. 681-687, 1989.

[82] L. Jones and I. Hunter, "A perceptual analysis of stiffness," *Experimental Brain Research*, vol. 79, no. 1, pp. 150-156, January 1990.

[83] L. Jones and H. Z. Tan, "Application of psychophysical techniques to haptic research," *IEEE Transactions on Haptics*, vol. 6, no. 3, pp. 268-284, December 2012.

[84] L. A. Jones, "Kinesthetic sensing," in *Human and Machine Haptics*, MIT Press, 2000.

[85] T. Kotuku, "A predictive display with force feedback and its application to remote manipulation system with transmission time delay," in *IEEE International Conference on Intelligent Robots and Systems*, Kowloon, China, 1992.

[86] A. Kron, G. Schmidt, B. Petzold, M. F. Zäh, P. Hinterseer, and E. Steinbach, "Disposal of explosive ordnances by use of a bimanual haptic telepresence system," in *Proceedings of IEEE International Conference on Robotics and Automation*, New Orleans, LA, USA, 2004.

[87] D. Kubus, I. Weidauer, and F. M. Wahl, "1khz is not enough how to achieve higher update rates with a bilateral teleoperation system based on commercial hardware," in *Proceedings of IEEE/RSJ International Conference on Intelligent Robots and Systems*, St. Louis, USA, 2009.

[88] A. Kuzu, E. A. Baran, S. Bogosyan, M. Gokasan, and A. Sabanovic, "Wavelet packet transform-based compression for teleoperation," *Journal of Systems and Control Engineering*, vol. 229, no. 7, pp. 639651, August 2015.

[89] L. D. Landau and E. M. Lifshitz, "Theory of elasticity," *Pergamon Press Ltd.*, 1959.

[90] D. Lawrence, "Stability and transparency in bilateral teleoperation," *IEEE Transaction on Robotics and Automation*, vol. 9, no. 5, pp. 624-637, October 1993.

[91] A. Leeper, S. Chan, and K. Salisbury, "Point clouds can be represented as implicit surfaces for constraint-based haptic rendering," in *Proceedings of IEEE International Conference on Robotics and Automation*, Saint Paul, May 2012.

[92] H. Li and A. Song, "Virtual-environment modeling and correction for force-reflecting teleoperation with time delay," *IEEE Transactions on Industrial Electronics*, vol. 54, no. 2, pp. 1227-1233, April 2007.

[93] Z. Li and Y. Xia, "Adaptive neural network control of bilateral teleoperation with unsymmetrical stochastic delays and unmodeled dynamics," *International Journal of Robust and Nonlinear Control*, vol. 24, no. 11, pp. 1628-1652, July 2014.

[94] Z. Li, Y. Xia, D. Wang, D. Zhai, C. Su, and X. Zhao, "Neural network based control of networked trilateral teleoperation with geometrically unknown constraints," *IEEE transactions on cybernetics*, vol. 46, no. 5, pp. 1051-1064, May 2015.

[95] B. Lloyd, G. Szekely, and M. Harders, "Identification of spring parameters for deformable object simulation," *IEEE Transactions on Visualization and Computer Graphics*, vol. 13, no. 5, pp. 1081-1094, September 2007.

[96] L. Love and W. J. Book, "Environment estimation for enhanced impedance control," in *IEEE International Conference on Robotics and Automation*, Nagoya, Japan, 1995.

[97] ——, "Force reflecting teleoperation with adaptive impedance control," *IEEE Transaction on Systems*, vol. 34, no. 1, pp. 159-165, February 2004.

[98] R. Lozano, N. Chopra, and M. Spong, "Passivation of force reflecting bilateral teleoperators with time varying delay," in *Proceedings of the 8th Mechatronics Forum*, Enschede, Netherlands, 2002.

[99] M. Mahvash and V. Hayward, "High-fidelity passive force-reflecting virtual environments," *IEEE Transaction on Robotics*, vol. 21, no. 1, pp. 38-46, February 2005.

[100] J. Marescaux, J. Leroy, F. Rubino, M. Smith, M. Vix, M. Simone, and D. Mutter, "Transcontinental robot-assisted remote telesurgery: Feasibility and potential applications," *Annals of surgery*, vol. 235, no. 4, pp. 487-492, April 2002.

[101] Z. C. Marton, R. Rusu, and M. Beetz, "On fast surface reconstruction methods for large and noisy datasets," in *Proceedings of the IEEE International Conference on Robotics and Automation*, Kobe, Japan, 2009.

[102] P. Mitra, D. Gentry, and G. Niemeyer, "User perception and preference in model-mediated telemanipulation," in *Proceedings of the IEEE World Haptics Conference*, Tsukaba, Japan, 2007.

[103] P. Mitra and G. Niemeyer, "Model-mediated telemanipulation," *International Journal of Robotics Research*, vol. 27, no. 2, pp. 253-262, February 2008.

[104] F. Mobasser and K. Hashtrudi-Zaad, "Predictive teleoperation using laser rangefinder," in *Canadian Conference on Electrical and Computer Engineering*, Ottawa, Canada, 2006.

[105] G. Niemeyer and J.-J. Slotine, "Stable adaptive teleoperation," *IEEE Journal of Oceanic Engineering*, vol. 16, no. 1, pp. 152-162, January 1991.

[106] M. V. Noyes and T. B. Sheridan, "A novel predictor for telemanipulation through a time delay," in *Proceedings of Annual Conference on Manual Control*, Moffett Field, USA, 1984.

[107] M. Oliveira, B. Bowen, R. McKenna, and Y. Chang, "Fast digital image inpainting," in *Proceedings of International Conference on VIIP*, Marbella, September 2001.

[108] P. G. Otanez, J. R. Moyne, and D. M. Tilbury, "Using deadbands to reduce communication in networked control systems," in *Proceedings of American Control Conference*, Anchorage, USA, May 2002.

[109] X. Pang, H. Tan, and N. Durlach, "Manual discrimination of force using active finger motion," *Perception and Psychophysics*, vol. 49, no. 6, pp. 531-540, June 1991.

[110] D. J. Park and B. E. Jun, "Selfperturbing recursive least squares algorithm with fast tracking capability," *Electronics Letters*, vol. 28, no. 65, pp. 558-559, March 1992.

[111] C. Passenberg, A. Peer, and M. Buss, "A survey of environment-, operator-, and task-adapted controllers for teleoperation systems," *Mechatronics*, vol. 20, no. 7, pp. 787-801, October 2010.

[112] ——, "Model-mediated teleoperation for multi-operator multi-robot systems," in *IEEE/RSJ International Conference on Intelligent Robots and Systems*, Taipei, China, 2010.

[113] L. F. Penin, "Teleoperation with time delay - a survey and its issue in space robotics," in *Proceedings of 6th ESA Workshop Advanced Space Technology Robotics Automation*, Noordwijk, The Netherlands, 2000.

[114] V. L. Popov, "Contact mechanics and friction - physical principles and applications," *Springer, 1st edition*, 2009.

[115] P. Prekopiou, S. Tzafestas, and W. Harwin, "Towards variable-time-delays-robust telemanipulation through master state prediction," in *Proceedings of IEEE/ASME International Conference on Advanced Intelligent Mechatronics*, Atlanta, September.

[116] J. Rebelo and A. Schiele, "Time domain passivity controller for 4-channel time-delay bilateral teleoperation," *IEEE Transaction on Haptics*, vol. 8, no. 1, pp. 79-89, October 2014.

[117] F. Ryden and H. Chizeck, "A proxy method for real-time 3-dof haptic rendering of streaming point cloud data," *IEEE transactions on Haptics*, vol. 6, no. 3, pp. 257-267, 2013.

[118] F. Ryden, S. Kosari, and H. Chizeck, "Proxy method for fast haptic rendering from time varying point clouds," in *Proceedings of IEEE/RSJ international conference on Intelligent Robots and Systems*, San Francisco, September 2011.

[119] J. Ryu, "Bilateral control with time domain passivity approach under time-varying communication delay," in *16th IEEE International Conference on Robot and Human Interactive Communication*, Jeju, Korea, 2007.

[120] J. Ryu, J. Artigas, and C. Preusche, "A passive bilateral control scheme for a teleoperator with time-varying communication delay," *Elsevier Journal of Mechatronics*, vol. 20, no. 7, pp. 812-823, Oct 2010.

[121] E. Saddik, "The potential of haptics technologies," *IEEE Instrumentation Measurement Magazine*, vol. 10, no. 1, pp. 10-17, April 2007.

[122] N. Sakr, N. Georganas, J. Zhao, and X. Shen, "Motion and force prediction in haptic media," in *Proceedings of IEEE International Conference on Multimedia and Expo*, Beijing, China, 2007.

[123] W. Schiff and E. Foulke, "Tactual perception: A sourcebook," Cambridge Univ Press, 1982.

[124] D. W. Schloerb, "A quantitative measure of telepresence," *Presence: Teleoperators and Virtual Environments*, vol. 4, no. 1, pp. 64-80, Winter 1995.

[125] C. Shahabi, A. Ortega, and M. R. Kolahdouzan, "A comparison of different haptic compression techniques," in *Proceedings of IEEE International Conference on Multimedia and Expo*, 2002.

[126] X. Shen, J. Zhou, A. E. Saddik, and N. D. Georganas, "Architecture and evaluation of tele-haptic environments," in *8th IEEE International Symposium on Distributed Simulation and Real-Time Applications*, 2004.

[127] J. Sheng and M. W. Spong, "Model predictive control for bilateral teleoperation systems with time delays," in *Canadian Conference on Electrical and Computer Engineering*, Canada, 2004.

[128] T. Sheridan, "Space teleoperation through time delay: Review and prognosis," *IEEE Transaction on Robotics and Automation*, vol. 9, no. 5, pp. 592-606, October 1993.

[129] M. Simsek, A. Aijaz, M. Dohler, J. Sachs, and G. Fettweis, "5g-enabled tactile internet," *IEEE Journal on Selected Areas in Communications*, vol. 34, no. 3, March 2016.

[130] J. Smisek, M. Paassen, and A. Schiele, "Naturally-transitioning rate-to-force controller robust to time delay by model-mediated teleoperation," in *IEEE International Conference on Systems, Man, and Cybernetics*, Kowloon, China, 2015.

[131] A. C. Smith and K. Hashtrudi-Zaad, "Adaptive teleoperation using neural network-based predictive control," in *IEEE International Conference on Control Applications*, Toronto, Canada, 2005.

[132] ——, "Neural network-based teleoperation using smith predictors," in *IEEE International Conference on Mechatronics and Automation*, Niagara Falls, Canada, 2005.

[133] O. J. M. Smith, "Closer control of loops with dead time," *Chemical Engineering Progress*, vol. 53, no. 5, pp. 217-219, 1957.

[134] E. Steinbach, S. Hirche, M. Ernst, F. Brandi, R. Chaudhari, J. Kammerl, and I. Vittorias, "Haptic data compression and communication," *Proceedings of the IEEE*, vol. 100, no. 4, pp. 937956, April 2012.

[135] E. Steinbach, S. Hirche, J. Kammerl, I. Vittorias, and R. Chaudhari, "Haptic data compression and communication," *IEEE Signal Processing Magazine*, vol. 28, no. 1, pp. 8796, January 2011.

[136] H. Z. Tan, M. A. Srinivasan, B. Eberman, and B. Cheng, "Human factors for the design of force-reflecting haptic interfaces," in *Proceedings of the ASME Dynamic Systems and Control Division*, Chicago, USA, 1994.

[137] H. Tanaka and K. Ohnishi, "Haptic data compression/decompression using dct for motion copy system," in *Proceedings of IEEE International Conference on Mechatronics*, Malaga, Spain, 2009.

[138] D. Terzopoulos, J. Platt, A. Barr, and K. Fleischer, "Elastically deformable models," *SIGGRAPH Computer Graphics*, vol. 21, no. 4, pp. 205-214, July 1987.

[139] W. Tiest and A. Kappers, "Cues for haptic perception of compliance," *IEEE Transactions on Haptics*, vol. 2, no. 4, pp. 189-199, May 2009.

[140] C. Tzafestas and S. Velanas, "Telehaptic perception of delayed stiffness using adaptive impedance control: Experimental psychophysical analysis," *Presence: Teleoperators and Virtual Environments*, vol. 22, no. 41, pp. 323-344, Fall 2013.

[141] C. Tzafestas, S. Velanas, and G. Fakiridis, "Adaptive impedance control in haptic teleoperation to improve transparency under time-delay," in *IEEE International Conference on Robotics and Automation*, Pasadena, USA, 2008.

[142] S. Velanas and C. Tzafestas, "Human telehaptic perception of stiffness using an adaptive impedance reflection bilateral teleoperation control scheme," in *IEEE International Conference on Robot and Human Interactive Communication*, Viareggio, Italy, 2010.

[143] ——, "Model-mediated telehaptic perception of delayed curvature," in *IEEE International Symposium on Robot and Human Interactive Communication*, Paris, France, 2012.

[144] D. Verscheure, J. Swevers, H. Bruyninckx, and J. Schutter, "On-line identification of contact dynamics in the presence of geometric uncertainties," in *Proceedings of IEEE International Conference on Robotics and Automation*, Pasadena, USA, 2008.

[145] I. Vittorias, J. Kammerl, S. Hirche, and E. Steinbach, "Perceptual coding of haptic data in time-delayed teleoperation," in *Proceedings of World Haptics Conference*, Salt Lake City, USA, March 2009.

[146] C. Weber, V. Nitsch, U. Unterhinninghofen, B. Färber, and M. Buss, "Position and force augmentation in a telepresence system and their effects on perceived realism," in *Third Joint Eurohaptics Conference and Symposium on Haptic Interfaces for Virtual Environment and Teleoperator Systems*, Salt Lake City, 2009.

[147] E. Weber, "Die lehre vom tastsinn und gemeingefuehl, auf versuche gegruendet," in *Vieweg: Braunschweig, Germany*, 1851.

[148] B. Willaert, J. Bohg, H. Brussel, and G. Niemeyer, "Towards multi-dof model mediated teleoperation: Using vision to augment feedback," in *IEEE International Workshop on Haptic Audio Visual Environments and Games*, Munich, Germany, October 2012.

[149] B. Willaert, H. Brussel, and G. Niemeyer, "Stability of model-mediated teleoperation: Discussion and experiments," in *Eurohaptics*, Tampere, Finland, 2012.

[150] R. C. Winck and A. Okamura, "Model-mediated teleoperation with predictive models and relative tracking," in *Proceedings of the ASME Conference on Dynamic Systems and Control Conference*, Stanford, USA, 2013.

[151] L. Winfield, J. Glassmire, J. Colgate, and M. Peshkin, "T-pad: Tactile pattern display through variable friction reduction," in *World Haptics Conference*, Tsukuba, Japan, 2007.

[152] B. G. Witmer and M. J. Singer, "Measuring presence in virtual environments: A presence questionnaire," *Presence: Teleoperators and Virtual Environments*, vol. 7, no. 3, pp. 225-240, June 1998.

[153] Y. Ye, Y. Pan, and T. Hilliard, "Bilateral teleoperation with time-varying delay: A communication channel passification approach," *IEEE Transactions on Mechatronics*, vol. 18, No. 4, pp 1431-1434, April 2013.

[154] Y. Yokokohji and T. Yoshikawa, "Bilateral control of master-slave manipulators for ideal kinesthetic coupling-formulation and experiment," *IEEE Transaction on Robotics and Automation*, vol. 10, no. 5, pp. 605-620, October 1994.

[155] W. Yoon, T. Goshozono, H. Kawabe, M. Kinami, Y. Tsumaki, M. Uchiyama, M. Oda, and T. Doi, "Model-based space robot teleoperation of ets - vii manipulator," *IEEE Transactions on Robotics and Automation*, vol. 20, no. 3, pp. 602-612, June 2004.

[156] Y. You and M. Y. Sung, "Haptic data transmission based on the prediction and compression," in *Proceedings of IEEE International Conference on Communications*, Beijing, China, 2008.

[157] C. Zhao, "Real time haptic simulation of deformable bodies," in *Ph.D Thesis, Institute of Applied Mechanics, Faculty of Mechanical Engineering, Technische Universität München*, 2010.

[158] C. Zilles and J. Salisbury, "A constraint-based god-object method for haptic display," in *IEEE/RSJ International Conference on Intelligent Robots and Systems*, Pittsburgh, 1995.

List of Figures

1.1 Overview of a bilateral teleoperation system with haptic feedback (adapted from [43]). . . . 2

2.1 Components of a position-force teleoperation architecture. 10
2.2 Illustration of the 1-DoF perceptual deadband approach. (a) The input signal, i.e., the sensor readings at the sender. (b) The reconstructed signal at the receiver. 15
2.3 Structure of the perceptual haptic data reduction scheme with predictive coding (adapted from [135]). 15
2.4 Principle of linear prediction. The red values are transmitted and used to predict the current haptic value. If the predicted value differs by more than the JND from the actual value, a new value is transmitted and the predictor is updated. 16
2.5 PD approach with passive ZOH reconstruction strategy (adapted from [65]). 17
2.6 Illustration of a one-port system (left) and a two-port system (right). 18
2.7 Overview of the wave-variable transformation for time-delayed teleoperation. 19
2.8 A time-delayed teleoperation system with the TDPA and the virtual mass-spring filter (adopted from [120]). 20
2.9 (a) Passivity-based teleoperation using the wave-variable transformation. (b) Passivity-based teleoperation using the time-domain passivity approach. For (a) and (b), the velocity and force signals are modified to guarantee system passivity. (c) A state-of-the-art model-mediated teleoperation architecture. The use of the local model enables non-delayed haptic rendering thus guaranteeing system stability. 24
2.10 First prototype of the MMT control architecture. The exchanged parameters $\hat{\theta}_{1,2}$ contain the effort (force/torque) and impedance on both the master and slave sides (adapted from [58]). 26
2.11 (a) An example system block diagram with delays. (b) The use of the Smith predictor to compensate for the delays (adapted from [133]). 27
2.12 (a) Predictive control architecture using a Smith Predictor for a position-force teleoperation system with the force feedback term. (b) Predictive control architecture using a Smith Predictor for a position-force teleoperation system without force feedback term. 29
2.13 The level of abstraction and data complexity with update rates and robustness to delays (adapted from [103]). 30
2.14 Overview of an MMT control architecture without force transmission in the backward channel. 34

2.15 Two methods for updating object position. Left: direct updating leads to suddenly increased penetration and thus injects energy into the system. Right: gradual updating without injecting energy into the system. Adapted from [103]. 35

3.1 Combination of the PD approach with the TDPA, type A. 43
3.2 Combination of the PD approach with the TDPA, type B. 44
3.3 Experimental results. (a) Packet rate vs. deadband parameters for different delays. (b) Mean and standard deviation of the subjective ratings vs. DBP. 47
3.4 Subjective rating vs. packet rate. 47
3.5 Teleoperation setup with adjustable time delay. 48
3.6 Illustration of the conservative control behavior of the PD+TDPA method. Delay 200 ms, DBP 0.3, average packet rate: 179 packets/s. (a) Computed and received energy signals at the slave side. (b) Computed and received energy signals at the master side. (c) Position signals. (d) Force signals with the PD approach. (e) Force signal without the PD approach. 49
3.7 Control architecture of the TDPA-based haptic data reduction approach with the use of the energy prediction scheme. 52
3.8 Measurements for the PD+TDPA+EP method. Delay 200 ms, DBP 0.3, average packet rate: 151 packets/s. (a) Computed and received energy signals at the slave side. (b) Computed and received energy signals at the master side. (c) Position signals. (d) Force signals. 53
3.9 The modified EP scheme for time-varying delay and packet loss. Average packet rate: 137 packets/s (10% packet loss). (a) Round-trip-delay in the communication channel. (b) Output energy at the slave side and delayed input energy at the master side. (c) Output energy at the master side and delayed input energy at the slave side. 55
3.10 The modified EP scheme for an extreme case. Average packet rate: 118 packets/s (50% packet loss). (a) Round-trip-delay. (b) Output energy at the master side and delayed input energy at the slave side. The system is still piece-wise passive. (c) Force signals. 55
3.11 Control architecture of the TDPA-based haptic data reduction approach with the use of the energy prediction and position drift compensation schemes (PD+TDPA+EP+PDC). The velocity signal v_{ad} is used to compensate for the position drift. 56
3.12 Output energy at the master side and delayed input energy at the slave side while simultaneously using the EP scheme and the PDC scheme. Limited active behavior is observed. 57
3.13 Bode plot of the displayed impedance in contact. 59
3.14 Simulation results of the average impedance errors and packet rates in different parameter settings. (a)(b) The PD+TDPA method. (c)(d) The PD+TDPA+EP method. (e)(f) The PD+TDPA+PDC method. (g)(h) The PD+WV method. Wave impedance is $b = 25$ Ns/m. 60
3.15 Boundaries of the region of perceived transparency for different control and compensation methods. The three tested parameter sets for Sec. 3.3.2.2 are A (0 ms, 0.1), B (20 ms, 0), and C (12 ms, 0.08). 63
3.16 Hypothetical subjective quality measure as a function of communication delay and packet rate. The subjectively best thresholds represent the lowest possible packet rate, at which the system remains subjectively transparent with respect to the corresponding reference signals. 65

3.17 Experimental setup. The communication network, the slave (represented by a haptic interaction point), and the virtual environment are simulated on a PC using the CHAI3D library. . . . 66
3.18 Detected DBP thresholds (mean and standard deviation) of the three tested methods across all subjects. . . . 67
3.19 Packet rates vs. deadband parameters for different delays in Fig. 3.14(d). The packet rate in the gray area can be achieved using the determined mean DBPs of the PD+TDPA+EP method for the tested delay. . . . 68

4.1 Overview of a point cloud-based model-mediated teleoperation system using a 3D sensor. . . 74
4.2 A depth image before filtering (left) and after filtering (right). The holes are filled by the median, average and inpainting filters. . . . 75
4.3 The definition of the proxy (left) and the estimation of the surface normal as well as master force (right). . . . 80
4.4 Comparison of the membrane deformation between the MSM and the proposed approach. Both models use the proxy-HIP haptic rendering method. (a) The MSM model developed by CHAI3D (www.chai3d.org) with 100 mass balls and 180 springs. (b) The proposed RFBD model with 150×150 points. . . . 83
4.5 Longitudinal deformation of an elastic half-space with a force applied to a small region. (a) The precise analytic solution ($z \sim 1/r$), and (b) the sixth-order polynomial approximation with finite deformation area. O denotes the collision position and x_s is the current slave position. . . . 84
4.6 The tangential deformation of the object surface approximated by shearing algorithms. The blue and black lines represent the object surfaces before and after the corresponding tangential deformations. (a) Surface without tangential deformation. (b) Small local dragging. (c) Critical local dragging. (d) Global sliding. . . . 85
4.7 Overview of the force rendering approach on the master side. . . . 87
4.8 Side and top views of the surface deformation. The blue and white spheres represent the master proxy and HIP. (a) $R : z_{max} = 3 : 1$. (b) $R : z_{max} = 6 : 1$. Please refer to http://www.lmt.ei.tum.de/forschung/projekte/prohaptics.html#demos/videos for more video demos. . . . 88
4.9 Position and locally rendered force signals of the master HIP during its interaction with the membrane. . . . 88
4.10 (a) Estimated stiffness values. (b) Estimated damping values. (c) Packet rate vs. time. . . . 92
4.11 A sampled-data master system with a spring-damper model. $\hat{\theta}$ represents the received model parameters, T is the sample period, and ZOH denotes zero-order hold. . . . 93
4.12 Simulation results for a linear stiffness increase. (a) Device position. (b) Object stiffness as a function of time. (c) The net energy output with and without the PMU method. (d) Adaptive damping for system passivity. . . . 97
4.13 Simulation results for the initial position change in the slave's approaching direction. (a) The change of the initial position. (b) The net energy output w/ and w/o the proposed PMU method. (c) Adaptive damping for system passivity. . . . 97
4.14 Experimental setup. . . . 99

4.15 (a) The setup of the teleoperation system. (b) The tested remote environment, which consists of two objects, one is a horizontally placed book with a smooth hard cover and the other one is a declining wooden plank. The green arrow from point A to point B denotes the trajectory of the slave motion during the test. 100
4.16 Experimental results. (a)(c)(e) the master and slave position in x, y and z directions, respectively. (b)(d)(f) the locally rendered master force and the remotely measured slave force in x, y, and z directions, respectively. The yellow region in (f) represents the 10% deadband with respect to the master force. 102
4.17 (a) Estimated stiffness. (b) Estimated friction coefficient. 103
4.18 Packet rate for transmitting the physical properties in the backward channel during the teleoperation. 105
4.19 Results of the subjective experiment. We only count the numbers of the "no difference" answers when the slave-master force signals are displayed. 106

5.1 (a) Various system performance measures can be applied to objectively compare the quality of different control and communication approaches. (b) Hypothetical performance measure for the previously proposed two joint solutions as a function of the end-to-end delay. 113
5.2 Experimental setup. The communication network, the slave (represented by a haptic interaction point), and the virtual environment are simulated on a PC using the CHAI3D library. 114
5.3 Measurements of the position and force signals and the estimated stiffness for the PD+MMT method. (a)(b) The master and slave position signals for 10 ms and 100 ms delays. (c)(d) The master and slave force signals for 10 ms and 100 ms delays. (e)(f) The estimated, transmitted, and applied stiffness values for 10 ms and 100 ms delays. 116
5.4 Measurements of the force signals for the PD+TDPA+EP method. (a) Delay of 10 ms. (b) Delay of 100 ms. 117
5.5 Experimental results. (a) The proportion of the subjects' choices in the two joint solutions based on the perceived stiffness similarity compared to the reference. (b) The average and standard deviation of the subjective ratings on the quality of experience for the two joint solutions. 119
5.6 Average packet rate over all subjects during the interaction with the soft object. 120

List of Tables

2.1 Overview of popular commercial kinesthetic haptic devices. . . . 11
2.2 Weber fraction of human perceptual discrimination for haptic signals [66]. . . . 14
2.3 A comparison of the existing haptic data reduction approaches for time-delayed teleoperation with the presented approaches in this thesis. . . . 23
2.4 A comparison of the state-of-the-art environment modeling methods for MMT with the extensions presented in this thesis. . . . 32
2.5 A comparison of the data reduction schemes for MMT. . . . 34
2.6 A comparison of the state-of-the-art model update methods for MMT with the approach presented in this thesis. . . . 36
2.7 Rating scheme for subjective evaluation. . . . 39

3.1 Determined thresholds for the three tested methods across all subjects. . . . 67
3.2 Results of the questionnaires for the second experiment. The remaining answers in Q1 are "both methods show similar impedance". . . . 69

4.1 Computational time of meshing and bounding-box creation for a spherical model with two different resolutions. . . . 90
4.2 Results of the subjective test. . . . 99
4.3 Slave status during the operation. . . . 101
4.4 Mean and standard deviation of the estimated stiffness values and friction coefficients for the two objects. . . . 103
4.5 Frame size and compression time for the depth images of the point cloud model. . . . 104

5.1 Parameter settings for the experiment. . . . 115